Characterization and Improvement of Oxygen Mass Transfer in a Rocking Disposable Bioreactor

by

Yun Bai

A thesis
presented to the University of Waterloo
in fulfillment of the
thesis requirement for the degree of
Doctor of Philosophy
in
Chemical Engineering

Waterloo, Ontario, Canada, 2020

Examining committee membership

The following served on the Examining Committee for this thesis. The decision of the Examining Committee is by majority vote.

External Examiner	Dr. Tingyue Gu Professor (Ohio University)
Supervisor(s)	Dr. William Anderson Professor (Department of Chemical Engineering)
	Dr. Murray Moo-Young Professor Emeritus (Department of Chemical Engineering)
Internal Member	Dr. Perry Chou Professor (Department of Chemical Engineering)
	Dr. Rajinder Pal Professor (Department of Chemical Engineering)
Internal-external Member	Dr. Trevor C. Charles Professor (Department of Biology)

AUTHOR'S DECLARATION

This thesis consists of material all of which I authored or co-authored: see Statement of Contributions included in the thesis. This is a true copy of the thesis, including any required final revisions, as accepted by my examiners.

I understand that my thesis may be made electronically available to the public.

Statement of Contributions

Some chapters in this thesis were based upon a combination of published work and a manuscript in preparation.

Section 4.1 consists of a paper that was co-authored by myself and both my co-supervisors Dr. William Anderson and Dr. Murray Moo-Young. My supervisors and I conceived the research idea and designed the experiments together. I carried out the model development, experimental validations, data analysis and the drafting of the manuscript. My supervisors and I reviewed and revised the manuscript.

Bai, Y., Moo-Young, M., Anderson, W.A., 2019. A mechanistic model for gas–liquid mass transfer prediction in a rocking disposable bioreactor. *Biotechnol. Bioeng*. 116, 1986–1998. https://doi.org/10.1002/bit.27000

Section 4.2 consists of a paper that was co-authored by myself and both my co-supervisors Dr. William Anderson and Dr. Murray Moo-Young. My supervisors and I conceived the research idea and designed the experiments together. I carried out experiments, data analysis and the drafting of the manuscript. My supervisors and I reviewed and revised the manuscript.

Bai, Y., Moo-Young, M., Anderson, W.A., 2019a. Characterization of power input and its impact on mass transfer in a rocking disposable bioreactor. *Chem. Eng. Sci*. 209, 115183. https://doi.org/10.1016/j.ces.2019.115183

Section 4.3 consists of a manuscript in preparation that was co-authored by myself, professor Jeff Gostick from our chemical engineering department and both my co-supervisors Dr. William Anderson and Dr. Murray Moo-Young. My supervisors and I conceived the research idea and designed the experiments together. I carried out experiments, data analysis and the drafting of the manuscript. Dr. Jeff Gostick provided help with pore size distribution analysis. My supervisors and I reviewed and revised the manuscript.

Bai, Y., Gostick, J., Moo-Young, M., Anderson, W.A., Sintered polyethylene sparger effects on gas-liquid mass transfer enhancement in a rocking disposable bioreactor (in preparation)

Abstract

Rocking disposable bioreactors use a cyclic rocking motion to induce mixing and oxygen transfer from the headspace gas into the liquid and are a novel type of bioreactor currently suitable for smaller-scale cell growth. At present they are used primarily for mammalian cell cultures. There are still unresolved knowledge gaps which render the broader applications of rocking disposable bioreactors challenging. These include adequate understanding of the gas-liquid mass transfer mechanism and the lack of quantitative correlations between the mass transfer capacity (to satisfy oxygen demand of a culture) and critical operational parameters, notably for scale-up applications in industry. This knowledge gap creates barriers for rational scale-up and application of these bioreactor systems in industrial biotechnologies. Industry is also interested about the applicability of these bioreactors to aerobic microbial fermentation processes which are faster than mammalian cultures for production of certain biological products.

In this work, the oxygen transfer pathways in a rocking disposable bioreactor were analyzed and a semi-empirical correlation for mass transfer coefficient based on a prediction ($k_L a$) model was developed that account for two types of aeration mechanisms, namely surface aeration and aeration via a breaking wave with air entrainment. Experimental $k_L a$ data across a range of possible operating conditions (rocking speed, angle, and liquid volume) supported the modelling approach, with most predictions falling within ±20% of experimental data. At low speeds (up to 20 rpm) the surface aeration mechanism was shown to be dominant with a $k_L a$ value of around 3.5 h^{-1}, while at high speeds (40 rpm) and angles the breaking wave mechanism contributed up to 91% of the overall $k_L a$ (65 h^{-1}). This model provides an improved mechanistic understanding of gas-liquid mass transfer for the operation, scale-up and potential design improvements for rocking bioreactors for aerobic fermentation processes.

Secondly, an electrical method was applied for measuring the specific power input into the liquid of the disposable rocking bioreactor at benchtop scales of 10 and 20 L volume capacities. Although power input varied periodically with the rocking motion, the peak power input was shown to be suitable for characterizing the impact of various operational parameters including

rocking frequency, rocking angle and liquid volumes. The average power inputs measured in this work ranged from 66.5 W/m^3 to 680.1 W/m^3 which were comparable with power inputs reported in the literature for stirred-tank and orbitally-shaken disposable bioreactors. The $k_L a$ was shown to correlate with the peak power input in a power law model, which confirmed that the gas-liquid mass transfer capacity rapidly improved as the power input increased, especially for power inputs of 600 W/m^3 and greater. The correlation between mixing time and power input indicated that a power input greater than 400 W/m^3 was more than enough to induce rapid mixing in the bioreactor.

Two potential improvements in the bioreactor design were tested for their capability to enhance the mass transfer capacity of rocking disposable bioreactors. First, an external rod baffle was installed diagonally on the rocking tray aiming to divert the dominant limited unidimensional liquid flow into both longitudinal and horizontal directions. This imposed diversion was shown to be very effective in reducing the mixing time of the bioreactor especially for liquid loadings at 50% of the total bag volume. The $k_L a$ however was reduced, especially when the rocking frequency was intensified to 30 and 40 rpm and the rocking angle was increased to 12 degrees This reduction was due to a diminished strength of the waves generated in the bioreactor which impacted the dominant mechanism contributing to the $k_L a$. Secondly, a submerged sintered polyethylene tube sparger was installed into the bioreactor to improve its oxygen gas-liquid mass transfer capacity. The gas flow condition and sparger surface wettability were changed to study the impact of these variables on the sparger performance. The results showed that the sparger could effectively increase the $k_L a$ of the bioreactor up to 8-fold when the rocking intensity was low with larger liquid volumes, but the improvements were diminished as the rocking intensity increased. The $k_L a$ of the modified bioreactor was observed to depend on the air flow but was not strongly affected by the sparger surface wettability unless the superficial gas velocity was decreased. Based on the progress in this study, future research is recommended for testing the applicability of the derived mass-transfer mechanistic models at larger scales, examining the proposed improvements on various types of cell cultures, especially aerobic microbial fermentations, and combining the modified bioreactor design with other process intensification techniques such as with perfusion and with microcarrier systems.

Acknowledgements

First and foremost, I would like to express my sincere gratitude to my supervisors Prof. William Andersons and Prof. Murray Moo-Young for not only their valuable guidance, support and encouragement throughout my doctoral study but also offering me such a precious opportunity to access to the world of knowledge I've never reached and allow me to explore freely in it.

I would like to thank all my Ph.D. thesis examination committee members: Prof. Perry Chou, Prof. Rajinder Pal, Prof. Trevor C. Charles and my external examiner Prof. Tingyue Gu from Ohio University for their time and efforts spent on examining my Ph.D. thesis and providing their comments.

I would also like to thank my fellow labmates especially Dr. Carol Moralejo and Dr. Shazia Tanvir for their help and guidance in my experiments and their talks that brought me lots of fun in lab.

I thank Mr. Bert Habicher for his help on mechanical and electronical re-designing of the rocking bioreactor instrument used throughout this study. I also want to thank Mr. Mingqian (John) Zhang for offering me consistent TA positions in the designated course CHE390L where I spent some enjoyable time with lots of undergraduate students and realized how accomplished teaching could be.

Financial support from the University of Waterloo, research funding from the Natural Sciences and Engineering Research Council of Canada (NSERC) and research support guidance with donation of the bioreactor system equipment from the GE Healthcare Inc is deeply acknowledged.

Lastly, I would like to thank all my friends who spent time with me on badminton courts, on road trips to national parks, on potluck gatherings, on boardgame nights and on building those ugly snowmen every winter. I am very grateful that you all accompanied me in part of this amazing four-year exploration of my life.

Dedication

This thesis is dedicated to my parents

Fengwu Bai and Li Dong

for their unconditional love and support of my academic pursuit

Table of Contents

List of Figures

List of Tables

List of Abbreviations

bDtBPP	Bis(2,4-di-tert-butylphenyl)-phosphate
BEVS	Baculovirus expression vector system
CAR-T	Chimeric antigen receptor T cell
CFD	Computational fluid dynamic
CHO	Chinese hamster ovary cell
CIP	Clean-in-place
CSTR	Continuous stirred tank reactor
COGs	Cost of goods
DC	Direct current
DI	De-ionized
DO	Dissolved oxygen
DtBP	2,4-di-tert-butylphenol
DtBPP	2,4-di-tert-butylphenyl dihydrogen phosphate
E&L	Extractable and leachable
EVA	Ethylene-vinyl acetate
FCI	Fixed capital investment
FEP	Fluorinated ethylene propylene
HEK	Human embryonic kidney cell
hHSC	Human hematopoietic stem cell
hiPSC	Human induced pluripotent stem cell
hMSC	Human mesenchymal stem cell

hPSC	Human pluripotent stem cell
LCA	Life cycle assessment
LDV	Laser doppler velocimetry
mAb	Monoclonal antibody
MDCK	Madin-Darby canine kidney cell
OTR	Oxygen transfer rate
OUR	Oxygen uptake rate
PCD	Peak cell density
PE	Polyethylene
PIV	Particle imaging velocimetry
QA/QC	Quality assurance and control
SIP	Sterilization-in-place
TBPP	Tris(2,4-di-tert-butylphenyl) phosphite
TOP	Tri-o-tolyl phosphate
UHMW	Ultra high molecular weight
ULDPE	Ultra low density polyethylene
1-D	1 dimensional
2-D	2 dimensional
3-D	3 dimensional

List of Symbols

Notation

A	Surface area (m^2)
a	Specific area (m^2/m^3)
B	Dimensionless bubble plume constant
b	Non-dimensional breaking parameter
C_{L0}	Initial concentration of oxygen in water (mol/L)
C_S	Saturated concentration of oxygen in water (mol/L)
c	Wave phase speed (m/s)
D	Diffusivity (m^2/s)
d_b	Bubble diameter (m)
DO	Dissolved oxygen level relative to saturation (%)
h	Liquid height (m)
h_w	Wave height (m)
$k_L a$	Volumetric mass transfer coefficient (h^{-1})
L	Length of the bag (m)
L_w	Wavelength (m)
L_c	Length of wave crest (m)
m_{wave}	Mass of wave (kg)
N	Rocking frequency (RPS)
pH_i	Initial pH value at time zero
pH_∞	Terminal pH value at infinite time
P/V	Specific power input (W/m^3)
Q_g	Volumetric gas flow rate (min^{-1} or vvm in some literature)
Re	Reynolds number
S	Wave slope
Sc	Schmidt number

t_e	Exposure time (s)
t_m	Mixing time (s)
t_S	Time to reach oxygen saturation in water (s)
t_{95}	pH probe response time (s)
u	Liquid velocity (m/s)
U_g	Superficial gas velocity (m/s)
V_L	Liquid volume (m^3)
$\bar{V}$	Average volume of air entrainment (m^3)
W	Bubble rise velocity (m/s)

Greek Letter

α	Rocking angle (^{o})
ε	Turbulent dissipation rate (m^2/s^3)
ϵ_l	Dissipation rate per crest length (kg m/s^3)
v	Kinematic viscosity (m^2/s)
ρ	Liquid density (kg/m^3)
$\emptyset$	Void fraction

Chapter 1 Introduction

1.1 Research Background

There has been a shift from traditional stainless-steel bioreactors towards disposable (also referred to as 'single-use') alternatives in the bio-manufacturing industry in recent years (Eibl et al., 2010a; Lopes, 2015; Shukla and Gottschalk, 2013). Compared with its stainless-steel alternatives, the disposable bioreactor holds several potential advantages which include a significant reduction in fixed capital investment, fast turnaround between production batches due to elimination of cleaning and sterilization processes, and minimization of potential cross contamination between batches. However, there are still some impediments to more extensive applications of the disposable plastic-bag bioreactor designs. Some of these challenges, such as the examination of leachables and extractables from plastic materials and their impact on cell growth and product quality, have been addressed in other studies (Noemí Dorival-García and Bones, 2017; Hammond et al., 2014, 2013). Other challenges are the inherent drawbacks of the bioreactor material itself, including the relatively weaker mechanical integrity of the plastic film and the environmental implications of the disposable plastic (Kelley, 2009; Langer and Rader, 2014). Some studies have also questioned the economics for switching established large-scale mAb production processes to disposables due to a negligible reduction in the cost of goods (Kelley, 2009). Nevertheless, the emergence of the contract manufacturing organization business model, the rise of small-to-medium size biopharmaceutical companies, and the rapidly growing biosimilar market in recent years requires potential upstream bioprocesses to achieve minimal capital investment, fast turnaround and high flexibility, which are the main advantages for the disposable bioprocessing systems over its permanent stainless-steel alternative (Gottschalk et al., 2012; Shukla and Gottschalk, 2013). Additionally, the 10-fold enhancement of mAb productivity from several hundreds of mg/L to several g/L titers in industry has reduced the scale requirements and enabled the wider application of 1000 to 5000 L bioreactors to be deployed as a basic workhorse for high-value biopharmaceutical production (Li et al., 2013). Continuing expansion of the single-use bioreactor market can be expected based on the robust overall growth in the biopharmaceutical market in combination with the steady maturation of products currently in development using single-use bioprocesses (Langer and Rader, 2014).

Rocking disposable bioreactors (or rocking bioreactors), which were first developed by Singh (Singh, 1999), have shifted the upstream bioprocess industry practices away from traditional stainless-steel vessels. Some of the disposable bioreactors' advantages include smaller initial capital investment, fast turnaround from batch to batch, and easier compliance with cGMP practices. These advantages have enabled them to win favor from industry over stainless steel equipment, especially in human and mammalian cell cultures and high value-added biopharmaceutical manufacturing (Eibl, Kaiser, Lombriser, & Eibl, 2010; Langer & Rader, 2014; Shukla & Gottschalk, 2013).

Applications of rocking bioreactors are mainly seen in mammalian cells, insect cells, plant cells and some microbial cells with minimal to moderate oxygen demand. Demonstration of mammalian cell cultivations has been performed on various cell types including CHO cultures (Clincke, Mölleryd, Samani, et al., 2013; Clincke, Mölleryd, Zhang, et al., 2013), Madin-Darby Canine Kidney (MDCK) cell culture (Genzel, Olmer, Schäfer, & Reichl, 2006) and Human embryonic kidney 293 (HEK293) cell culture (Jardin et al., 2008). Insect cells, including *Spodoptera frugiperda* 21 (Sf-21), *Spodoptera frugiperda* 9 (Sf-9) and *Drosophila melanogaster* Schneider 2 (S2) cells, were tested by several researchers using bench-top scale rocking bioreactors from different suppliers under varied conditions (Imseng et al., 2014; Wang et al., 2012; Weber, Weber, Geisse, & Memmert, 2002). Additionally, cultivations of anaerobic but shear sensitive microbial cells and cyanobacteria cells were also reported in some previous work (Cirés, Alvarez-Roa, & Heimann, 2015; Jonczyk et al., 2013).

The rocking bioreactor was designed de novo as a novel disposable bioreactor, unlike its counterparts such as stirred and orbitally-shaken disposable bioreactors which were adapted from their non-disposable predecessors. This makes the characterization of the rocking bioreactor rather challenging, due to a lack of precedents. Despite the abundant work on the characterization of stirred, orbitally shaken and pneumatic disposable bioreactors published in recent years, the characterization work reported on rocking bioreactors has been relatively limited. For example, Eibl et al. examined the engineering characteristics of the rocking bioreactor including power input, flow pattern, mixing time and gas-liquid mass transfer coefficient using a BioWave® bioreactor as a model (Eibl, Werner, & Eibl, 2009). Kalmbach et al. investigated the hydrodynamic properties of the liquid flow in the bag using experiments as well as computational fluid dynamic simulation tools (Kalmbach et al., 2011; Öncül, Kalmbach, Genzel, Reichl, & Thévenin, 2010).

Marsh et al. used phase-resolved particle image velocimetry (PIV) to experimentally characterize the fluid flow in a 2 L mimic of a disposable bag (Marsh et al., 2017).

Despite the progress to date in the characterization of rocking bioreactors, the previous work has put an emphasis on using previous experience and concepts acquired from cylindrical vessels, and has neglected to some extent the unique geometry, non-steady state flow patterns and mass transfer mechanisms occurring within the rocking bioreactor. A lack of mechanistic understanding of the mixing and mass transfer phenomena makes it difficult or uncertain to use and compare previous works for scale-up and optimization purposes.

Another challenge for the rocking bioreactor is its present more limited gas-liquid mass transfer capacity. Though sufficient for most mammalian and other animal cell cultivation purposes, it remains a limitation for its application to microbial or other cell cultures with a more intensive oxygen demand (Glazyrina et al., 2010; Mikola, Seto, & Amanullah, 2007). A lack of mechanistic understanding of mass transfer in rocking bioreactors presents a potential barrier to making improvements.

1.2 Research Objectives

The core objective of this research was to explore the potential of improving the oxygen mass transfer capacity of a commercially available rocking disposable bioreactor. To reach the ultimate milestone of the research, four specific sub-objectives were proposed. First of all, noticing the lack of a competent model describing the oxygen mass transfer between the gas and liquid phases in this rocking bioreactor, the first step of the research aimed to establish a mechanistic model capable of describing the unique oxygen mass transfer mechanism occurred in this rocking bioreactor. Following the modelling and understanding of the mass transfer mechanism in the bioreactor, some key parameters assumed to be influential to the gas-liquid mass transfer were investigated in the second phase of the study. Based on the modelling and experimental characterization of the gas-liquid mass transfer mechanism of the bioreactor, two potential improvements namely implanted baffle and sparger designs were added to the existing bioreactor configuration to try to improve the mass transfer capacity of the current rocking disposable bioreactor which could be represented by key parameters namely mixing time and volumetric mass transfer coefficient. Results and subsequent discussion yielded from these four sub-sections together were compiled into the overall outcome this study proposed to conclude. The wide-range of results will allow a

more rational understanding of this disposable type of bioreactors for applications to cell cultures in general, and with a special view to expansion of its potential use for aerobic microbial fermentation processes of increasing industrial interest compared to the current usual use for less-aerobic mammalian-cell cultures.

1.3 Thesis Structure

This thesis consisted of mainly four sections which included a review of published works (Chapter 2); a summary of experimental setup, model development and all measurement methods applied in this study (Chapter 3); a summary of all experimental results and related discussion yielded based on the four research sub-objectives mentioned in the above section (Chapter 4.1-4.4) and a conclusion and recommendation section for the indicated future work drawn from this work. Figure 1-1 below shows detailed content regarding each chapter.

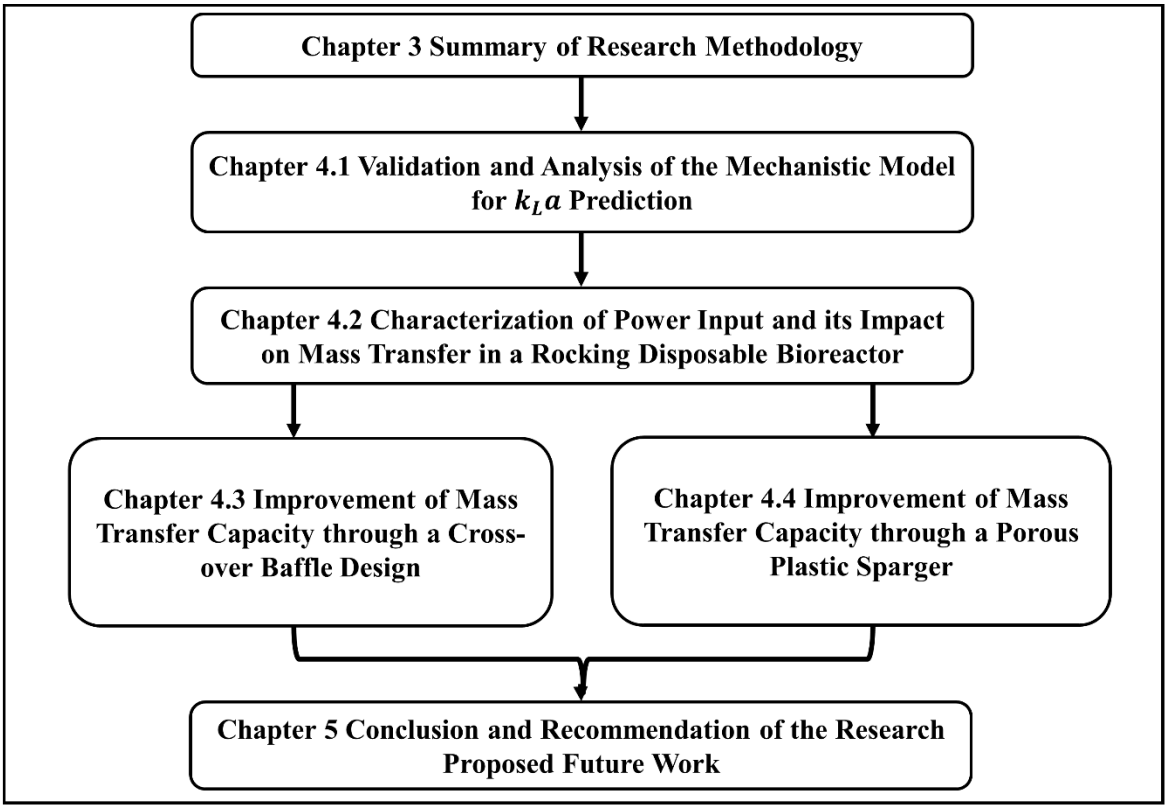

Figure 1-1 Structure of the thesis illustrated based on the content of each chapter, excluding introduction and literature review chapters.

In Chapter 2, a literature review closely related to the nature of this research is presented. This review contains an analysis of the feasibility of disposable bioprocess equipment both economically and environmentally; a revisit of the recent research progress reported on a variety of disposable bioreactors and their applications to some commonly used types of cells in industry. Additionally, a summary of reported research efforts on the transport phenomena characterization of these disposable bioreactors is provided in the review. Lastly, conclusive comments are provided identifying knowledge gaps still existing at this time.

In Chapter 3, a summary of all research methods applied in this research was presented. This included the experimental setup of the bioreactor and all measuring equipment, the measurement methods of mass-transfer related parameters, re-design of the bioreactor and statistical and analytical methods involved in the analysis of the experimental outcomes.

In Chapter 4, all results and discussion were summarized. There were four sections in this chapter each corresponded to the four proposed research objectives. In Chapter 4.1, the mechanistic model was developed to describe the $k_L a$ of the rocking bioreactor and validated against experimental results acquired from this study and the established model was analyzed parameter sensitivity and weight of each mass transfer mechanism. In Chapter 4.2, an experimental characterization investigating the correlation between power input and mass transfer performance was reported and the impact from varied operational parameters was discussed. In Chapter 4.3, a baffle design was tested for its capacity to improve the mass transfer comparing to the original bioreactor design, key parameters like t_m and $k_L a$ were selected for the comparison. In Chapter 4.4, varied sparger designs were evaluated for their capacity to improve the $k_L a$ of the bioreactor and the improvement is discussed relative to the sparger material and bubble profiles generated.

Finally, in Chapter 5, conclusions were drawn upon summarizing all results and discussion reported in the previous chapters. Recommendations and proposals for potential future research directions were subsequently provided based on these conclusions.

Chapter 2 Literature Review

2.1 Economic and Environmental Assessments of Disposable Bioprocess

After the establishment of the disposable bioprocess concept, the first question raised by many is whether adopting disposable bioprocesses would bring more benefits than their cost to the manufacturers and researchers both economically and environmentally. It is a critical question surrounding the disposable bioprocess that needs to be clearly addressed prior to other efforts to be deployed in expanding its applications. Economic assessment of disposable bioreactors could be divided mainly into two categories namely capital investment and operating costs (referred by some literatures as running costs). Additionally, modelling software such as BioSolve, SIMBIOPHARMA, SuperPro and Aspen Batch Process Developer^{TM}, have gained growing recognition and application in the assessment of bioprocess economic feasibility and environmental impact.

2.1.1 Economic assessment of disposable bioprocess

For bioprocess capital investment estimation, there are mainly three sections to be considered: fixed capital investment (FCI), labour capital and start-up and validation cost (Petrides et al., 2015). A straightforward approach for capital investment estimation was the direct summation of all three sections involved during the establishment of the whole bioprocess which combines an estimating "Lang" factor (Lang, 1947) with cost of equipment and utilities involved during installations (Peters and Timmerhaus, 1991). When applying this approach for estimating FCI of a disposable bioprocess, several aspects need to be considered include equipment and utilities, pipework and installation, process control and instrumentation, electrical power, building, detail engineering, construction and validation (Peters and Timmerhaus, 1991).

Several economic assessment studies comparing disposable bioprocess with traditional stainless-steel-tankk based bioprocess agreed that establishing a fully disposable bioprocess would help significantly reduce the capital investment, although the specific reduction ranged from 30 to 70 % without consensus (Lopes, 2015; Novais et al., 2001). Such discrepancy could be attributed to different cell systems of interest and subsequently different process parameters e.g. product titer, yield and productivity. Operating cost estimation usually consists of two main categories namely

direct operating cost which contains raw materials, utilities, labour, quality assurance and control (QA/QC), management and indirect operating cost which contains annual maintenance, insurance, general utilities and capital depreciation (Vermasvuori and Hurme, 2011). Contrary to the cut in capital investment, whether deployment of disposable bioprocess would decrease or increase the operating cost is still disputable and so far, no conclusive general remark could be drawn. The expenditure on raw material was claimed to increase if choosing disposable bioprocess due to procurement of disposable components such as bags, tubings and sensors (Lopes, 2015; Novais et al., 2001). Meanwhile, operating costs involving utilities would be reduced significantly thanks to drastic cut in water-for-injection demand and labor cost involved in sterilization-in-place and cleaning-in-place processes. It was estimated by some researchers that labour cost during operation would be increased if switched to disposable bioprocess (Shirahata et al., 2017), especially when the production scale expanded up to 2000 L. This was probably due to the smaller available scale of disposable bioreactors which required multiple production batches and thus required more frequent assemblies and dismantles of the instruments. A cross-comparison conducted recently by Pereira Chilima et al. among four potential bioreactor candidates for mesenchymal stromal cells expansion indicated that single-use stirred bioreactors coupled with microcarriers showed their economic feasibility as production scale and cell density elevated (Pereira Chilima et al., 2018). Arnold et al. demonstrated in their study that by adopting the continuous process strategy, a fully disposable bioprocess was capable of replacing a convential stainless-steel bioprocess due to cuts in capital, consumables and labor expenditures (Arnold et al., 2019). Regarding the application of single-use components in downstream processes, Xenopoulos proposed a novel single-use focus downstream recovery processes which were shown to be more cost-effective than conventional stainless-steel focus processes at 1000 to 5000 L commercial manufacturing scales (Xenopoulos, 2015).

A further development of the economic assessment model incorporated the uncertainty of the manufacturing process such as scale-up complexity and process consistency into the cost of goods sold (COGs) calculation and by doing so, the advantage of disposable bioprocess in reducing riskiness of the process as well as overall COGs of the product was strengthened (Farid et al., 2008, 2005; Jenkins and Farid, 2018). Moreover, the integration of disposable components into both upstream and downstream bioprocesses helped effectively reduced the current risks as well as improved process control quality in the manufacturing processes which in turn fostered the

maturation of continuous bioprocess strategy in industry. Such transition from existing batch or fed-batch cell culture to perfusion cell culture also helps enhance the productivity as well as final product titer, thus enables better profitability for fully disposable bioprocesses (Arnold et al., 2019; Bunnak et al., 2016; Cataldo et al., 2020; Xenopoulos, 2015).

2.1.2 Environmental impact assessment of disposable bioprocess

Besides the evaluation of economic feasibility of disposable bioprocess, another essential assessment of the disposable bioprocess focus on the environmental impact it generated. Life cycle assessment (LCA) methodology was commonly applied when analyzing the environmental impact of disposable bioprocess. A comprehensive life cycle assessment comprised of four main components e.g. process scope definition, inventory data acquisition, impact assessment and lastly sensitivities and uncertainties analysis (Ramasamy et al., 2015). Pietrzykowski et al. reported in their LCA study that disposable bioprocess holds significant comparative advantage over traditional stainless-steel bioprocess in alleviating environmental impact released from monoclonal antibody (mAb) manufacturing at 100 L up to 2000 L production scale (Pietrzykowski et al., 2013).

Future improvements could be focused on refining more accurate assessment models as more data from disposable bioprocesses would be disclosed from manufacturers and researchers. It is worth noticing that while some economic assessment works published so far have successfully demonstrated the economic drivers for adopting disposable bioprocesses in reducing operational costs reflected by lower COG out of the bioprocess, there is still a lack of convincing evidence to prove that costs spent on replacing existing stainless-steel bioprocesses could be fully recovered later from deployment of disposable bioprocess. Besides, so far most reported economic and environmental assessments of disposable bioreactors were performed using either human stem cells (chimeric antigen receptor modified T cells, mesenchymal stromal cells) for cell therapy or mammalian cells (CHO, HEK) for mAb manufacturing while similar assessments for other types of cell lines haven’t been reported, at least to our knowledge. Assessments of disposable bioprocesses on other cell lines would be helpful for stakeholders to develop better-informed decision-making strategy.

2.2 Disposable Bioreactor Designs and Types

There have been so far several types of commercially available bioreactors in the market with different designs suitable for different types of cell applications. The most commonly and widely applied types include stirred tank, wave rocking, orbitally shaken disposable, hollow fibre and fixed bed bioreactors.

Table 2-1 A summary of up to date commercially available disposable bioreactors with their scales and applications on reported cell systems.

Mass Transfer Mechanism	Bioreactor Product Name (manufacturer)	Scale (L)	Cell culture applied
Stirred	Ambr® Mini Bioreactor (Sartorius)	0.015 – 0.25	CHO cells (Janakiraman et al., 2015; Kelly et al., 2018; Kreye et al., 2019; P. Xu et al., 2017);
	DASbox® Mini Bioreactor (Eppendorf)	0.25	hPSC (Kropp et al., 2016);
	BIOSTAT® STR (Sartorius)	50	Bacteria cells (Dreher et al., 2013);
	Xcellerex™ (GE Healthcare)	50 – 200	HEK293T cells (Yang et al., 2019);
	Hyclone® (Thermo Fisher Scientific)	50 – 1000	MDCK cells (George et al., 2010);
Wave rocking	WAVE (GE Healthcare)	1 – 10	CHO cells (Clincke et al., 2013a, 2013b); yeast cells (Mikola et al., 2007); stem cells (Timmins et al., 2012, 2011); rice cells (Kwon et al., 2013); algae cells (Jones et al., 2017); insect cells (Weber et al., 2002);
	BIOSTAT RM (Sartorius)	1 – 10	Bacteria cells (Glazyrina et al., 2010);
	CellTainer	1 – 200	Bacteria cells (Westbrook et al., 2014);
	Wave and Under Tow	1 – 10	Soya and tobacco cells (Kwon et al., 2013);

Orbitally shaken	TubeSpin® (Techno Plastic Products AG)	0.001 – 0.6	Insect cells (Monteil et al., 2016);
	SB200-X (Kuhner AG)	10 – 200	Tobacco cells (Raven et al., 2015);
Air-Wheel	Air-Wheel® (PBS Biotech)	1 – 500	CHO cells (Lee et al., 2011); hMSC (de Sousa Pinto et al., 2019)
Membrane Diffusion	G-Rex® (Wilson Wolf Manufacturing)	0.01 – 5	Cancer cells and CAR-T cells (Bajgain et al., 2014); red blood cells (Heshusius et al., 2019)
Hollow-fibre Membrane	Quantum® (Terumo BCT)	0.01 – 1	hMSC (Hanley et al., 2014; Mennan et al., 2019), white blood cells (Uslu et al., 2019) or T cells (Nankervis et al., 2018)
Packed-bed	iCELLis (Pall Life Science)	0.1 – 100	Insect cells (Valkama et al., 2018)
Multiplate	Xpansion® (Pall Life Science)	10 – 200	hPSC (Lambrechts et al., 2016);

2.2.1 Rocking motion disposable bioreactor

Rocking disposable bioreactor was the first-of-its-kind design that brought the disposable concept and bioreactor design in focus. The mixing was achieved by waves generated by the oscillatory rocking motion of the rocking tray while the gas-liquid mass transfer was realized through surface aeration. Such design could minimize the shear stress derived from agitation and bubbling (in conventional stirred-tank bioreactor designs) meanwhile maintain sufficient mixing and gas-liquid mass transfer capacity. Following its debut, the versatility of the rocking bioreactor makes it suitable for a variety of cell lines including some industrial workhorses CHO cells (Clincke et al., 2013b, 2013a), HEK293 cells, Sf-9 insect cells, S2 insect cells and some emerging cell therapy applications like chimeric antigen receptor (CAR) T cells and iPSC/hPSC cells. Surface aeration in combination with wave mixing enables the rocking bioreactor to easily scale up to 50 L equipped with abundant characterization works on $k_L a$, liquid velocity distribution and shear rates readily available. Further scale-up could be challenging possibly due to two factors: 1) sufficient surface area for gas-liquid mass transfer is hard to maintain as the scale of the bioreactor increases and 2) mechanical strength of the bag building material needs to be resilient enough to tackle with intensive hydraulic forces exerted on the bag. Despite potential limitations on the bioreactor's scale-up, the rocking disposable bioreactor still has the market share in animal and human cell bioprocess applications primarily due to their minimal shear stress environment achieved by the mild agitation strategy.

2.2.2 Stirred tank disposable bioreactor

Another widely used type of disposable bioreactor was the stirred tank disposable bioreactor which inherited the classical stirred vessel design while replacing stainless steel building material with in-stalled disposable plastic containers. By doing so, all SIP, CIP and validation processes and associated labour costs are eliminated and downtime between batches was significantly reduced. Potential drawbacks include mechanical issues brought by using disposable plastic material. Compared with steel vessel, heat transfer of the stirred disposable bioreactor might be complicated because of two challenges: 1) installing cooling coil within the disposable bioreactor was impractical and 2) plastic film and air in between film and stainless steel support could add additional resistance for the heat transfer across the wall (Müller et al., 2018, 2017). The strength

of the plastic film as well as the magnetic impeller design renders the agitation power lower than what could be realized in stainless steel vessels. Despite of the mass and heat transfer limitations compared with traditional stainless-steel stirred tank bioreactor, stirred tank disposable bioreactor still holds several advantages over other types of disposable bioreactors. The stirred tank design is still the most capable design in terms of mass and heat transfer capacities compared with other types of disposable bioreactors. Its classical and well characterized shape and geometry makes scale-up straightforward and predictable as well. All these advantages make the disposable stirred tank suitable for cells with intensive mass and heat transfer requirement especially those aerobic industrial microorganisms such as *Escherichia coli*, *Saccharomyces cerevisiae* and *Pichia pastoris*. This disposable bioreactor type was also more commonly applied for large-scale cultivation processes up to 200, 1000 or even 2000 L scale as reported by several studies (Dreher et al., 2014a; Minow et al., 2014a, 2014b; S. Xu et al., 2017; Yang et al., 2019).

2.2.3 Membrane based disposable bioreactor

G-Rex® disposable bioreactor differentiates itself from other types of disposable bioreactor by its unique gas permeable membrane-based gas-liquid mass transfer mechanism. The mixing and circulation of media was realized by convection induced by thermal difference along the distance from the heat source. Applying such technologies enables the G-Rex® bioreactor to eliminate disruptive shear stress induced by agitation or bubbling aeration. The absence of shear stress creates an optimal growth environment for suspension cells that are susceptible to shear damages e.g. human stem cells or mammalian cells. An early optimization study reported a 100-fold expansion potential and about 1×10^6 cells/ml medium final cell density for K562 cancer cells (Bajgain et al., 2014). For primary T cells used for producing chimeric antigen receptor, final cell density could reach up to 3×10^6 cells/ml medium within 11 days of culture (Bajgain et al., 2014; Gagliardi et al., 2019). Another type of membrane based disposable bioreactor is the Quantum® cell expansion system, which is a disposable hollow fibre membrane bioreactor. Different from the G-Rex®, Quantum® is capable of growing adherent cells within the hollow fibre unit. However, it shares the same challenge with G-Rex® regarding scale-up. Hence the Quantum® disposable bioreactor is primarily used in patient-specific cell therapy applications such as expansion of mesenchymal stem cells (Hanley et al., 2014; Mennan et al., 2019), white blood cells (Uslu et al., 2019) or T cells (Nankervis et al., 2018). A common challenge for membrane disposable

bioreactors is their scalability and so far no known studies have reported any efforts in this area. This limits the membrane disposable bioreactor currently to only the area of patient-specific cell expansion purposes. As cell therapy rapidly evolved in recent years, allogeneic cell expansion might be the future direction of cell manufacturing as demand for treatment cells grows with the maturation of the technology. Such a trend requires increasing the scale of cell expansion which could yield more cells per batch of expansion. The scalability of membrane-based disposable bioreactors could be its bottleneck in a wider range of applications that is worth more devoted research efforts.

2.2.4 Orbitally shaken bioreactor

Orbitally shaken disposable bioreactors are promising novel disposable bioreactors designed primarily for less oxygen-demanding cell applications such as human, animal, insect and plant cells. As depicted in Figure 2-1, they share a 3-D vessel geometry similar to stirred tank bioreactors which requires less footprint for a large scale, above 1000 L. There are several advantages that make orbitally shaken disposable bioreactors quite appealing, namely simplicity and cost-effectiveness in the bioreactor design, readily scale-up based on simple geometry, and minimum hydrodynamic damage induced by agitation (Klöckner et al., 2013a). Currently available orbitally shaken disposable bioreactors range from 10 mL up to 1000 L. For example, the TubeSpin bioreactor is a miniaturized benchtop laboratory scale disposable bioreactor with working volumes between 1 and 400 mL. It has been tested to be suitable for several types of mammalian (Monteil et al., 2013; Raven et al., 2015), insect (Liu and Hong, 2001; Monteil et al., 2016) and plant cells (Lehmann et al., 2014) mainly for process screening applications. The bioreactor selected for Figure 2-1 is a SB50-X (Kuhner AG) disposable bioreactor belonging to the SB-X series of orbitally shaken bioreactors. This series of bioreactors includes a benchtop scale of 1 L and pilot scale of 200 L. Successful demonstrations using tobacco cells (Raven et al., 2015) avian cells (Coronel et al., 2019) or microalgal cells (Hillig et al., 2013) have been reported. Raven et al. showed that the scale-up of an orbitally shaken disposable bioreactor from shake flask culture with a 200-fold increase was still consistent and predictable for plant cells. Hillig et al. demonstrated that orbitally shaken bioreactors were quite suitable for shear sensitive oxygen demanding microalgae growth and showed the direct scalability between TubeSpin and SB200-X bioreactors.

Recently Coronel et al. tested the feasibility of producing influenza virus particles for vaccination applications using avian cells in a SB10-X disposable bioreactor. The reported cell density could reach and be maintained at 50×10^6 cells/mL with cell specific virus yields of 1000-3500 virions/cell and productivities of $0.5\text{-}2.2\times10^{12}$ virions/L/d which proved that orbitally shaken disposable bioreactors are capable of cultivating high-density suspension animal cells in a perfusion mode. Compared with other types of disposable bioreactors, the potential application of orbitally shaken bioreactors lies predominantly in growing shear sensitive cells which require moderate mass transfer capacity at 1 to 1000 L scales. Due to the classical shaking vessel design, characterizations of orbitally shaken disposable bioreactors are sufficient which make the scale-up of these bioreactors quite straightforward. Hydrodynamic parameters including shear stress distribution and energy dissipation rate have been analyzed and related to geometrical parameters, and the investigation not only showed the dependence on these geometrical parameters but also proved that the shear stress profile at all operational conditions could be still maintained below critical values that minimize hydraulic damage to mammalian cells (Zhu et al., 2018a). The study of flow patterns in orbitally shaken bioreactor related to viscosity of the liquid was also reported (Ducci and Weheliye, 2014). In addition, mass transfer characterizations such as $k_L a$ and t_m were also characterized based on varying operational parameters and geometrical factors. Klöckner et al. established an empirical correlation between $k_L a$ and parameters including: cylinder diameter, shaking diameter, shaking frequency, liquid volume, diffusion coefficient of oxygen and kinematic viscosity and validated their correlation at pilot scale up to 50 L (Klöckner et al., 2013b). Werner et al. applied computational fluid dynamic (CFD) simulation to predict $k_L a$ and t_m during the scale-up between two orbitally shaken disposable bioreactors with completely different geometries (Werner et al., 2013). In the characterization of orbitally shaken bioreactors, a unique 'out-of-phase' phenomenon that described the inconsistency between shaking frequency and liquid oscillation frequency was identified and shown to be influential on the mixing and gas-liquid mass transfer capacities of orbitally shaken bioreactors (Ducci and Weheliye, 2014; Klöckner et al., 2012; Maier and Büchs, 2001). Such phenomenon is worth special attention when dealing with the mass transfer characterization of orbitally shaken bioreactors.

2.2.5 Other types of disposable bioreactor

Besides above-mentioned types of disposable bioreactors that are commonly seen in the current biomanufacturing sector, there are other types of bioreactors with unique designs. Pneumatic disposable bioreactors such as the Air-Wheel disposable bioreactor use bubble flow to both agitate the liquid and to drive the impeller for mixing. Thanks to the presence of bubbles, the gas-liquid mass transfer capacity of these bioreactors is usually superior compared to other disposable bioreactors that applying surface aeration strategies. Successful applications have been reported using CHO cells (Kim et al., 2013), human mesenchymal stem cells (hMSC) (de Sousa Pinto et al., 2019; Sousa et al., 2015) and human induced pluripotent stem cells (hiPSC) (Nogueira et al., 2019; Rodrigues et al., 2018). As bubbles are generated in such bioreactors, the shear impact on vulnerable cells is a critical factor to consider when applying this type of bioreactor. To circumvent the shear stress brought by bubbles in the liquid as well as support adherent cell growth, some researchers use microcarriers to anchor cells in bioreactors. Reported stem cell cultivations in pneumatic bioreactors could be scaled up to 1 L so far while much more robust mammalian cells could grow in much larger bioreactors up to 250 L.

Another type of disposable bioreactor currently available is the fixed-bed disposable bioreactor represented by the iCELLis bioreactor. Such bioreactors are suitable for growing adherent cells from benchtop to pilot scales. Though the packed bed design could minimize the mechanical strength requirement which is much higher for other types of bioreactors like stirred tanks, rocking motion and orbitally shaken bioreactors, the mass transfer capacity would be a significant limiting factor during the scale up of the process. Nevertheless, several types of cells including insect cells (Ventini-Monteiro et al., 2015) and animal cells (Emmerling et al., 2016; Leinonen et al., 2019; Powers et al., 2016). HEK293 cell line is the most widely tested cells for packed-bed bioreactors due to their superior growth and cell density in adherent environments.

Figure 2-1 A summary of some commercially available disposable bioreactors, distinguished by their designs and mass transfer mechanisms including Air-Wheel bioreactor manufactured by PBS Biotech, BIOSTAT STR® bioreactor manufactured by Sartorius AG, SB50-X bioreactor manufactured by Kuhner AG, WAVE bioreactor manufactured by GE Healthcare, iCELLis® bioreactor manufactured by Pall Life Sciences and Quantum bioreactor manufactured by Terumo BCT (photos cited from manufacturers' official websites).

2.3 Applications of Disposable Bioreactors

As a critical component of rapidly expanding disposable bioprocesses, a disposable bioreactor is steadily replacing traditional stainless-steel equipment in newly established as well as recently upgraded manufacturing facilities. A variety of designs for disposable bioreactors enable them to be extensively adopted to various types of cells for different applications including customized cell therapy using human stem cells, mAb and vaccine production using industrial mammalian cells or insect cells, therapeutic protein production using microbial cells. Depending on the targeted cell system and operational parameters selected, performance on each disposable bioreactor could differentiated among each other. All these current or potential cell applications using various disposable bioreactors and their performances will be discussed in the following few sections.

2.3.1 Mammalian cells

Animal cell lines are currently widely applied by biopharmaceutical manufacturers as cell hosts for most of their biopharmaceutical production needs, although an on-going trend of switching from animal cell lines to human cell lines for some biopharmaceutical products have been observed due to less immunological concerns. Animal cells are generally vulnerable to shear stress but require sufficient mixing and gas-liquid mass transfer capacities for CO_2 and O_2 transport during their proliferation. Additionally, as proliferation of most types of animal cells is much slower, stringent requirements for clean-room and sterilization are highly emphasized by all manufacturers and researchers.

The CHO cell is a powerful workhorse cell line favored by industry for recombinant mAb production thanks to its robust proliferation capacity in both adherent and suspension culture, simplicity in host cell engineering and efficient selection techniques (Wurm, 2004). The rocking disposable bioreactor, as the first bioreactor ever developed employing a disposable concept (Singh, 1999), was specifically designed for all the characteristics required by the CHO cell line. Later several types of disposable bioreactors were introduced to the market which are suitable for CHO cells including orbitally-shaken, stirred tank, fixed bed and pneumatically mixed bioreactor designs. (Kuiper et al., 2019; Lee et al., 2011; Minow et al., 2014b; Raven et al., 2015; Stettler et al., 2007).

2.3.2 Insect cells

Insect cells are another promising multifunctional host cell system capable of producing recombinant proteins or virus particles. Compared to mammalian cells, insect cells as hosts for recombinant protein production hold several inherent advantages such as ease of culture, lower cost of medium, and are capable of efficiently expressing intracellular proteins and high level expression when using baculovirus expression vector system (BEVS) (Ikonomou et al., 2003; McKenzie and Abbott, 2018). It was one of the three cell lines being tested when the first disposable bioreactor was developed, and also was the first cell line successfully scaled up to 10 L during the initial tests in a fed-batch culture with a peak cell density reaching 3×10^6 cells/mL with a inoculum cell density of 5×10^5 cells/mL (Singh, 1999). A further optimization was performed based on the initial reported test yielding an optimized protein (intercellular adhesion molecule 1/mouse cκ fusion protein) up to 100 mg/L which was realized by supplementing medium with yeastolate, using a peak cell density (PCD) of 3×10^6 cells/mL before infection, 0.5 MOI virus and TOI of 33 % of PCD (Weber et al., 2002). Based on the optimized protocol, the following studies focused on three main directions: 1) testing a variety of disposable bioreactors for cultivating insect cells (Imseng et al., 2014; Lu et al., 2005; Monteil et al., 2016; Ventini-Monteiro et al., 2015), 2) testing different types of insect cell expression systems namely Sf-9/BEVS and S2 expression systems (Decarli et al., 2018; Lu et al., 2005; Sun et al., 2016; Ventini-Monteiro et al., 2015; Wang et al., 2012) and 3) further improving process performance through novel cultivation strategies e.g. perfusion culture (Ventini-Monteiro et al., 2015; Wang et al., 2012), continuous culture (Schlaeppi et al., 2006) or upstream and downstream process integration. All these efforts could further enhance the peak cell density to reach 10^7 cells/mL, lowering the costs spent on labour and medium while achieving an increased level of expression of target protein products.

2.3.3 Human cells

Developments in cell therapy in recent years have led to a very promising technology for various disease treatments. Despite the promising potential for cell therapy, as cells acquired from either patients or matching donors are limited in quantity by their nature, large-scale efficient expansion of these stem cells is still a major hurdle for the full deployment of the technology. Disposable

bioreactors are viewed as competent candidates for the expansion of various types of human stem cells e.g. CAR-T cells, mesenchymal stromal cells, hematopoietic stem cells, and iPSCs.

For human mesenchymal stromal cells (hMSCs), several types of disposable bioreactors have been tested for their potential for cell expansion purpose (de Sá da Silva et al., 2019; de Sousa Pinto et al., 2019; Lawson et al., 2017; Mennan et al., 2019; Schirmaier et al., 2014). Both immunophenotype and differentiation potential of the hMSCs grown in all types of bioreactors were confirmed as being well maintained. Other process parameters though vary among the different types of bioreactors. The maximum cell number could reach 2.61×10^8 cells with a 25.6-fold expansion and a doubling time of 28.9 h in a 600 mL working volume WAVE™ disposable bioreactor after 10 days of processing (de Sá da Silva et al., 2019) which was a further improvement on the previously reported 14.9-fold expansion in a 500 mL working volume WAVE™ bioreactor (Timmins et al., 2012). A disposable hollow fibre bioreactor was also demonstrated as a capable choice for a single-dose hMSC expansion with maximum cell numbers of roughly 2.8×10^8 cells in a single batch expansion of 7 days with a doubling time of 19.2 h and highest achievable 57.1-fold expansion (Mennan et al., 2019). In addition, a trial on a Vertical-Wheel™ disposable bioreactor was performed at a 100 mL scale yielding 5.3×10^5 cells/mL with 21-fold expansion in a 8 day cell expansion process (de Sousa Pinto et al., 2019). A further scale-up study reported a cell density of 3×10^5 cells/mL and 12-fold expansion achieved in a 2.2 L scale Vertical-Wheel™ bioreactor (Sousa et al., 2015). While there exist diverse types of disposable bioreactors for bench-top scale hMSC expansion applications, as the demand further grows, so far only a stirred tank disposable bioreactor provided successful scale up to a 50 L pilot scale culture. For the stirred tank disposable bioreactor, final cell numbers on day 7 could reach 5.3×10^8 cells with a 35.4-fold expansion and a doubling time of 25.6 h in a 2 L working volume, while at a 35 L pilot scale volume, total cell numbers could reach 1×10^{10} cells which was estimated to be sufficient for 20 clinical doses (Schirmaier et al., 2014). Another scale-up research reported a comparable maximum cell number of 9.5×10^9 cells at a 50 L working volume with a 36-fold expansion during 11 days of cultivation (Lawson et al., 2017). It should be noted that the process parameters summarized above should only be viewed as reference indexes. It is neither meaningful nor practical to directly compare the performances of these bioreactors using the parameters reported due to inconsistencies and variations existing among each experiment. Process conditions regarding medium composition, cell line source, microcarrier selection,

dissolved oxygen (DO) level and seed cell concentration chosen by each study vary to different levels and thus render a direct comparison rather challenging.

Hematopoietic stem cells (hHSCs) were another potential beneficiary of the disposable cell expansion technique. The first ever test in a disposable bioreactor was reported by Timmins et al. in a 1 L BIOSTAT RM rocking disposable bioreactor generating up to 2.25×10^8 -fold expansion in cell number with competent enucleation frequency above 90 % (Timmins et al., 2011). Such a large-scale expansion strategy was further refined by Heshusius et al. in a G-Rex disposable membrane bioreactor reaching 1×10^9 -fold expansion of $CD34^+$ cells per peripheral blood mononuclear cell (PBMC) with enucleation frequency maintained above 90% (Heshusius et al., 2019). However, further improvements aimed at manufacturing cost reduction, especially medium cost reduction, was still required to fully realize the clinical potential of hHSC expansion. Additionally, human induced pluripotent stem cells (hiPSCs) were tested under suspension culture in a disposable stirred bioreactor with 125 mL initial working volume (Kropp et al., 2016). Cell density was reported reaching up to 3.6×10^6 cells/mL with 6.7-fold expansion yielding totally 3×10^8 cells per batch of 100 mL culture volume. While in another study using the Vertical-Wheel™ bioreactor combined with microcarriers, comparable results were acquired where cell density was observed to reach 8.55×10^6 cells/mL yielding a total 2.6×10^8 cells in a 300 mL working volume with a 4.8-fold expansion of seed cells (Nogueira et al., 2019; Rodrigues et al., 2018).

2.3.4 Microbial cells

Microbial cells are often a first choice for testing regarding recombinant protein expression duty. Compared to most mammalian cells, microbial cells hold a quite different membrane protein composition as well as an either absent or if existing high mannose modified glycosylation metabolic pathway which renders itself sometimes unsuitable for some therapeutic protein expression applications. However, its superior growth rate, higher cell density and subsequent product titer achievable in combination with its extremely simple and cheap cultivation process enables the microbial cell to stand out if needed for certain therapeutic product manufacturing. Nevertheless, those advantages of microbial cells require certain pre-requisites including more intensive requirements for oxygen mass transfer, heat removal and mixing in suspension which are sometimes challenging to fulfill.

Some researchers investigated the potential of using existing disposable bioreactors as novel types of photobioreactors. Cires et al. (Cirés et al., 2015) proved that a WAVE^{TM} bioreactor was capable of growing a N_2-fixing cyanobacterium *Anabaena siamensis* at 1 L benchtop scale with better performance observed in CO_2 fixation rate, biomass productivities and protein content when compared to growth in the bubbled suspension. Jones et al. reported a proof-of-concept test using another algal strain *Scenedesmus* sp. in a WAVE^{TM} bioreactor modified photobioreactor, where the biomass productivity reported in their study reached 0.187 $gL^{-1}d^{-1}$ (Jones et al., 2017). Compared with the rocking disposable bioreactor, a stirred tank disposable bioreactor might be a better choice for those microbial cells that are robust to shear stress but more oxygen demanding. *E. coli* is an example of such a microorganism and scaled up growth was recently reported in a 50 L stirred disposable bioreactor (Dreher et al., 2014b). *Aspergillus niger* was another microbe tested for its potential to be cultivated in a disposable bioreactor (Kurt et al., 2018). As several parameters including agitation strength and dissolved oxygen tension could influence both cell morphology as well as heterologous protein productivity (Wang et al., 2003), these parameters were monitored during their cultivation in the 2-D rocking disposable bioreactor. Results indicated that the bioreactor's gas-liquid mass transfer capacity as well as rocking intensity could meet the growth requirements of this type of filamentous fungal species.

2.4 Progresses in Disposable Bioreactor Characterizations

2.4.1 Characterization of extractables and leachables

Leachables are defined as chemical entities extracted from single-use components, i.e. the bioreactor container bag, into the manufacturing process solution under general working conditions. Extractables are chemical entities that are extracted out of the single-use components but under more exaggerated process conditions or an artificial extraction environment (Ding, 2013; Rao et al., 2009). Process conditions potentially contributing to the extraction include pH, temperature, time of exposure and medium composition. For the single-use bioprocess, typical extractables and leachables (referred as E&Ls in the following context) come from two major sources: 1) polymers and additives during plastic film manufacture and 2) the degradation of plastic materials during the sterilization process which was usually achieved by gamma irradiation (Ishii-Watabe et al., 2015). Earlier when the concept of the single-use bioreactor was first

introduced, concerns regarding the leachables and extractables from disposable plastic films emerged almost simultaneously and were identified as a major barrier for the deployment of single-use bioprocesses.

Fortunately, E&Ls characterization was not a new challenge to the biomanufacturing industry, as investigation of potential E&Ls of plastic materials had been established since disposable plastic was involved in media storage, product packaging and bottling processes. There had been significant progress on both identification and characterization of E&Ls in disposable bioreactors as well as improvements in bag film material ever since the issue was brought to the spotlight immediately after the introduction to the market. Jenke et al. (Jenke et al., 2007) reported several E&Ls they detected including small-chain organic acids (formic acid and acetic acid), long-chain fatty acid (myristic acid, palmitic acid and stearic acid) and amides (erucamide, hexadecanamide and octadecanamide) using multiple chromatography methods in combination from two EVA films and two polyethylene films respectively. Noemí et al. proposed a 2-propanol solution suitable as a model solvent for E&Ls characterizations of plastic bag materials and by coupling with a dispersive liquid-liquid microextraction and UHPLC-MS analytical method (N. Dorival-García and Bones, 2017; Noemí Dorival-García and Bones, 2017). Several target compounds were measured in their study including bDtBPP, DtBPP, DtBP, Irgafos 168® (TBPP) and TOP. In their flow-up study, an extensive characterization of E&Ls for 34 disposable bags from 5 suppliers validated the role of high resolution mass spectrometry (HRMS) in E&Ls detection and measurement and a reduction of specific toxic E&Ls amount was observed on newer bags potentially thanks to the technology advances and stringent regulations in recent years (Dorival-García et al., 2018). The removal of some potentially toxic leachables e.g. bDtBPP and silver metal was demonstrated to improve the CHO cell growth in a comparative study between a newer bag and its previous generation (Kelly et al., 2019). Additionally, a novel broad-spectrum analytical method proposed by Marghitoiu et al. (Marghitoiu et al., 2015) successfully identified 53 organic entities in total out of four disposable bioreactor bags from anonymous suppliers. One specific group of E&Ls from *tris*(2,4-di-tert-butylphenyl)phosphite (TBPP) degradation was reported to be worthy of researchers notice as degradation by-product bis(2,4-di-tert-butylphenyl)phosphate (bDtBPP) was firstly identified as a leachable toxic to mammalian cells even at very low level of concentration (ppb) (Hammond et al., 2014).

In addition to the concern on E&Ls of the bag material, the change of contact surface physical property as plastic material replaced stainless-steel was reported to impact the cell growth process in the bioreactor to some extent. Kadarusman et al. firstly noticed that the low-density polypropylene film material, due to its pore structure, had a significant binding affinity for cholesterol which resulted in cholesterol retention on the bag inner contact surface and subsequently induced cholesterol depletion during their NS0 cell growth (Kadarusman et al., 2005). Altaras et al. reported a similar observation of cholesterol binding to polyethylene (PE) materials as well and additionally found that such binding would be exacerbated in the presence of cyclodextrin, a common additive to cell culture media (Altaras et al., 2007). To fix this issue, alternative plastic materials e.g. fluorinated ethylene propylene (FEP) or ultra-low-density polyethylene (ULDPE) was suggested as the inner contact film material in the bag design. Continuous progress has been witnessed in the characterization of E&Ls during the past few years as more and more biologics manufacturers switched from stainless-steel equipment to disposable plastic alternatives. Equipped with these reported works on E&Ls characterization, researchers and other technical staff could develop a better understanding of the potential impact by the building material on product quality issues.

2.4.2 Characterization of disposable bioreactors

Depending on the application, at present, disposable bioreactors range from 5 mL up to 2000 L as described in Figure 2-2. Such a variation in the bioreactor scale requires in-depth understanding of transport phenomenon in the bioreactor. Key process parameters like $k_L a$, t_m, liquid velocity, flow pattern and their correlation with P/V and liquid properties need to be accurately described in order to perform successful scale-up or scale-down tasks. With the steadily growing popularity of the disposable bioreactor and established characterization work from traditional bioreactors with similar geometry and design, a significant amount of research effort has been devoted in characterizing these novel disposable bioreactors with some progress which will be summarized in this section.

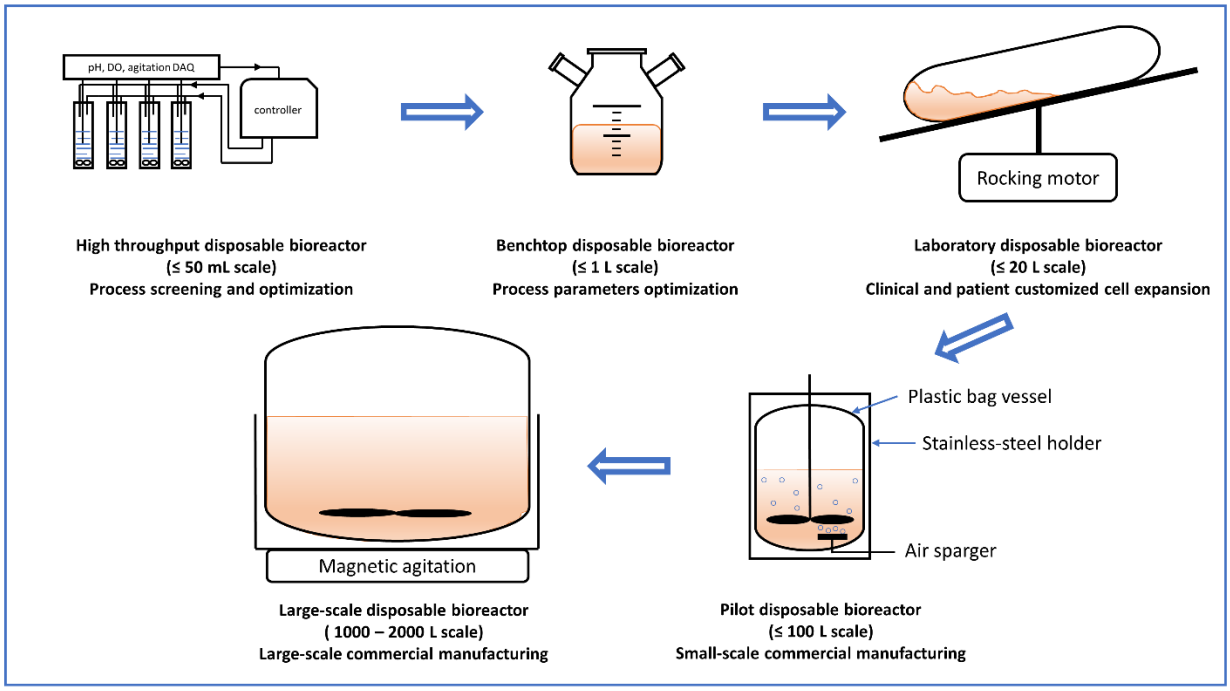

Figure 2-2 Disposable bioreactors currently available across all scales and their applications (Dreher et al., 2013; Janakiraman et al., 2015; Minow et al., 2014b; Tsai et al., 2017; P. Xu et al., 2017).

2.4.2.1 Fluid dynamics in disposable bioreactors

Fluid dynamics studies on bioreactors mainly focus on the key parameters such as liquid velocity, shear rate, flow pattern and energy dissipation rate, which could impact the shear environment, mixing performance and inter-phase mass transfer capacity. Such parameters could either be estimated by computational fluid dynamics (CFD) modelling techniques or measured through fluid flow visualization experiments using techniques such as laser doppler velocimetry (LDV), particle image velocimetry (PIV) (Odeleye et al., 2014) or hot-wire anemometry (Kalmbach et al., 2011). For some types of disposable bioreactors that were re-designed based on pre-existing stainless-steel or glass vessels, i.e. stirred tank or orbitally shaken bioreactors, the fluid dynamics studies focus on either transferring the well established knowledge from conventional bioreactors to their disposable successor based upon the similarity in geometry and momentum transfer mechanism, or if unsuccessful investigating the disparities lying between the two. Thanks to continuous progress in model development and computing capacity, CFD simulation has been accepted as a reliable technique in modelling the fluid flow in disposable bioreactors across a variety of designs

including stirred tank (Maltby et al., 2018), orbitally shaken (Zhu et al., 2018b, 2018a) and rocking wave (Öncül et al., 2010; Zhan et al., 2019). The most widely applied software packages for disposable bioreactors CFD simulations includes commercial packages such as ANSYS Fluent (Amer et al., 2019; Öncül et al., 2010; Schirmaier et al., 2014; Zhan et al., 2019) and COMSOL (Tsai et al., 2017) and open-source package like OpenFOAM (Ansoni and Seleghim, 2016; Rahimi et al., 2018). Thanks to the limitation on the scale of disposable bioreactors (≤ 2000 L in most cases) and the symmetrical geometry of most bioreactors, current CFD techniques don't have to deal with a serious bottleneck on computing capacity and CFD simulations up to 1000 L have been reported on stirred tank disposable bioreactors (Delafosse et al., 2018; Maltby et al., 2018). Based on numerous successful cases reported on scale-up designs facilitated by CFD simulations and the growth in both computing capacity and modelling techniques, it can be expected that CFD assisted scale-up and mass transfer characterizations would be more widely adopted as predominant tools for future disposable bioreactor design applications. Experimental techniques to characterize the fluid dynamics in the bioreactor are studied more intensively prior to the development of CFD techniques. Even now, a well established CFD model in the bioreactor still requires experimental characterization to validate its accuracy in prediction. Among various techniques available for flow characterizations, PIV technique gains growing applications as it can provide a multi-dimensional tracing of the flow despite of the cost and complexity performing such a measurement. Several PIV studies were reported on rocking (Marsh et al., 2017), orbitally shaken (Ducci and Weheliye, 2014; Weheliye et al., 2013) and stirred (Odeleye et al., 2014; Schirmaier et al., 2014) disposable bioreactors. Additionally, there were studies using other techniques such as a hot-wire anemometer (Kalmbach et al., 2011) which was an invasive measurement technique to acquire the point-based spatial distribution of fluid flow profile in a disposable bioreactor as well. Due to the fragility and molding of the plastic material, non-invasive measurement methods are more favorable compared with invasive methods.

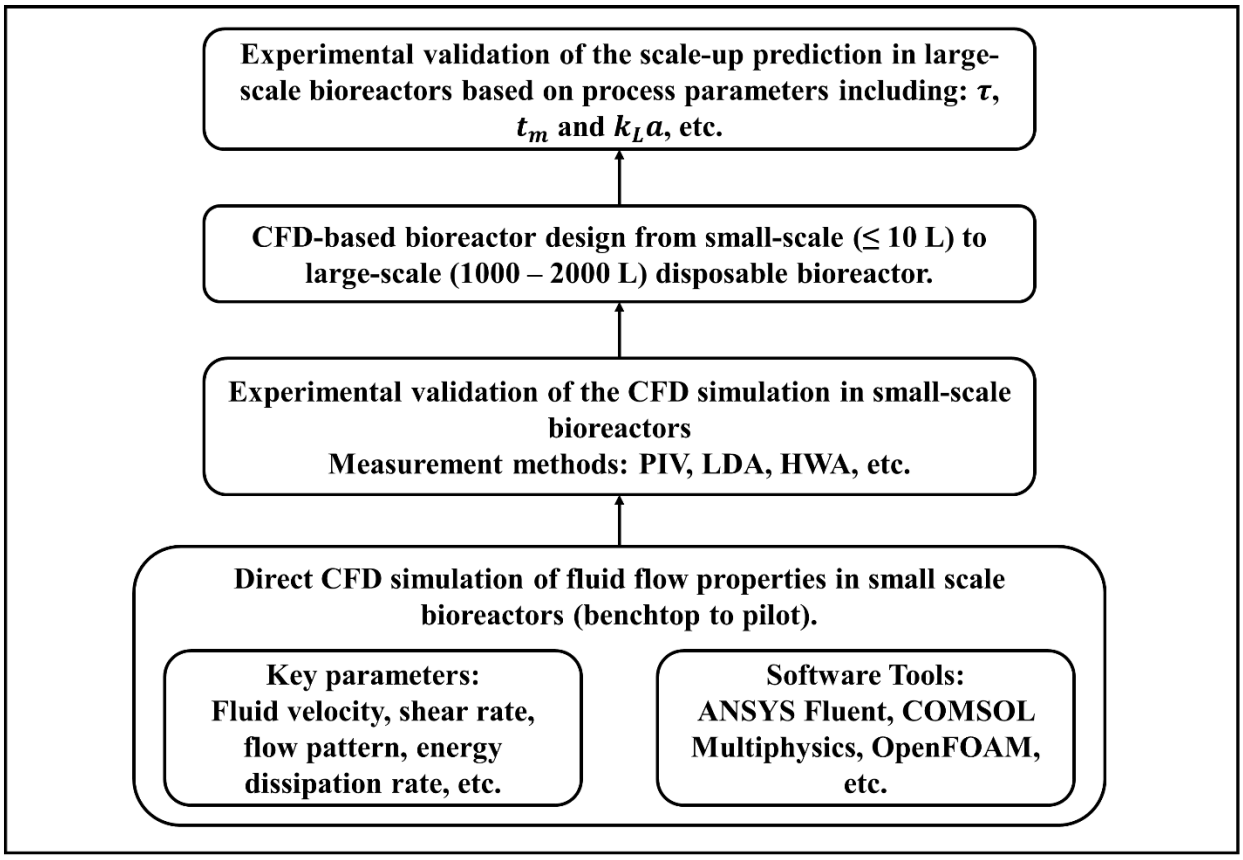

Figure 2-3 A CFD-based disposable bioreactor scale-up design process flow diagram.

Figure 2-3 summarizes a standard scale-up design combining both CFD and experimental validation processes. This design flow integrates up-to-date progress in CFD and flow visualization techniques. Such a design process is also expected to expedite the overall scale-up design and cut time and labor costs spent on scale-up and optimization of the bioreactor.

2.4.2.2 Mass transfer in disposable bioreactors

Mass transfer is another critical aspect involved in bioreactor design and characterization. Key process parameters of bioreactor mass transfer capacity include mixing time, residence time distribution, volumetric mass transfer coefficient, mass transfer rate and concentration profile in suspension. These parameters together determine whether a bioreactor could provide a homogeneous and nutrient sufficient environment for cells to proliferate.

For disposable bioreactors, additional characterization studies on mass transfer needed to be performed due to the different agitation equipment installed on the bioreactor, unique geometry and influence from the plastic building material. Among all types of disposable bioreactors, rocking wave disposable bioreactor received most intensive investigation mainly because of its novel design in geometry and wide applications in research and development sectors. Rodrigues et al. found that the residence time distribution in a 2 L rocking disposable bioreactor was quite similar to the distribution profile acquired from a 2 L stirred tank bioreactor but deviated from ideal-model predictions including CSTR and plug-flow models (Rodrigues et al., 2012). Based on their results, a rocking disposable bioreactor could maintain similar mixing capacity in alignment with a stirred system regarding mammalian cell expansion conditions while such mixing capacity was still insufficient to reach the assumptions for a CSTR or plug-flow model. Studies on the t_m characterization in rocking bioreactors revealed that rocking frequency and rocking angle could be influential on mixing time. For benchtop scale, rocking frequency above 15 rpm combined with a rocking angle higher than 8^o could reduce the t_m below 50 s (Eibl et al., 2010b; Jones et al., 2017). Similar results were also reported for a 2-D rocking bioreactor t_m measurement. However, as the bioreactor scale reached up to 200 L, the same rocking conditions resulted in a mixing time between 100 and 300 s (Eibl et al., 2010b) which could result in an insufficient mixing situation. Comparatively t_m data acquired from a stirred tank disposable bioreactor provided superior performance regarding the mixing capacity where t_m was maintained below 20 s at a 2 L scale with P/V remaining below 1.5 W/m^3 (Grein et al., 2016). Even when the bioreactor scale was elevated, t_m could still be contained below 30 s at a 200 L scale with P/V at around 15 W/m^3 (Dreher et al., 2014a). Mixing studies on an orbitally shaken disposable bioreactor reported a t_m ranging between 10 and 100 s at a 50 L scale with a rotation speed of 80 to 120 rpm (Zhang et al., 2010).

Besides mixing performance, another key parameter characterizing the mass transfer in a disposable bioreactor is the volumetric mass transfer coefficient ($k_L a$). This parameter is especially important for oxygen transfer within the bioreactor which, thanks to the low oxygen solubility in liquid phase, requires continuous transport of oxygen between gas phase and liquid phase in the bioreactor. For mammalian and insect cells, as the specific oxygen uptake rate (q_{O_2}) ranges between $0.1 - 0.4 \times 10^{-12}\ mol\ O_2\ cell^{-1}h^{-1}$ for varied types of cells among all growth

phases which is moderate (Palomares and Ramírez, 1996; Ruffieux et al., 1998), $k_L a$ around 20 h^{-1} is sufficient to maintain a 10^6 cells/mL cell density. Some robust industrial cell lines like CHO, Sf-9 and HEK293 could reach much higher cell density up to 10^8 cells/mL under optimal growth environment (Clincke et al., 2013b, 2013a) which is favoured by industry but required much higher $k_L a$ (nearly 200 h^{-1}) from the bioreactor. For more oxygen demanding microbial cell lines like *E. coli*, *S. cerevisiae* and *P. pastoris*, q_{O_2} mostly ranges between 10^{-4} and 10^{-3} mol O_2 $cell^{-1}$ h^{-1} (Garcia-Ochoa et al., 2010) which is much higher comparing to animal cells. For such oxygen intensive microbial cell expansion, $k_L a$ above 100 h^{-1} is usually required for optimal cell growth performance. In addition to understanding the $k_L a$ capacity required for difference types of cell applications, it is important to clearly describe the dependence of $k_L a$ on process parameters such as liquid properties, power input and agitation conditions. Such characterization efforts have been reported using various types of disposable bioreactors. For stirred tank disposable bioreactors, thanks to sufficient characterization work reported on traditional stirred tank bioreactors which share many similarities in both geometry and mixing mechanism, most studies focused on transferring existing characterization knowledge from stainless-steel or glass vessels to plastic bag containers and identified any inconsistency found during such transfer (Dreher et al., 2014a). For orbitally shaken disposable bioreactors, an semi-empirical correlation of $k_L a$ was established and validated at 2 – 200 L scale under a BY-2 cell suspension condition relating $k_L a$ to multiple variables including bioreactor dimensions, liquid volume and viscosity, oxygen diffusion coefficient and gravitational acceleration (Klöckner et al., 2013b). A $k_L a$ prediction model was validated at 10 L scale under DI water system based on the CFD simulation of fluid flow in an orbitally shaken disposable bioreactor (Zhu et al., 2018a). For rocking disposable bioreactors, most reported characterizations of $k_L a$ were performed experimentally relating $k_L a$ to either operational parameters such as rocking frequency, rocking angle and liquid volume, or process parameters like P/V and liquid viscosity (Jones et al., 2017; Pilarek et al., 2018; Westbrook et al., 2014). For other types of disposable bioreactor, specific characterization works are scarce and usually $k_L a$ was studied as a process parameter that could potentially affect cell density, cell viability and product quality without in-depth description of how it would change with different operational conditions.

2.4.2.3 Heat transfer in disposable bioreactors

Compared with momentum transfer and mass transfer, heat transfer capacity of the bioreactor traditionally does not draw significant concern for animal cell cultivations as the respiratory intensity of many types of animal cells is relatively low which renders heat generated during cell cultivation moderate. Even for intensive microbial cell cultivation, a well-designed cooling coil and baffle is sufficient for most heat transfer capacity requirement. The heat transfer capacity of disposable bioreactors is expected to underperform in comparison to their stainless-steel or glass predecessors mainly due to the inferior heat conductivity of plastic as well as the difficulty in designing a proper cooling system within the closed plastic container. Dreher et al. demonstrated in their research that for a 50 L stirred disposable bioreactor, its heat transfer coefficient was roughly 20% of an equivalent stainless-steel stirred bioreactor (Dreher et al., 2014b). Müller et al. while confirming similar heat transfer coefficient values with results reported by Dreher et al., went a step further by establishing a more detailed characterization of the dependence of the overall heat transfer coefficient on process parameters like agitation speed and cooling liquid flow (Müller et al., 2018, 2017). For animal cell applications, the heat transfer capacity is not expected to be the limiting parameter involved in the design of disposable bioreactor due to low heat release rates during the much slower growing phase of those cells compared to rapidly growing microbial cells. However, the heat transfer capacity should be taken into careful consideration when applying disposable bioreactors as microbial fermenters.

Chapter 3 Methodology

3.1 Disposable Bioreactor System

Experiments were performed on a nominal 20 L WAVE^{TM} bioreactor platform (WAVE Bioreactor^{TM} 20/50 EHT system, GE Healthcare Canada) using either 10 L or 20 L cellbags containing varied loading of de-ionized water as a consistent model test liquid. Figure 3-1 below showed the instrumentation in detail including bioreactor rocking tray, bioreactor bag, bioreactor controller, tracer injection port, air inlet and outlet. Depending on specific research goals, certain modifications might be applied to the existed system which were mentioned in the next few sections.

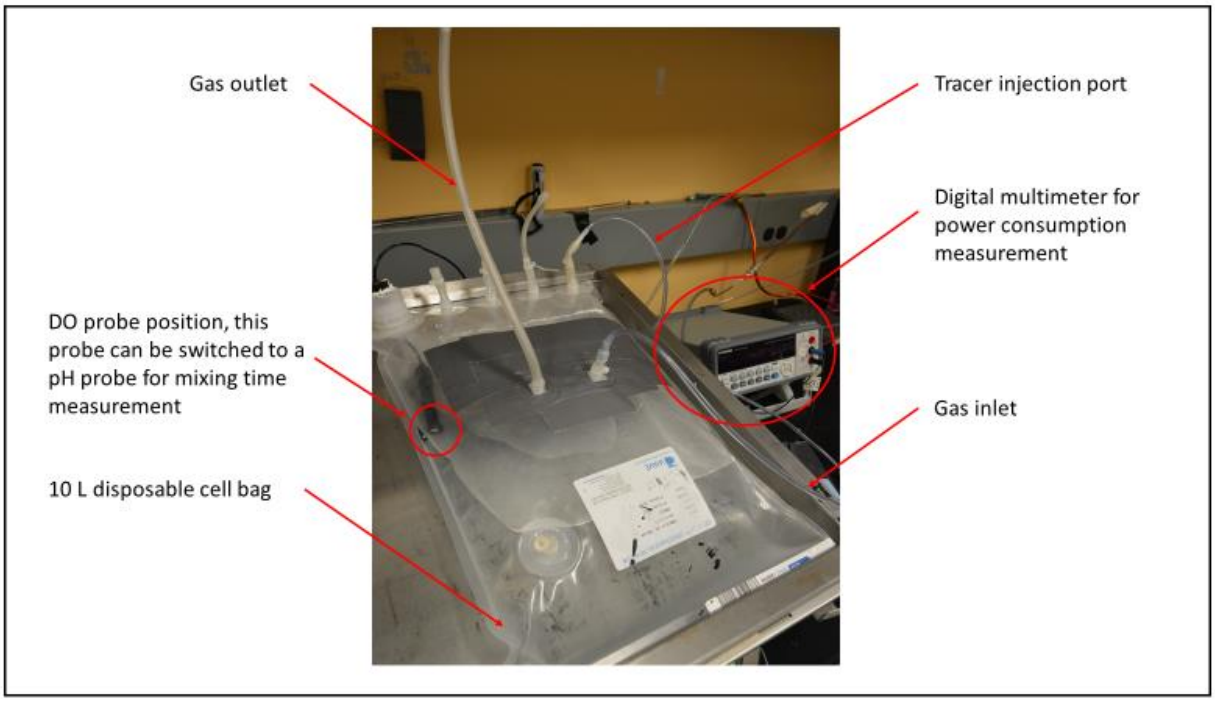

Figure 3-1 Photo of the 20 L WAVE^{TM} bioreactor platform (WAVE Bioreactor^{TM} 20/50 EHT system, GE Healthcare Canada) loaded with 6 L DI water used in this study.

Figure 3-2 shows a schematic of the experimental apparatus including the WAVE^{TM} bioreactor platform, measurement probe position, power measurement instrumentation as well as the data acquisition system. The DO and pH probes were both anchored at the bottom of the bioreactor bag thanks to the much higher density of the building material than DI water which could ensure that

the DO and pH measured in during experiments represent real-time values at the bottom of the liquid body.

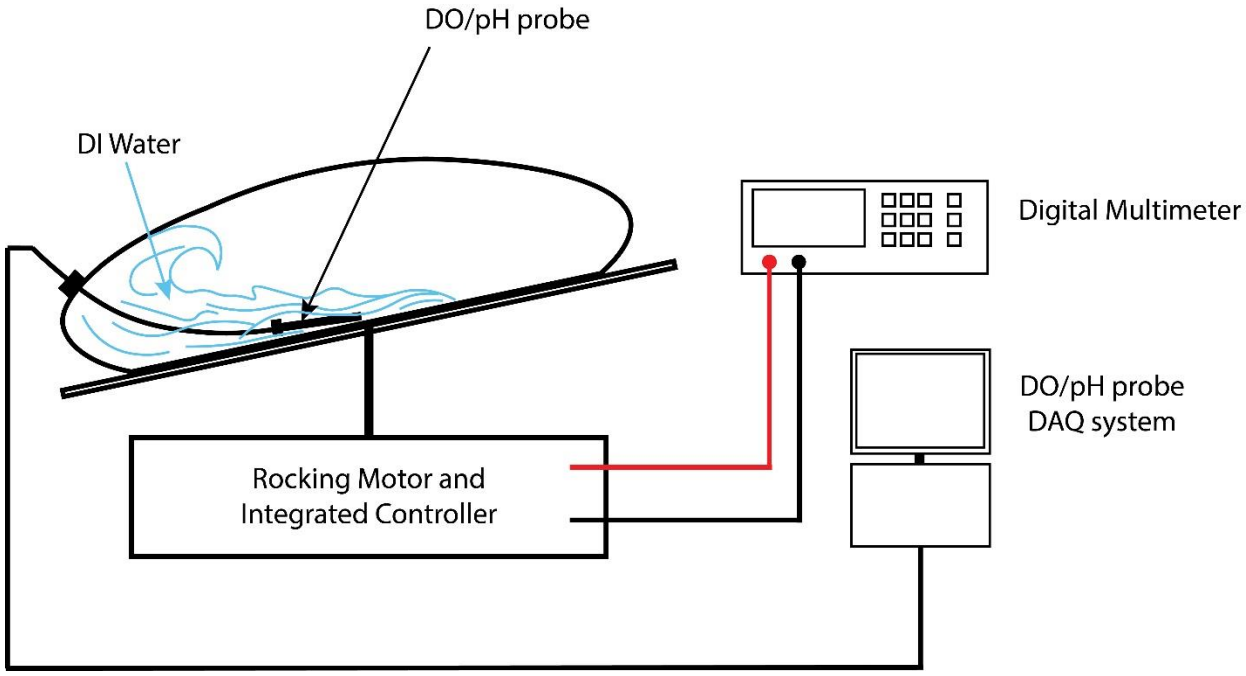

Figure 3-2 Schematic of the WAVE™ bioreactor platform, and all additional measurement instrumentations including DO/pH probe, digital multimeter and DAQ system.

3.2 Process Parameters

There were three types of operational process parameters being changed in this study in order to investigate the mass transfer capacity. Liquid volume of DI water used in experiments ranged from 3 and 5 L in a 10 L bioreactor bag to 6, 8 and 10 L in a 20 L bioreactor bag. Rocking frequency of the rocking tray chose four different values which were 10, 20, 30 and 40 rpm respectively. Two rocking angles which were 8º and 12º were used during experiments. These varied operational process parameters in combination constructed a comprehensive experimental condition matrix which was capable of capture the bioreactor's performance in a wide range of operational conditions.

Besides the manipulation of operational process parameters, another parameter changed in this study was the viscosity of the model liquid. In addition to the DI water used in most experiments, a 400 g/L sucrose solution was used to model a high viscosity liquid. The viscosity was measured using a Brookfield viscometer and pre-established calibration table kindly provided by Prof. Pal.

3.3 Mass Transfer Characterization Techniques

3.3.1 Volumetric mass transfer coefficient $k_L a$ measurement

Since DI water was used without any cells for convenience , similarly as in previous established research work the dynamic gassing out method was adopted for $k_L a$ measurements with the oxygen uptake rate (OUR) taken as zero for these experiments (Bandyopadhyay et al., 1967; Garcia-Ochoa and Gomez, 2009). A fast-response dissolved oxygen (DO) probe (ENV-40-DO, Atlas Scientific LLC) with response time t_{95}<30 s was used during experiments in order to minimize the error due to probe response time (Tribe et al., 1995). The position of the DO probe was depicted in both Figure 3-1 and Figure 3-2. Under these conditions, $the\ mass\ transfer\ coefficient,\ k_L a,$ can then be calculated using equation (3.1). An example plot was also illustrated by Figure 3-3, the slope in the plot was extracted as the $k_L a$ value of interest.

$$\ln \frac{(C_{L0} - C_L)}{(C_{L0} - C_S)} = k_L a(t - t_s) \tag{3.1}$$

Prior to the first use, the DO probe was calibrated by a two-point calibration method as suggested by the probe manufacturer at both an atmospheric condition for 100% DO and a nitrogen-purged condition for 0% DO. Once conditioned for initial start, the DO probe later was re-calibrated using single-point calibration method at atmospheric condition prior to experiments.

During the $k_L a$ measurement, the bag was first purged with nitrogen at 0.4 vvm and 30 rpm rocking rate to expel all dissolved oxygen from the liquid phase. Once the DO value dropped below 5% of saturation, the rocking was paused, and nitrogen flow was terminated. The bag was manually compressed to remove most of the residual gas in the headspace. The gas flow was then switched to compressed air and the bag headspace was filled and left to flushed with air for 5 min at 0.4 vvm. After the head space gas flushing was completed, the rocking was resumed with continuous compressed air flow into the headspace to ensure that the gas phase oxygen concentration did not change significantly. The increasing liquid phase DO was tracked by a data acquisition system based on LabView software (LabView 17.0). Three replicates were performed for each $k_L a$ measurement condition.

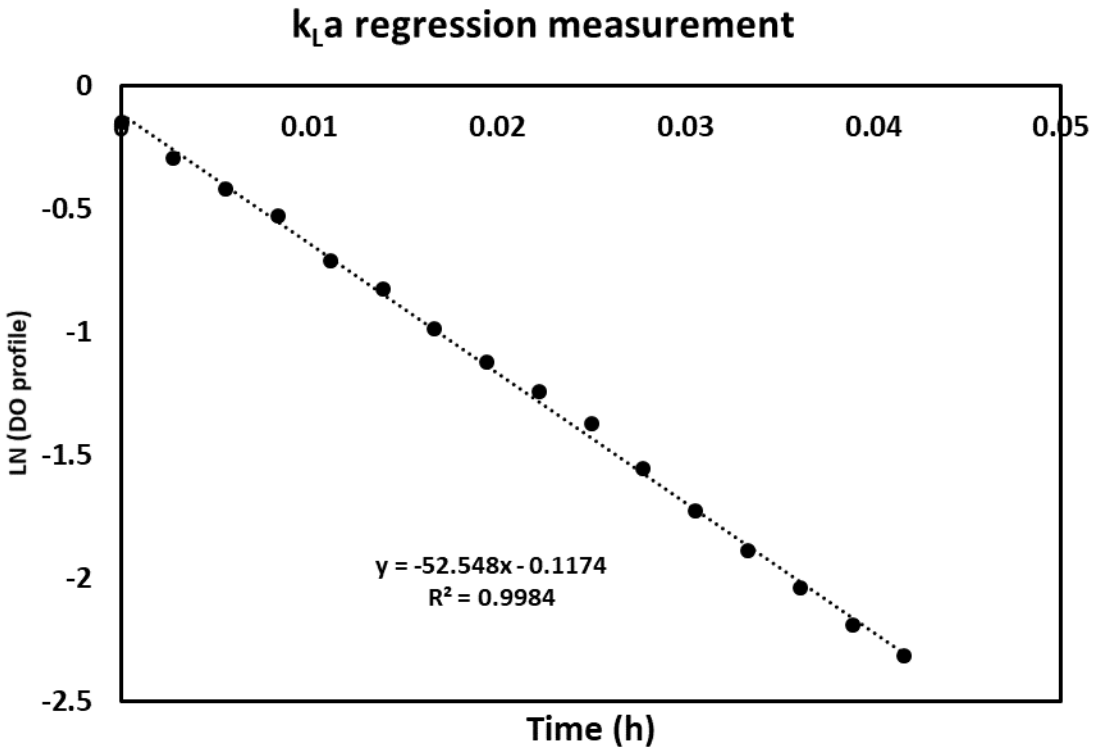

Figure 3-3 An example plot of $k_L a$ measurement using dynamic gassing method described by equation (3.1) at 6 L volume, 12° angle and 30 rpm condition in a 20 L bag.

3.3.2 Impact of gas phase exchange time on $k_L a$ measurement

During the initial validation trials of the $k_L a$ measurement method, it was noticed that the gas phase exchange time would affect the $k_L a$ value measured in the experiment. Such effect used not to be very substantial for the $k_L a$ measurements in stirred tank or bubble column bioreactors because the headspace was relatively small comparing to liquid phase in the vessel in these bioreactors and the gas-liquid mass transfer in these bioreactors relies heavily on bubble liquid contact surface rather than the surface aeration between headspace and liquid. In this rocking bioreactor however, it was concerned that such pre-requisites might not hold valid. Liquid loading in the bioreactor bag could not exceed half of the total bag volume as required by most bioreactor suppliers which means the headspace would take up over half of the total bag volume. Besides, the gas-liquid mass transfer in the rocking bioreactor with the absence of a sparger is realized mainly through either surface aeration or wave air entrainment which relied on the oxygen exchange between headspace atmosphere and liquid body. Those factors combined make the gas

content in the headspace a potential variable that could affect the $k_L a$ measurement and brought inconsistency among different experimental conditions.

To address this uncertainty, a series of experiments were performed to check whether such variation was significant and if significant to quantify such variation in the measurement. Five different headspace exchange times were selected namely 0, 1, 3, 5 and 10 min for comparing the impact on $k_L a$ induced by varied headspace exchange situations. Liquid volume was fixed at 10 L in a 20 L disposable bag.

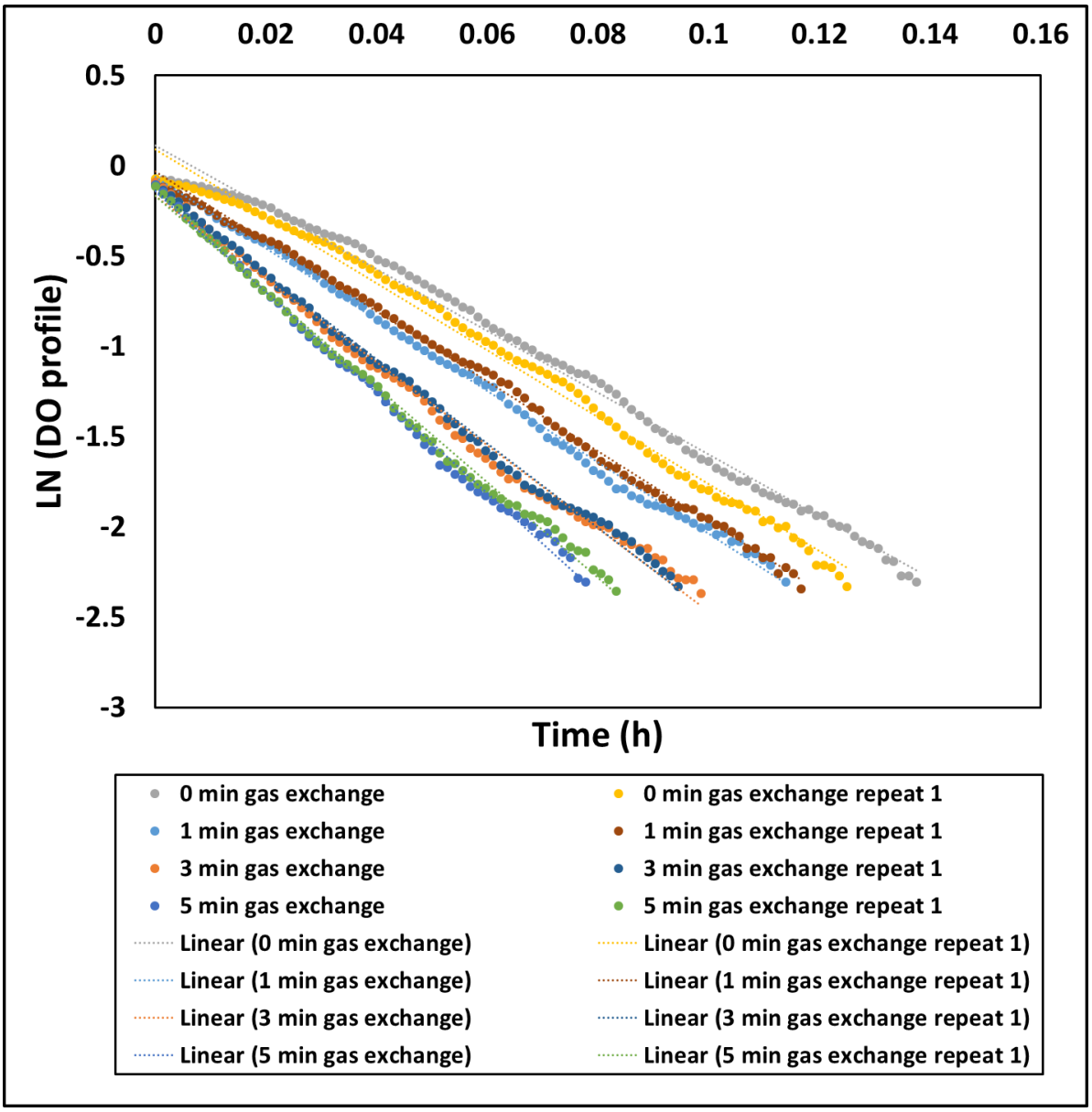

Figure 3-4 Summary of the $k_L a$ measurements linear regression plots with different headspace gas exchange time of 0, 1, 3, 5 and 10 min.

Results summarized in Figure 3-4 revealed that the gas exchange time did affect the $k_L a$ values measured. Such influence could be attributed to the dynamic gas composition alteration with time which subsequently affected the saturated dissolved oxygen concentration (C_S) in equation (3.1). As C_S was treated as a constant in equation (3.1), a deviation from this pre-requisite would render the measurement inaccurate. Previous studies of mass transfer in the rocking bioreactor either

neglected the headspace gas exchange or adopted a fixed exchange time but none of them seemed to notice the impact brought by differences in gas exchange time. In this work, this inconsistency has been identified and as demonstrated by experimental results acquired at different gas exchange times, $k_L a$ could vary between 17.82 and 41.15 at 30 rpm and 10 L liquid volume in a 20 L bioreactor. Such a difference was too significant to be neglected and thus should be treated with caution when comparing $k_L a$ values reported by various other studies.

A much longer headspace exchange time such as 10 min was seen to significantly increase the $k_L a$ measured in experiments. Such high $k_L a$ was viewed inaccurate as an air enriched diffusion layer could be formed on the top of the liquid body where it was in contact with the headspace gas phase. On the other hand, lack of headspace gas exchange rendered the gas composition unstable during the $k_L a$ measurement which was reflected in Figure 3-4 as the deviation from linearity in the regression for 0 min data (yellow and grey data points). Based on above considerations, the headspace gas exchange time in this study was fixed at 5 min for all experiments. This would enable the results acquired from this research to be compared directly with some other researches (Ghasemi et al., 2019; Westbrook et al., 2014) run under the same gas exchange time without any potential discrepancy as well as maintain a robust linear regression calculation.

3.3.3 Mixing time t_m measurement

Mixing time was measured using an acidic tracer method. A pH probe (ENV-40-pH, Atlas Scientific LLC) was inserted into the bag to monitor the liquid pH during the experiment, and the data was recorded using LabView software. The pH probe used the same position as the DO probe in the bioreactor, and the tracer injection position was located on the corner of the bag. Before the injection of acidic tracer, the pH of the liquid was adjusted using 0.1 M NaOH solution to 9.00 ± 0.10. Once the pH reading was stabilized, rocking was paused and 2 mL acidic tracer (0.1 M HCl) was injected into the bioreactor. Following the injection, rocking was immediately resumed. As illustrated in Figure 3-5, the pH in the liquid decreased until it stopped fluctuating and stabilized again. The time it took for the pH to reach 95% degree of homogeneity was determined to be the mixing time of the bioreactor. The degree of homogeneity is described by equation (3.2) below.

$$degree\ of\ homogeneity\ = \frac{pH_\infty \pm 0.05(pH_i - pH_\infty)}{pH_\infty} \times 100\% \qquad (3.2)$$

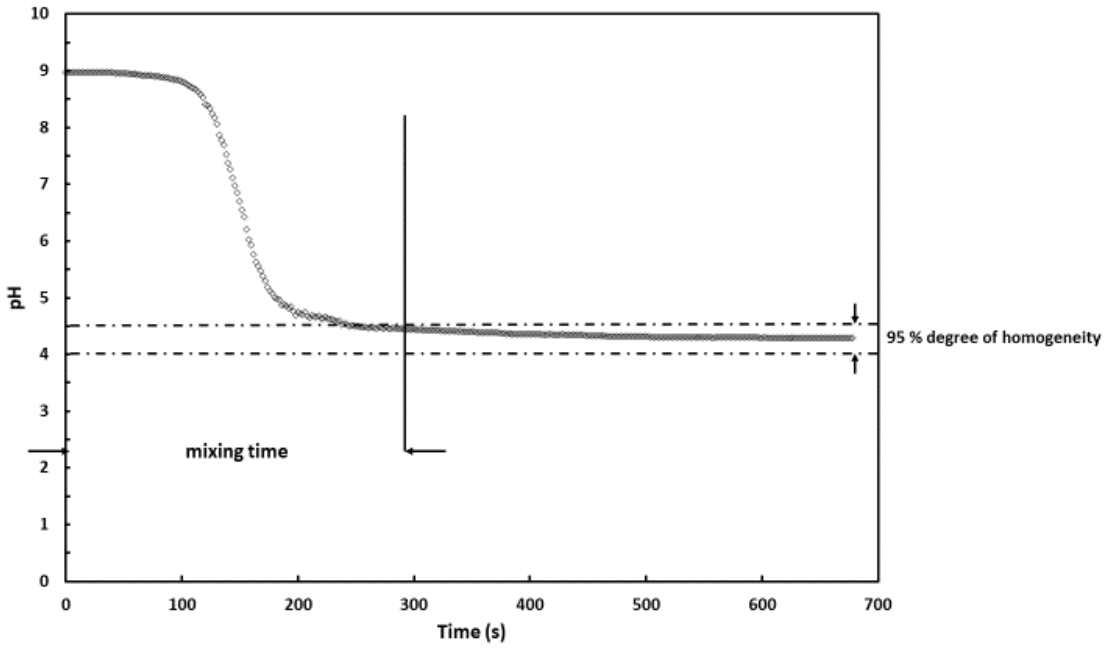

Figure 3-5 Example mixing time determination at 10 L volume, 12º angle and 10 rpm condition in a 20 L bag.

Additionally, to identify any dead zones appearing in the liquid mixing, phenolphthalein was added to the liquid to trace the transient mixing results visually in local regions of the liquid using color change as the pH varied. Photographs were compiled in Figure 4-11 to illustrate the phenolphthalein experiments as well as the tracer injection position and pH probe location.

3.4 Power input measurement

A digital multimeter (InstekGW GDM-8342, Good Will Instrument Co., Ltd) was connected directly to the DC motor (SM23165DT Class 5 D-Style SmartMotor™, Moog Animatics) that drives the rocking platform. The DC power is the direct product of DC voltage and DC current measured. The DC voltage was determined to be a constant value of 24 DCV throughout the rocking action. The fluctuating DC current was measured at 10 readings per second by the digital multimeter as rocking continued. The DC current data acquisition process for each condition lasted for at least 5 min of stable current oscillations. A 1 min selection of data, including approximately 600 DC current data points, was selected for determination of the peak, average and base current.

The specific power input (P/V) was then calculated using the calculated power consumption divided by the known liquid volume in the bioreactor. As illustrated in Fig. 2 for one set of data, the motor current and subsequently the motor power consumption varied periodically along with the rocking motion. Hence three types of power consumptions, namely peak power, average power and base power, were determined for later analysis of their relationship with mass transfer performance. Temperature control of the bioreactor heating plate was shut off during these measurements to eliminate disturbances on the power consumption measurements.

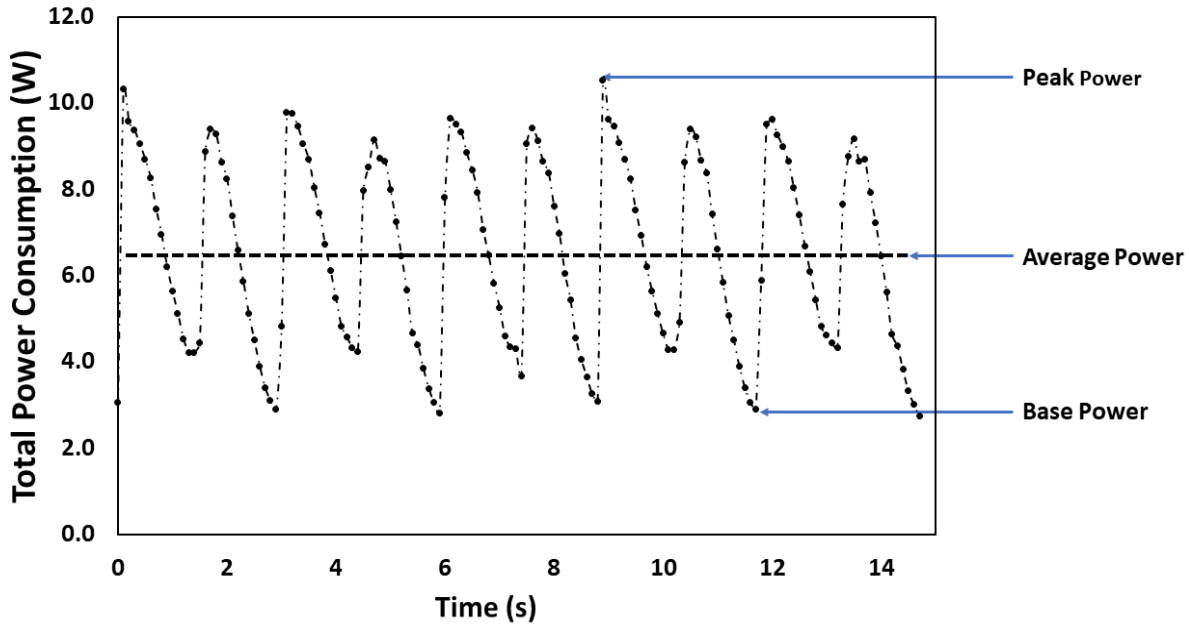

Figure 3-6 Definition of three types of power consumption measured in this work as illustrated for a 6 L liquid volume in a 20 L bag operating at 20 rpm and a 12º rocking angle

To account for the effects of mechanical friction and the weight of the stainless-steel tray rocking in combination with the bioreactor bag, a power consumption baseline was established with an empty bag loaded onto the rocking tray. The net power consumption was then calculated by subtracting the empty-bag baseline power from the directly measured power. This net power

consumption was used in the calculation of specific power input (W/m^3). Three replicates were performed for each power consumption condition.

3.5 Bioreactor Design Improvements

3.5.1 Baffle design and characterization

The baffle used in this study was a polypropylene rod 1.5875 cm in diameter (5/8 inches) and 27 cm in length. Depending on the bag volume, the total number of baffles installed might be either 1 or 2 which made the total length of the baffle either 27 or 54 cm.

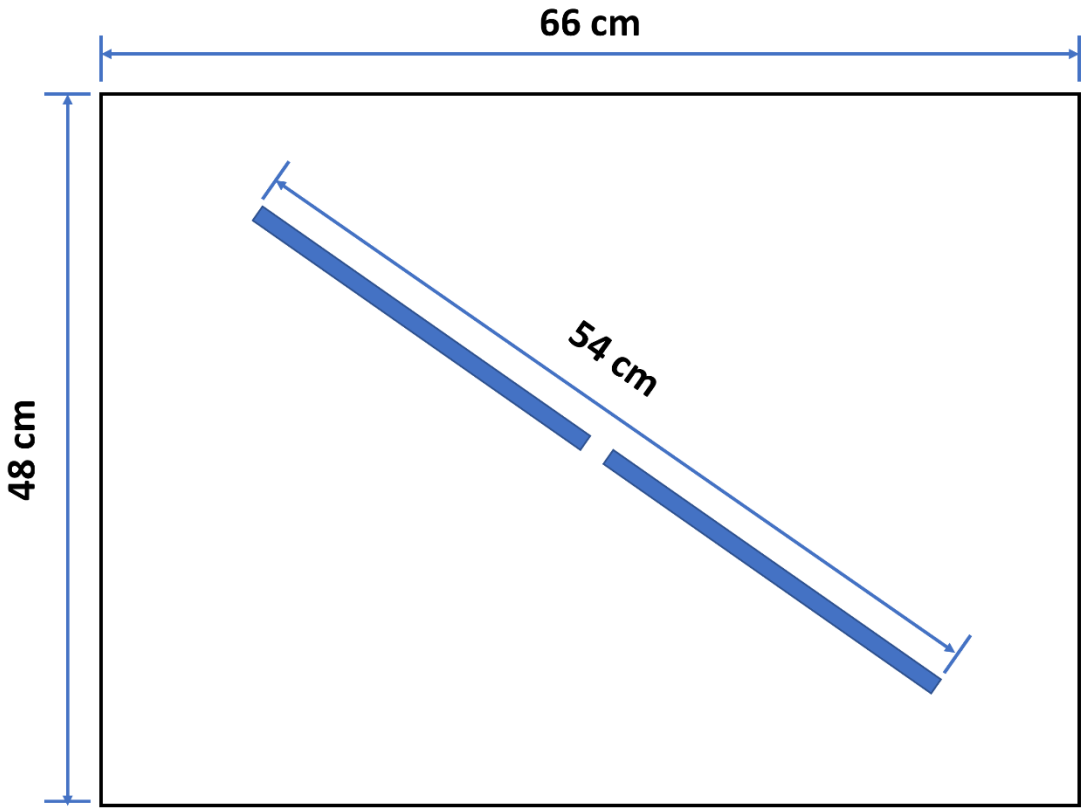

Figure 3-7 Baffle position at the rocking tray with 20 L bag volume which required two rod baffles to be aligned together.

Figure 3-7 illustrates the alignment of two baffles in between the rocking tray and bioreactor bag in a 35^{o} angle position. The baffle was fixed on top of the rocking tray by plastic glue and duck tape might be attached depending on the requirement of the baffle attachment on the rocking tray surface. For a 10 L bioreactor bag, 1 rod baffle was used taking only half of the rocking tray area. The angle of the baffle for a 10 L bioreactor bag was required to be adjusted to a 50^{o} angle position.

3.5.2 Sparger design and characterization

The sparger tested in this experiment was a customized hollow tubular material using ultra high molecular weight (UHMW) polyethylene and polyethylene co-polymers, supplied by GenPore (Reading, PA, USA). Three nominal pore diameters were employed, namely 5 µm (Model No.: BB2062-1814-5SP), 10 µm (Model No: BB2062-1814A) and 50 µm (Model No.: BB2062-1814B). The inner and outer diameters of all sparger tubes installed during experiments were 3.175 mm (1/8 inch) and 6.350 mm (1/4 inch), respectively. The sparger, as illustrated by Figure 3-8, was installed on one edge of the bag and was fixed at the bottom of the bag to ensure that it remained submerged during the rocking action.

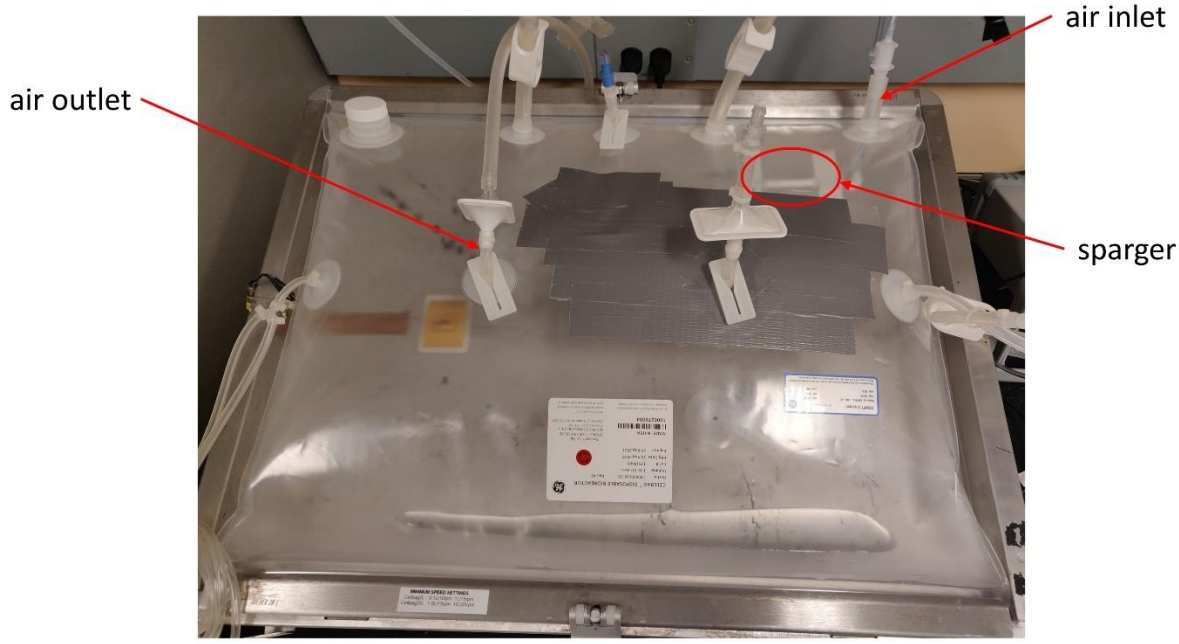

Figure 3-8 Sparger layout in a 20 L bag container loaded on a WAVE™ Bioreactor 20/50 EHT system.

The porosity of the sparger was characterized by both back scattered SEM and 3-D X-ray microscopy (Xradia 410 Versa, Carl Zeiss Microscopy GmbH, Baden-Württemberg, Germany). A sample of the scanning is provided in Figure 3-9. As illustrated, images acquired from both measurements were processed using the Porespy package in a Python 3 environment for porosity, mean pore diameter and pore size distribution. A detailed sample code of analysis was available in the appendix. Additionally, porosity was also calculated based on material density to verify the measurements from the Porespy program.

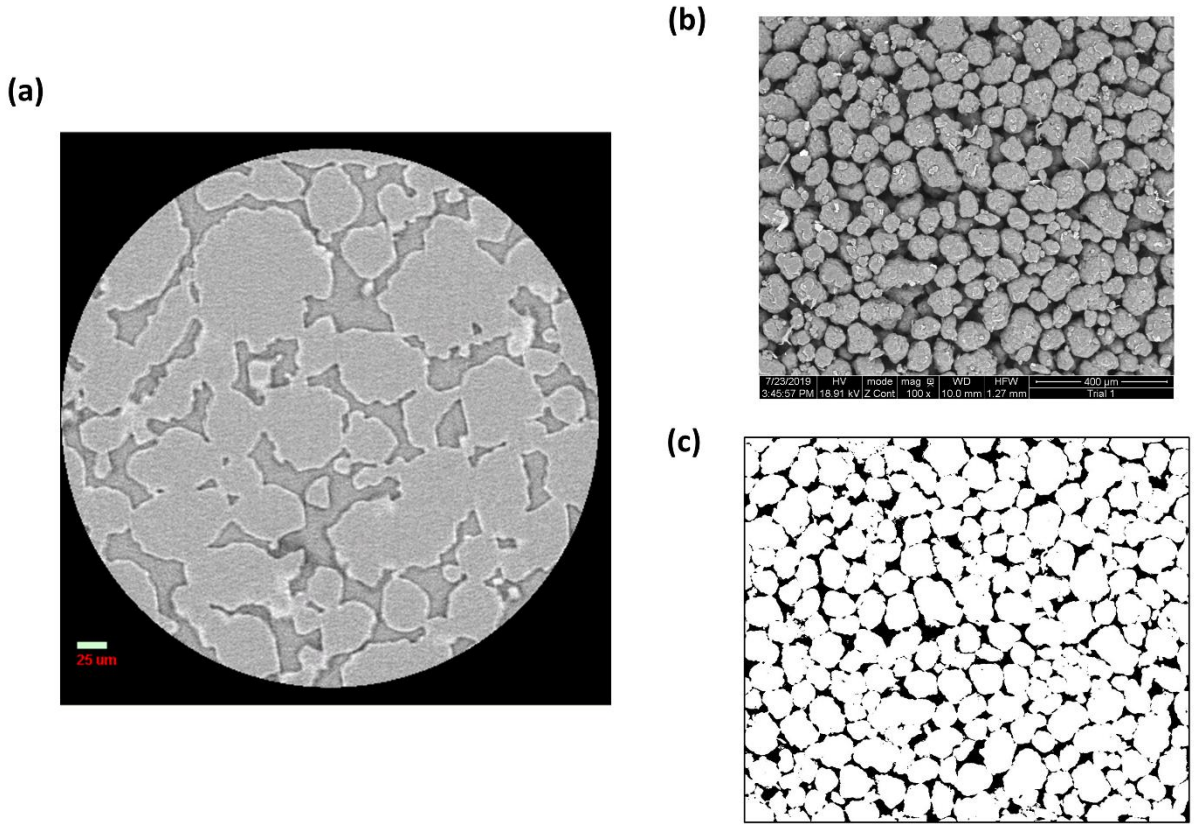

Figure 3-9 An example of (a) NanoCT X-ray Scanning (b) back scattered SEM scanning and (c) image J analysis threshold criteria on SEM image acquired

3.6 Bubble Profile Characterization

Measurement of bubble size and shape profile was achieved using slow-motion photography captured by a 20 megapixels F1.7 mobile phone camera (OnePlus6, OnePlus, China) at a frame rate of 480 fps. The images acquired were processed using ImageJ (National Institute of Health, Bethesda, USA) software to extract information including mean Sauter diameter, bubble size distribution and bubble circularity.

Chapter 4 Results and Discussion

4.1 Validation and Analysis of the Mechanistic Model for $k_L a$ Prediction

4.1.1 Mechanistic $k_L a$ model development

By observation of the operation, gas-liquid mass transfer in the rocking disposable bioreactor was hypothesized to occur by a combination of surface aeration as well as air entrainment in breaking waves, as illustrated in Figure 4-1. Models for both mechanisms of mass transfer were established separately and their contribution towards the total mass transfer performance was estimated by experimental observations shown in the later discussion section.

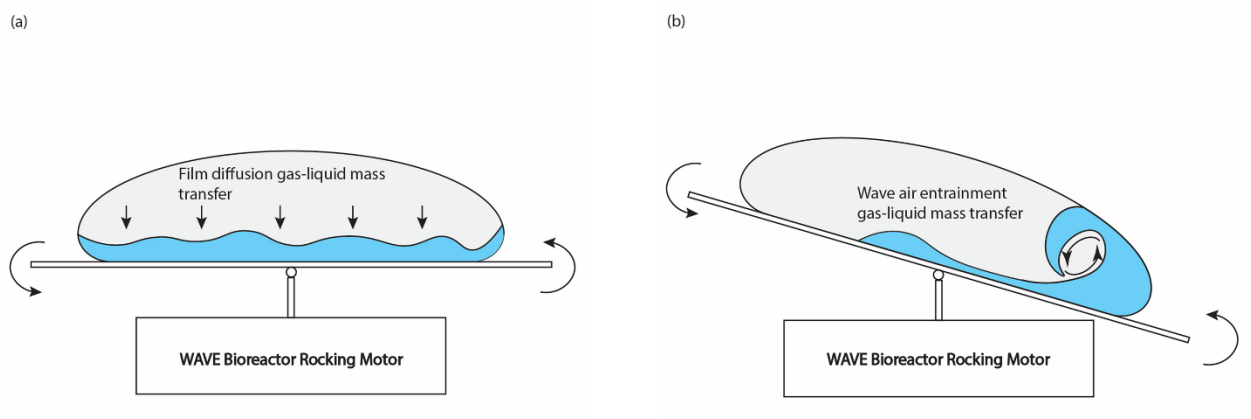

Figure 4-1 Two oxygen gas-liquid mass transfer mechanisms: (a) Film surface interface diffusion gas-liquid mass transfer (b) Wave air entrainment gas-liquid entrapment mass transfer.

4.1.2 Surface aeration mass transfer model

Before presenting the surface aeration mass transfer model, it is necessary to clarify the definition of Reynolds number in the rocking bioreactor. There are various definitions of Reynolds number that have been proposed in previous works (Eibl et al., 2010b; Marsh et al., 2017; Öncül et al.,

2010), as summarized in Table 4-1, where different characteristic length and velocities have been chosen.

Table 4-1 Summary of previous proposed definitions of Reynolds number in rocking disposable bioreactor

Reference	Re definition	Characterization Method	Bioreactor scale	Re range
Eibl et al., 2009	$Re = \frac{u \cdot k \cdot C}{v \cdot (2h + L)}$	Experimental	2 L to 200 L	300-2500
Öncül et al., 2010	$Re_{mean} = \frac{u_{mean} h_{mean}}{v}$	CFD	2 L and 20 L	0-8000
Marsh et al., 2017	$Re = \frac{\alpha N L^2}{4v}$	Experimental	2 L	1443-2424
Zhan et al., 2019	$Re = \frac{uL}{v}$	CFD	10 L	3000-20000

In the present work, it was observed that the fluid flow in the filled bag has similarities to open channel fluid flow and thus it is reasonable to take the hydraulic perimeter which is equivalent to the three wetted boundaries between the fluid and channel as the characteristic length in the definition of Reynolds number (Moog and Jirka, 1999). It was observed in our 10 L and 20 L bag that the change of liquid width is constrained by the bag geometry and is relatively small compared with the change of liquid depth. Therefore, we further reduce the hydraulic perimeter to the liquid height (h) in the definition of Reynolds number shown in Equation (4.1). This is similar to the definition proposed by Zhan et al. (2019), except that liquid height is used instead of bag length.

$$Re = \frac{u^* h}{v} \tag{4.1}$$

It was hypothesized that a portion of the oxygen mass transfer occurs at the top surface of the liquid where it is in contact with the gas headspace. Currently there are several types of models proposed that try to describe the gas-liquid interfacial mass transfer. The film model proposed by Whitman (Whitman, 1923) simplifies the gas-liquid interface into two thin layers of gas and liquid film with a boundary constantly in equilibrium. Such a model characterizes the mass transfer

coefficient k_L being directly proportional to diffusivity (D_L) which has been demonstrated to be unrealistic by experimental observations but is often employed for its simplicity. The penetration model proposed by Higbie (Higbie, 1935) has gained wide acceptance and application in describing gas-liquid mass transfer in dispersed flows, e.g. bubbly flows. The penetration model characterizes the k_L being not only proportional to ${D_L}^{0.5}$ but also dependent on exposure time (t_e) which can only be estimated rather than directly measured due to its transient nature. The surface renewal model, proposed by Danckwerts (Danckwerts, 1951), relates the k_L to both D_L and surface renewal rate (r). The surface renewal rate, although not directly measurable, could be estimated by either the large-eddy assumption (Fortescue and Pearson, 1967) or the small-eddy assumption (Lamont and Scott, 1970), which lead to the large-eddy surface renewal model and small-eddy surface renewal models, respectively. Another approach was the development of the surface divergence model and its integration with the surface renewal model (McCready et al., 1986). The surface divergence model replaces the surface renewal rate in the surface renewal model with a parameter named surface divergence strength (β). Recently Turney and Banerjee (Turney and Banerjee, 2013) tried to bring together both the surface renewal and surface divergence models into a uniform model which contains r as well as β. This requires experimental efforts to validate and accurately estimate both r and β, which is another challenging task.

Based on these considerations, in this work a small-eddy surface renewal model (Lamont and Scott, 1970) was adopted to describe the air-water surface aeration process in the rocking bioreactor, as described by Equation (4.2). This model is widely used to characterize the mass transfer on the surface of a turbulent liquid, which is similar to the situation observed in the rocking bag where the surface of the liquid is wavy and uneven due to liquid movement with each cycle back and forth.

$$k_L a = C_1 Sc^{-0.5} (\varepsilon v)^{0.25} \left(\frac{A}{V_L}\right) \tag{4.2}$$

The parameter C_1 in Equation (4.2) was estimated to be 0.161 by Moog and Jirka (Moog and Jirka, 1999) using non-linear regression in their work with channel flow. The surface area A in Equation (2) can be calculated from the directly measured liquid width and length at stationary state, and the total liquid volume V_L is measured and controlled during experiments. Meanwhile ε in Equation (4.2), which according to Moog and Jirka is the near-surface turbulent energy dissipation

rate for a smooth channel condition, can be estimated using Equation (4.3) taken from Nakagawa et al. (Nakagawa et al., 1975):

$$\varepsilon = \frac{u^{*3}}{h} \tag{4.3}$$

where u^* in Equation (4.3) represents the shear velocity (also described as the friction velocity). In the present work, this was evaluated using the characteristic horizontal liquid velocity in the logarithmic law of the wall as described by Equation (4.4) (Nezu and Rodi, 1986) with the von Kármán constant κ taken as 0.40 and the roughness length z_0 taken as 10 μm (Larena and Pinto, 1991) taking wear and tear of the film into account for the low-density polyethylene film used for the bioreactor bag:

$$\frac{c}{u^*} = \frac{1}{\kappa} ln\left(\frac{z}{z_0}\right) \tag{4.4}$$

The Schmidt number (Sc) is calculated by its definition $Sc = \frac{\nu}{D}$. As in this work both ν and D_L are constant in the air-water system at constant temperature (around 20ºC), the Schmidt number thus has a constant value of 428.12.

4.1.3 Wave turbulence mass transfer model

By observation, it was hypothesized that a portion of the mass transfer would be related to the breaking of the wave created by each rocking motion cycle, and the air that is entrained by this wave. Therefore, a $k_L a$ prediction model for turbulent mass transfer induced by wave motion was established by modelling the mass transfer coefficient and specific area separately, as follows.

There are three commonly cited theoretical models describing the gas-liquid interfacial mass transfer mechanism: the two-film theory (Whitman, 1923), the penetration theory (Higbie, 1935) and the surface renewal theory (Danckwerts, 1951). For this work, Higbie's penetration theory (Equation 4) was adopted for modelling the mass transfer coefficient (k_L) as it can capture the time-varying nature of the wave moving in the rocking vessel in a more direct manner compared with the two-film or surface renewal theories.

$$k_L = 2\sqrt{\frac{D}{\pi \cdot t_e}} \tag{4.5}$$

As is shown in Equation (4.5), D_L is the diffusivity of the liquid phase which is treated as a constant value at the maintained temperature. Exposure time (t_e) can be estimated by applying Kolmogorov's isotropic turbulence theory. Assuming a Newtonian fluid, such as the de-ionized water used in this work, Equation (4.6) was derived using the isotropic turbulence theory:

$$t_e = \frac{\eta}{u} = \frac{\left(\frac{v^3}{\varepsilon}\right)^{\frac{1}{4}}}{(v \cdot \varepsilon)^{\frac{1}{4}}} = \left(\frac{v}{\varepsilon}\right)^{\frac{1}{2}} \tag{4.6}$$

In Equation (4.6), v is the fluid kinematic viscosity and ε is the rate of dissipation of energy per unit mass.

Specific area can be derived by assuming that rigid spherical bubbles with uniform diameter are entrained into the breaking wave, as given in Equation (4.7):

$$a = \frac{total\ interfacial\ area\ of\ bubbles}{total\ volume\ of\ liquid} = 6\frac{\emptyset}{d_b} \tag{4.7}$$

where ∅ is the gas hold-up or void fraction, d_b is the average bubble diameter.

Instead of using gas hold-up models from existing aerated stirred tank or bubble column bioreactors, ∅ is expressed as the total volume of air entrained by breaking waves divided by the total volume of liquid. The total volume of air entrained can be described by the air entrainment model proposed by Deike et al. (Deike et al., 2016) in their work analyzing air entrainment by breaking waves for ocean-atmosphere interfaces. The model from Deike et al. is summarized in Equation (4.8).

$$\bar{V} = B\frac{\epsilon_l L_c}{\rho W g} \tag{4.8}$$

where B is a dimensionless constant which describes the proportionality between the work done against buoyancy forces in bubble entrainment and the mechanical energy dissipated, ϵ_l is the wave turbulence dissipation rate per length of wave crest, L_c is the crest length, and W is the weighted bubble rise velocity. According to Deike et al., the parameter ϵ_l in Equation (4.8) can be characterized using $\epsilon_l = b\rho c^5/g$ (Duncan, 1981; Phillips, 1985) where c is the linear phase speed of the breaking wave and b is an estimated breaking strength parameter. Additionally b can be

estimated by $b = 0.4(S - 0.08)^{2.5}$ (Romero et al., 2012), where S is a measure of the wave slope at breaking, and the wave geometrical definitions are illustrated in Figure 4-2.

By combining the models for k_L and a, the $k_L a$ model was derived as given in Equation (4.9):

$$k_L a = 12 \frac{D_L^{0.5} B(\epsilon_l L_c)(\frac{\epsilon_l L_c}{m})^{0.25}}{\pi^{0.5}(v)^{0.25} V_L \overline{d_b} W g \rho} \tag{4.9}$$

A scaling analysis confirms the dimensional validity of equation (4.9):

$$unit\ (k_L a) = \frac{\left(\frac{L^2}{T}\right)^{\frac{1}{2}} (\frac{ML^2}{T^3})}{\left(\frac{\frac{L^2}{T}}{\frac{L^2}{T^3}}\right)^{\frac{1}{4}} L^3 L (\frac{L}{T})(\frac{M}{L^3})(\frac{L}{T^2})} = \frac{\frac{LML^2}{T^{\frac{7}{2}}}}{T^{\frac{1}{2}} \frac{ML^3}{T^3}} = \frac{LML^2T^3}{T^4 L^3 M} = T^{-1} \tag{4.10}$$

Substituting $\epsilon_l = b\rho c^5/g$ and $b = 0.4(S - 0.08)^{2.5}$, after rearrangement Equation (4.9) can then be expressed as follows in Equation (4.11):

$$k_L a = (\frac{12}{\pi^{0.5}}) \cdot \frac{D_L^{0.5} B[0.4(S - 0.08)^{2.5} c^5 L_c]^{1.25} \rho_{wave}^{0.25}}{(v)^{0.25} m_{wave}^{0.25} V_L \overline{d_b} W g^{2.25}} \tag{4.11}$$

Some parameters are constant for the experiments performed in this work, namely:
$\rho = 1000\ kgm^{-3}$; $D_L = 2.31 \times 10^{-9}\ m^2 s^{-1}$; $g = 9.81\ ms^{-2}$; $v = 0.8927 \times 10^{-6}\ m^2 s^{-1}$;
Now the remaining problem is the measurement or estimation of some of the other parameters in Equation (4.11). First, L_c is the length of the breaking crest which in this work can be directly measured through the transparent film of the rocking bioreactor culture bag. The linear phase velocity is given by $c = (\frac{L/\cos\alpha}{2/N})$ which is derived based on the length between wave crests from both ends divided by the time required for the liquid to move between crests. Despite a difference from the traditional definition of linear phase speed in ocean waves, this definition captures the physical meaning under the bioreactor operating conditions where there is not a series of continuously moving waves. The parameter *B* is a dimensionless bubble plume constant. In the Deike et al. model, $B \approx 0.1 \pm 0.05$ based on comparisons with existing experimental data. The

parameter W is the weighted bubble rise velocity which, according to Deike et al., is a value with an order of approximately 10 cm·s^{-1} and this value is assumed in this work as a constant.

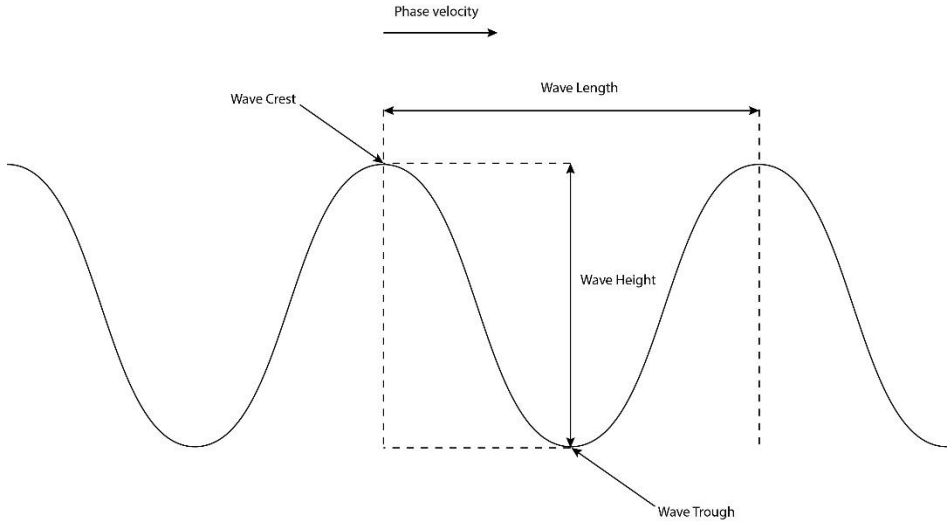

Figure 4-2 Illustration of wave parameters including wavelength and waveheight. Wave slope is the ratio of wavelength/waveheight. Linear phase velocity is the speed of the wave between either crests or troughs.

It is assumed that the mass transfer contributions from the two components, i.e. surface aeration and wave breaking, are independent. Therefore, the overall $k_L a$ can be acquired by combining the $k_L a$ values calculated from both models, resulting in the expression shown in Equation (4.12):

$$k_L a = Sc^{-0.5} \cdot \left(\frac{\varepsilon}{v}\right)^{0.25} \cdot \left(\frac{A}{V_L}\right) + \left(\frac{12}{\pi^{0.5}}\right) \cdot \frac{D_L^{0.5} B[0.4(S-0.08)^{2.5} c^5 L_c]^{1.25} \rho_{wave}^{0.25}}{(v)^{0.25} m_{wave}^{0.25} V_L \overline{d_b} W g^{2.25}} \qquad (4.12)$$

The model given by Equation (4.12) can then be experimentally tested under a variety of rocking bioreactor operating conditions to assess its capabilities for fitting the data and predicting performance.

4.1.4 Experimental $k_L a$ values: summary

The experimental $k_L a$ data is summarized in Table 4-1. These $k_L a$ values gathered under varied rocking speeds and angles have a good agreement with results reported by some others using similar equipment (Jones et al., 2017; Westbrook et al., 2014). However, $k_L a$ values measured in our experiments are much higher compared with some previously reported results (Mikola et al.,

2007; Pilarek et al., 2018) by a factor of approximately 20% to 100%. By comparing experimental conditions and methods, such differences could be attributed to two factors: 1) the gas flow rate is much higher in this work, 0.4 vvm, compared with 0.01 to 0.1 vvm reported in other works, and 2) a head space gas exchange lasting 5 min was used in this work to ensure the complete removal of residual nitrogen in the headspace as well as to establish an inflated and rigid structure of the bag to facilitate proper wave generation. Despite the differences in the exact $k_L a$ value, the effect of rocking angle and rocking frequency on $k_L a$ observed in our experiment was consistent with previous results reported by others.

Table 4-2 Summary of experimental data of $k_L a$ acquired under varied conditions in 10 L (with 3 L and 5 L working volumes) and 20 L (with 6 L, 8 L and 10 L working volumes) CellBag® of a WAVE™ Bioreactor 20/50 EHT system

Working volume (L)	3 L	5 L	6 L	8 L	10 L
Rocking angle (°)	8°				
Rocking speed (rpm)	Volumetric oxygen transfer coefficient $k_L a$ (h^{-1}), mean±std				
10	7.35±0.33	1.65±0.04	7.18±0.95	4.19±0.43	1.62±0.09
20	24.12±0.15	8.32±0.48	24.31±1.01	16.61±0.52	11.25±1.00
30	51.31±1.39	24.81±1.12	56.06±0.99	39.34±0.55	33.11±0.50
40	84.60±2.36	N/A	109.55±2.40	87.80±3.37	64.89±2.45
Rocking angle (°)	12°				
Rocking speed (rpm)	Volumetric oxygen transfer coefficient $k_L a$ (h^{-1}), mean±std				
10	7.33±0.23	2.21±0.09	9.82±0.43	5.64±0.23	3.76±0.25
20	26.10±1.45	11.68±0.39	31.68±1.43	23.04±0.28	16.02±0.59
30	64.58±4.02	31.38±0.94	82.95±1.67	59.52±0.47	41.45±1.12
40	107.30±5.07	N/A	142.52±2.84	116.66±5.73	91.08±5.55

The calculated Reynolds number, based on the definition presented in Equation (4.1), ranges from a low of 4114 at 3 L, 8° rocking angle and 10 rpm rocking speed to a high value of 26249 at 10 L, 12° rocking angle and 40 rpm. This range is higher than in previously reported works due to the

different definition used in this work, as well as a wider range of employed experimental conditions (Eibl et al., 2010b; Marsh et al., 2017; Öncül et al., 2010). However, from visual observations during the experiments and the nature of wave movement, it is reasonable to characterize the flow patterns in the wave bioreactor into different categories. Laminar flow is more likely to happen at low rocking speed and low liquid level conditions. As the rocking speed and filling level increase, the flow patterns tend to switch into a type of transitional flow or even turbulent flow which, at intensive rocking conditions i.e. 40 rpm, was frequently observed under various liquid levels.

Others (Marsh et al., 2017) also suggested such transitions from their research which was observed based on the turbulent kinetic energy acquired between 33.5 rpm and 42 rpm. It was observed in our experiments that at 10 rpm, the liquid flow pattern presented in the bag was dominantly laminar-like flow despite the rocking angle, with the highest Reynolds number reaching 6600 with a liquid depth of 0.024 m and a maximum liquid velocity of 0.22 m/s. As the rocking frequency increased to 20 rpm and rocking angle increased, the liquid flow showed deviations from a laminar flow pattern and a wave vortex was observed at the edge of the bag. The liquid in the bag exhibited a mix of laminar flow in the middle and weak transitional to turbulent flow at both edges. After the rocking frequency was further elevated to 40 rpm, the laminar-type flow was no longer observed even in the middle region of the bag and the liquid showed a vigorous turbulent behavior, for which the Reynolds number was calculated to be 13600 at a minimum. It is worth noting that as recently reported, the Reynolds number can oscillate over a broad range in a single rocking cycle (Zhan et al., 2019). This indicates that there could exist two patterns of flow during a single rocking motion, which distinguishes the wave bioreactor significantly from other types of bioreactors when it comes to engineering characterizations. Such observations also support the argument to consider two mechanisms of gas-liquid mass transfer, i.e. surface diffusional as well as turbulent wave air entrainment, into consideration when developing the model for gas-liquid mass transfer in the wave bioreactor.

4.1.5 Model sensitivity test

While examining the developed wave mass transfer model shown in Equation (4.11), it was noted that two variables, wave slope (S) and linear wave phase velocity (c), may have a major influence on $k_L a$ values due to their exponents of 2.5 and 5, respectively. As illustrated in Figure 3, it is

observed that $k_L a$ increases in a steep trend after slope and phase velocity both reach certain threshold values, thus indicating a synergistic effect from both parameters. It is widely accepted that the wave breaking motion can be characterized by different types namely spilling, plunging, collapsing and surging breakers. According to Deike et al., the slope for a spilling breaker falls between 0.35 and 0.42, while for a plunging breaker, the slope is ≥ 0.42 (Deike et al., 2016). In addition, Duncan mentioned that the average inclination of a non-breaking wave could reach approximately 18^o, corresponding to a wave slope of 0.3, which suggested that waves are more likely to break when they reach a steep enough slope (Duncan, 1981). Linear phase velocity characterizes the momentum a wave carries towards its moving direction. As in our model, the phase velocity is related to the length of the bag, rocking angle and rocking speed. Increased rocking angle and frequency transports more energy into the liquid through more intensive agitation. At lower rocking intensity, due to insufficient velocity, liquid moving towards the edge of the bag was reflected towards the opposite direction rather than moving upwards along the edge of the bag to fully develop into a breaking wave. Such barriers for the wave formation and breaking based on the slope and phase velocity could explain the observed threshold for $k_L a$ seen in Figure 4-3.

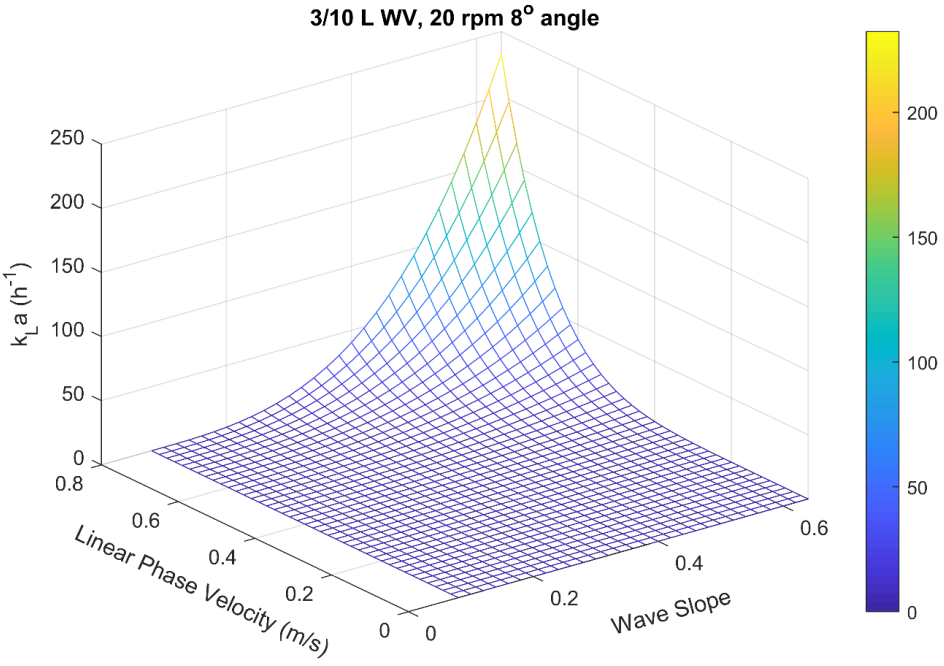

Figure 4-3 Sensitivity test on the influence of wave slope and linear phase velocity on $k_L a$ at 3 L working volume, 20 rpm and 8° angle condition.

4.1.6 Model predictions compared to experimental values

The derived model given in Equation (4.12) was applied for each experimental condition using the appropriate operating and geometrical parameters. As demonstrated in Figure 4-4, predicted values of $k_L a$ generally matched with the experimental measurements over a wide range with an estimated slope of 1.006 (95% confidence interval ranging between 0.982 and 1.119). By examining each working volume in detail, it was observed that relatively large deviations existed at 3 L and 6 L working volumes, but as working volume increased to nearly 50% of total bag volume, such deviations narrowed significantly. Additionally, $k_L a$ values acquired from experiments at 30 rpm rocking frequencies exhibited relatively more difference from theoretical predictions than any of the other three conditions. While the predicted phase velocities of wave motion are about 10 to 20% higher than the liquid velocity reported by Marsh et al. (Marsh et al., 2017), it is possible that the slope estimated from the work of Deike et al. (Deike et al., 2016) might not accurately represent the wave slope generated in the bag vessel. The maximum slope Deike et al. used in the model was 0.65, which might underestimate the real slope of the wave generated in the bag. An examination of the work of Marsh et al. showed a slope of the liquid at

42 rpm could reach as high as 0.8 under 1 L working volume. However, due to differences between their experimental conditions and ours as well as insufficient information, it is difficult to provide a thorough estimation of slope of wave for all conditions run in our experiments. Such differences in slope could be attributed to the differences in the wave generation mechanism. The wave generated in the bag was a reflective wave motion bouncing from the restricted boundary of the bag, which is not exactly the same as the wave studied in either deep ocean or shallow water regions where the wave moves with a free surface and only gravity or the bed of the surf zone contributes to the alteration of wave structure and movement.

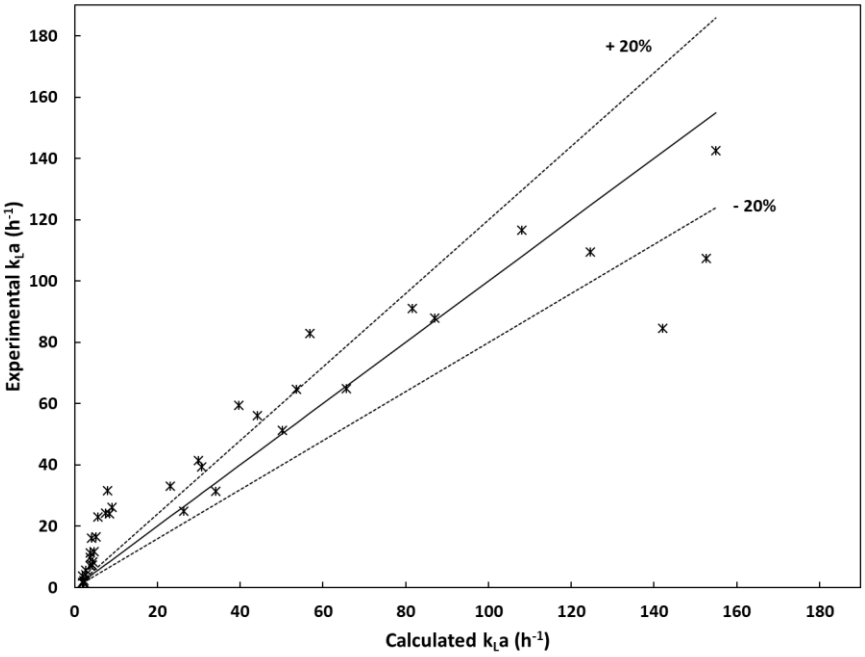

Figure 4-4 Experimental k_La vs model based calculated k_La with crossed data points indicating experimental k_La values from Table 4-2, solid line representing slope of 1 and dotted lines representing 90% of prediction interval.

It was also noticed from Figure 4-4 that the model developed in our work tended to underestimate the k_La value at most 20 rpm conditions (some lower values of k_La) and overestimate the k_La at some 40 rpm conditions (some higher values of k_La). This issue might indicate that while the model is capable of reflecting the gas-liquid mass transfer at fully laminar and turbulent conditions, it could not accurately capture some of the transitional states developed in the bioreactor. The model may be insufficient for characterizing the out-of-phase movement which, hypothesized by

Marsh et al. (Marsh et al., 2017), was observed at a very high rocking intensity of 40 rpm. According to Marsh et al., when moving out of phase, the liquid body in the bag tends to flow faster than the rocking speed of the bioreactor platform. Such a phenomenon might explain the enhancement in the experimental values compared with the model estimation and thus requires further consideration of the model in future work.

Based on the calculation using Equation (4.7), the average air void fraction induced by each wave is small with a maximum value of 1.7%. Although experimental studies on breaking waves usually showed a much larger value of void fraction, it should be noted that their void fraction calculation frame is focused only on the localized wave structure instead of the whole body of fluid. As was shown by various studies (Blenkinsopp and Chaplin, 2007; Lamarre and Melville, 1991), the void fraction of the breaking wave is a heavily time and space dependent value. While the void fraction of the top layer of the liquid after wave breaking could reach almost 100%, it rapidly drops to almost zero within a small depth. In these experiments it was observed that within seconds of the wave breaking, the void fraction created by air entrainment and wave break down was dissipated and the bubbles rose back to the liquid surface. Hence only a small void fraction can be maintained by each rocking movement. As the rocking speed increases, it is expected that the void fraction per second would increase accordingly in a linear trend. During low rocking intensity the rapid disappearance of such void fraction was observed, and thus a lesser oxygen transfer by the wave mechanism is expected.

4.1.7 Relative effects of surface and wave aeration contributions in the overall $k_L a$

Since the proposed combined model predicts the overall mass transfer relatively well across the full range of rocking bioreactor operating conditions, it is useful to consider the amount each mechanism of gas-liquid mass transfer contributes to the total observed $k_L a$ value. Predicted results from five working volumes were summarized in Figure 4-5. As the figure shows, the contribution from air entrainment by wave breaking is negligible at all five working volumes when the rocking intensity is weak and surface aeration plays a dominant role instead. Nevertheless, as the rocking intensified, the $k_L a$ contribution from air entrainment became increasingly significant. Figure 4-5 (i) and (j) showed that at 30 rpm rocking frequency, air entrainment could contribute

around 80% of the total gas-liquid mass transfer capacity in the wave bioreactor. At 10 L liquid volume condition, the contribution of breaking-wave aeration further increased to 90% at the highest rocking frequency of 40 rpm. Similar trends were observed in all working volumes, indicating that the increase in oxygen transfer by wave breaking is significant mainly at the 30 rpm and 40 rpm rocking conditions while most of gas-liquid mass transfer capacity at low rocking intensity was realized by surface aeration.

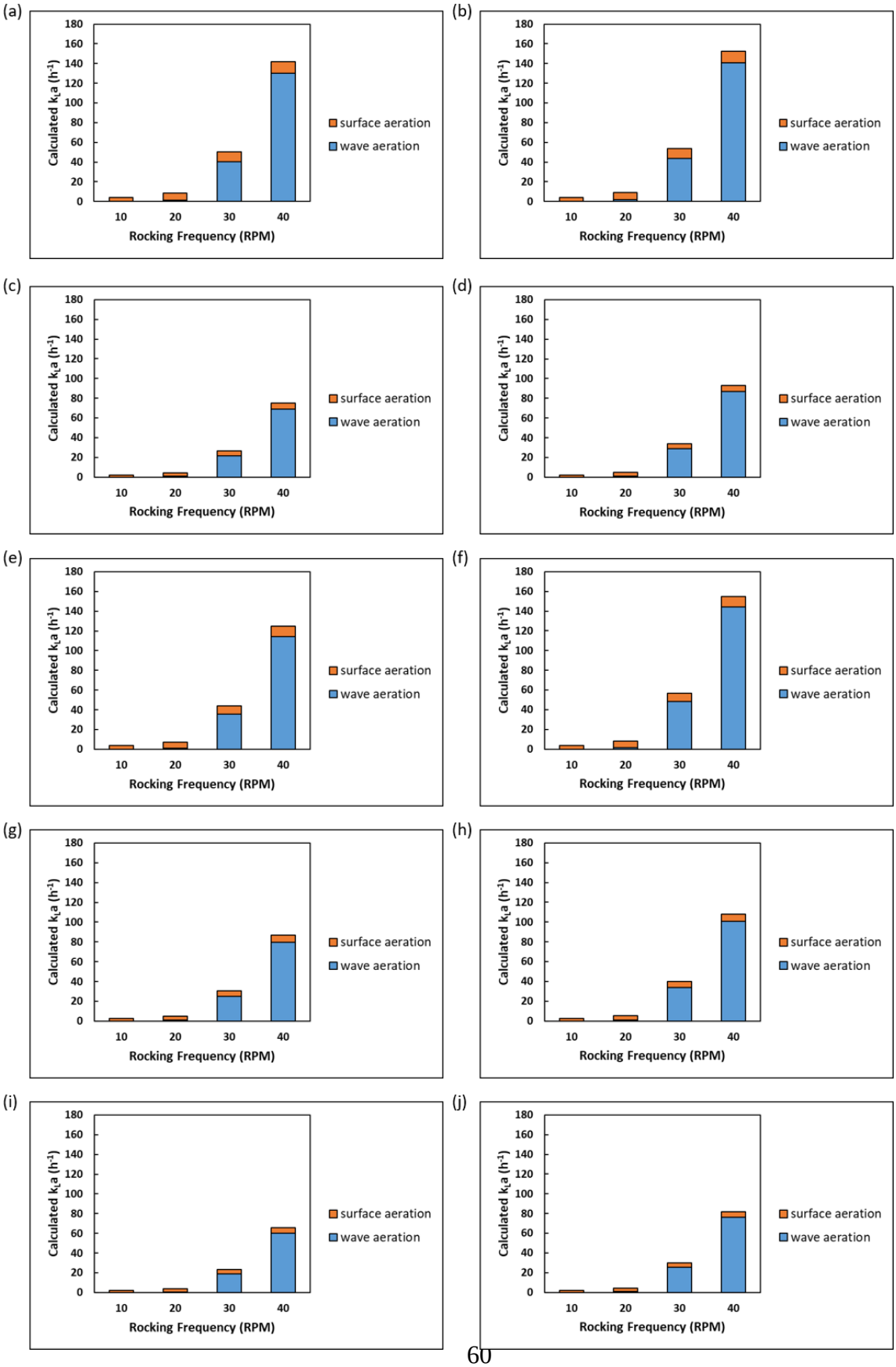
(a)
(b)
(c)
(d)
(e)
(f)
(g)
(h)
(i)
(j)
Calculated k_La (h^{-1})
0
20
40
60
80
100
120
140
160
180
10
20
30
40
Rocking Frequency (RPM)
surface aeration
wave aeration

Figure 4-5 Examination of the contributions of surface aeration and wave aeration in the total calculated $k_L a$ based on the developed model using equation (12). Fig (a), (c), (e), (g), (i) showed the predicted 8º rocking angle $k_L a$ at 3 L, 5 L, 6 L, 8 L and 10 L respectively. Fig (b), (d), (f), (h), (j) showed the predicted 12º rocking angle $k_L a$ at 3 L, 5 L, 6 L, 8 L and 10 L respectively.

It is important to note that previous research had usually assumed that the rocking bioreactor achieved its oxygen transfer primarily by the bubble-free surface aeration mechanism, and concludes that this is insufficient for microbial cultivation due to its higher oxygen transfer requirements versus animal cells (Singh, 1999). Nevertheless, it is clear in this analysis that most of the oxygen transfer improvement induced by higher rocking intensity is realized by a different air entrainment process induced by the breaking wave. This indicates that a higher oxygen transfer capacity can be achieved if the rocking intensity and the wave-breaking contribution can be further increased through operating or design changes.

4.2 Characterization of Power Input and its Impact on Mass Transfer in a Rocking Disposable Bioreactor

4.2.1 Power input analysis

It has been demonstrated in previous work that oxygen transfer from the bioreactor headspace to the liquid occurs through two mechanisms, namely surface aeration and air entrainment by the breaking wave (Bai et al., 2019). The breaking-wave mechanism can provide the majority of the oxygen transfer capacity of the bioreactor when the rocking "intensity" (i.e. the combination of rocking frequency and angle) is high enough to generate a significant wave. Characterizing the mass transfer in terms of power input provides an alternative way to examine and quantify this wave-breaking phenomenon and its effect. Therefore, the specific power input (P/V) was first measured as a function of operating conditions, including liquid volume, rocking frequency and angle. As defined in the Figure 3-6, there are three ways to characterize specific power input, namely base, average, and peak P/V.

As illustrated by the results in Figure 4-6, the peak, average and base power inputs exhibited slightly different trends as rocking intensity varied. It was noted from Figure 4-6 (a) to (e) that base power inputs for both 8^o and 12^o between 10 rpm and 30 rpm for all liquid volumes were negative. This phenomenon can be attributed to the effect of gravity forces generated during the liquid rocking movements. As the main liquid volume tilted across the centerline of the bag, the action of gravity on the liquid would facilitate its movement towards the edge of the bag. Hence the power required to drive the liquid from the centerline to the edge of the bag would be even lower than that required to drive an empty bag on the rocking tray. The momentum of the liquid at the edge of the bag where the wave generation occurred thus came from the combination of mechanical power delivered by the rocking motor as well as the gravity force on the liquid. As the rocking frequency was elevated, it was seen that the base power inputs increased to positive values for almost all the 40 rpm rocking conditions. At this higher frequency rocking, the action of gravity alone is insufficient and additional power input is still required to move the liquid volume at the higher rate, compared to the power required to move an empty bag.

The peak P/V tended to increase from the 10 to 30 rpm conditions but flatten out at higher rocking rates, especially for the 8° angle, as seen in Figure 4-6 (a) to (e). This trend, in combination with the increase of base P/V value at the 40 rpm condition, is likely evidence of the so called 'out-of-

phase' movement of the liquid reported by Büchs et al. (Büchs et al., 2001) observed in orbitally-shaken disposable bioreactors, but also confirmed by Marsh et al. (Marsh et al., 2017) for rocking disposable bioreactors. According to Büchs et al., in an out-of-phase condition, the liquid movement would lag behind the oscillatory rocking of the platform. This could lead to the rocking platform and liquid moving in opposite directions at certain points, which would alter the way the mechanical power was delivered into the liquid. The general trend of peak power input in these experiments is in agreement with previous observations reported by Eibl et al. (Eibl et al., 2010b), where the specific power input would increase in a linear manner up to 20 rpm and then level out as the rocking frequency further increased.

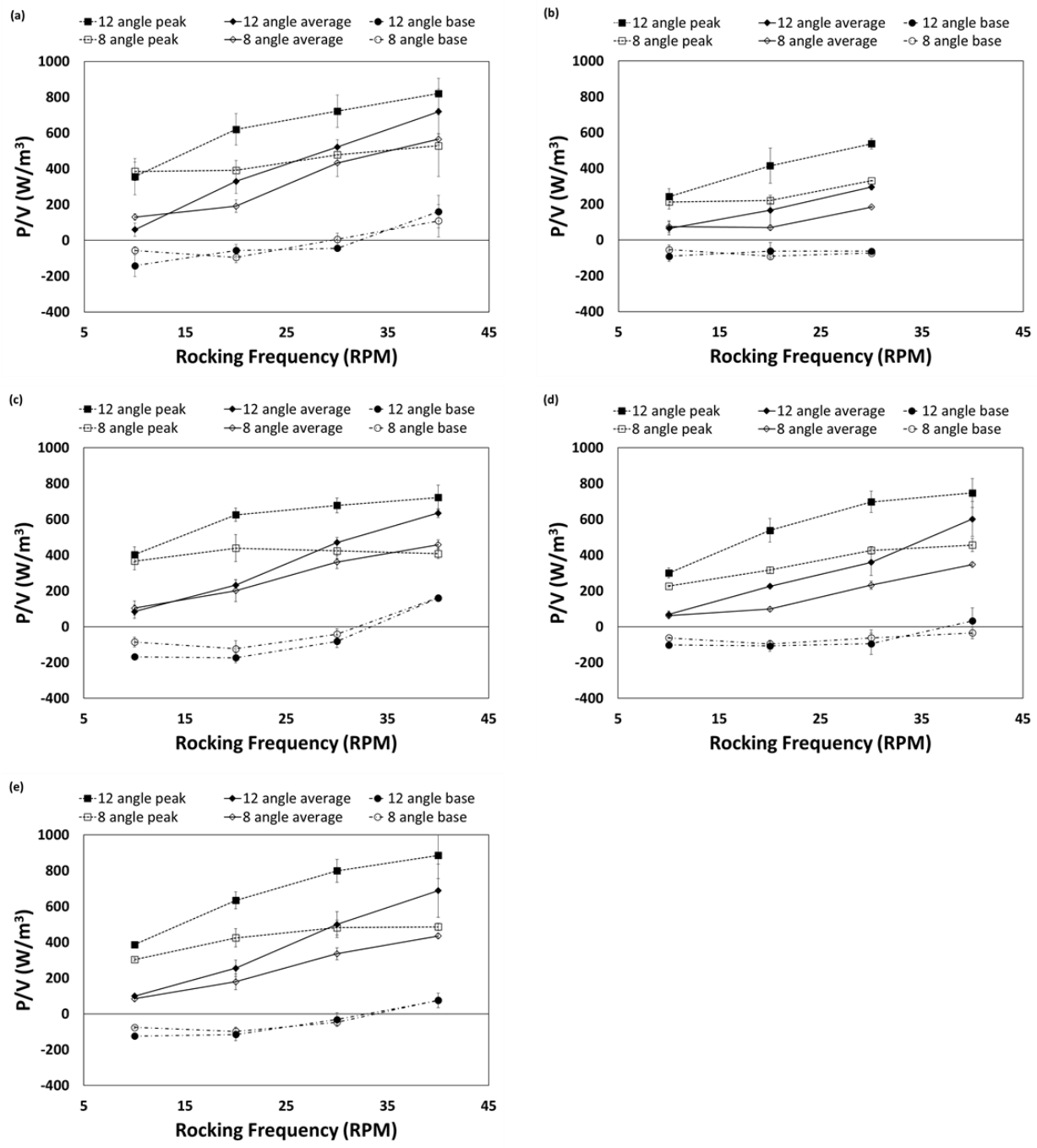

Figure 4-6 Net peak, average and base power input at different rocking frequencies and angles for (a) 3 L liquid in a 10 L bag, (b) 5 L liquid in a 10 L bag, (c) 6 L liquid in a 20 L bag, (d) 8 L liquid in a 20 L bag, (e) 10 L liquid in a 20 L bag.

The average power input shown in Figure 4-6, as might be expected, appeared to be a combination of base and peak power input trends. The average power across all conditions was summarized and is compared in Figure 4-7. The results of the 5 L liquid volume at 40 rpm with either 8^o or 12^o rocking angles are excluded because it was noticed during the experiments that a high rocking frequency at an 8^o angle would induce irregular wave motion and splashing of liquid in the bioreactor. This resulted in the flooding of the air venting filter positioned on the top of bag, causing the filter to be blocked and an elevated air pressure within the bag. Hence the experiments at these specific two conditions could not be performed.

From statistical t-tests it was determined that the influence of different liquid volumes within the same bag scale was not significant (p value >0.05) for nearly all experimental conditions with the only exceptions being 3 and 5 L (in 10 L bag) at 20 and 40 rpm rocking frequencies. Nevertheless, the effect of different rocking angles and rocking frequencies on power input was distinguishable between the experimental conditions, except for the 10 rpm conditions where the impact on power input from different rocking angles was not significant according to t-tests. This indicates that the electrical method used in this work was sufficiently sensitive to distinguish between power inputs in a benchtop scale wave bioreactor from medium to high rocking intensity conditions, which are of most practical interest.

Compared with other power consumption measurement methods in bioreactors, such as calorimetric and torque methods, the electrical method can be more capable of characterizing power consumption in medium to large scale bioreactors (Ascanio et al., 2004). These results suggest that the electrical method can be readily scaled down and applied to benchtop wave bioreactors. This may be helpful for unifying the power input measurement methods and to help reduce the errors potentially introduced by different types of methods used for different scales of rocking bioreactor.

Table 4-3 Comparison of power input measurement from previous works on rocking disposable bioreactors

Liquid volume (L)	Rocking frequency/angle rpm/degree^o	P/V (W/m^3)	Reference
2	10-40/2-10^o	64-633	(Jones et al., 2017)
0.2-1	6-30/7-10^o	8-561	(Eibl et al., 2010b; Eibl and Eibl, 2008)
3-10	10-40/8 or 12^o	59.82-719.68	This study

A summary of the P/V measurements from previous works is shown in Table 4-3. The measured net average power input data in this work can be compared with previously reported average experimental power inputs from Jones et al. (Jones et al., 2017) who used a calorimetry method. The average power input at 30 rpm and 8^o rocking angle with 2 L liquid in a 10 L bag from Jones's work was approximately 300 W/m^3 while the power input ranged from 169.9 to 469.1 W/m^3 at 30 rpm with rocking angles changing from 2^o to 10^o. In this study, the power input acquired at a similar condition with 3 L DI water loaded in a 10 L bag rocking at 30 rpm with 8^o and 12^o rocking angles was 433.2±76.5 and 521.2±41.2 W/m^3 respectively. Eibl et al. (Eibl et al., 2010b) reported a power input estimation using a CFD technique by modeling the change of the bag's centre of gravity and the surface area of the fluid. In that study, the power input at a 50% filling level (1 L liquid in a 2 L bag) changed from 8 to 50 W/m^3 based on the 7^o rocking angle and a rocking frequency ranging from 9 to 30 rpm. This is slightly lower than our experimental measurements under same 50% fractional filling (5 L liquid in a 10 L bag). However, some of the conclusions drawn from Eibl's computational work were validated in these results, including the trend of decreasing power input with elevated liquid volumes and the proportionality between rocking frequency and power input up to 20 rpm.

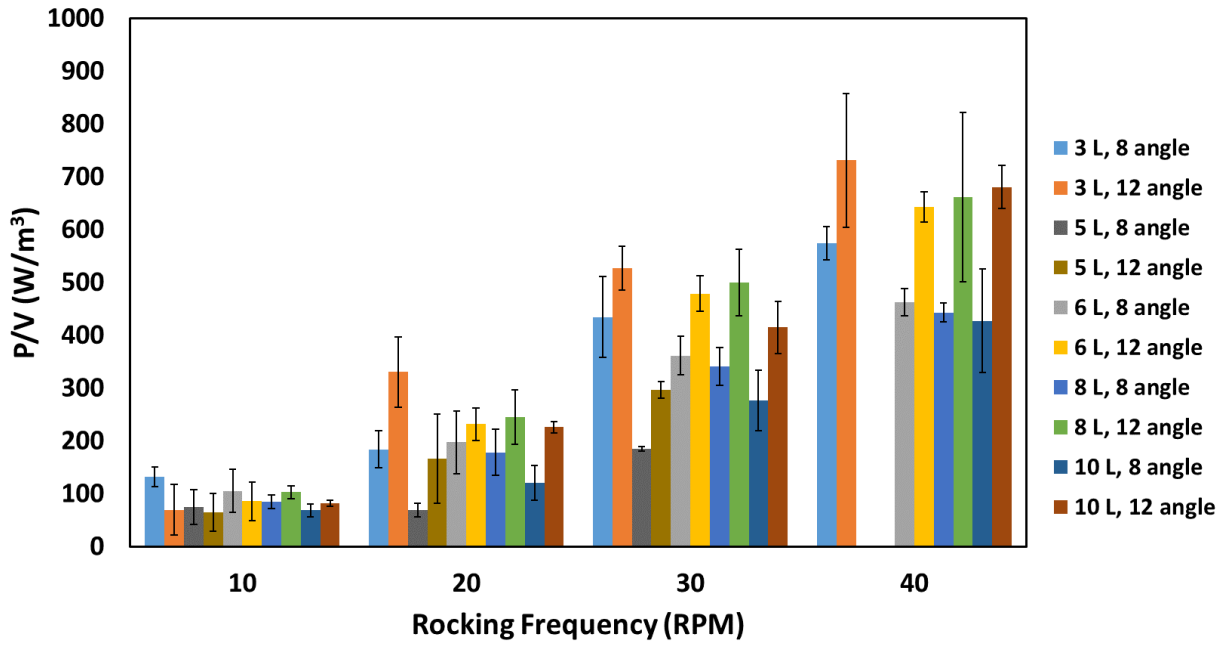

Figure 4-7 Summary of average net power input measurement at various experimental conditions

The power inputs measured here can also be compared with other disposable bioreactor configurations, such as the orbitally-shaken and stirred tank versions. For example, the average power input measured here (458.4 W/m^3) for 6 L liquid, 8^o rocking angle and 40 rpm is similar to the power input for several disposable orbitally-shaken bioreactors (500 W/m^3) for 6 L liquid, 140 rpm and 5 cm shaking diameter (Klöckner et al., 2012). In addition, the average power (635.2 W/m^3) for 6 L liquid, 12^o rocking angle and 40 rpm was approximately equal to the power input (625 W/m^3) for 6 L liquid, 150 rpm and 5 cm shaking diameter. Table 4-4 summarized a cross-comparison between the rocking bioreactor and other types of bioreactors with either glass, stainless-steel or disposable materials, including data acquired in this work together with previously reported data from various sources.

Table 4-4 Summary of $k_L a$ for various types of bioreactors under different liquid volumes and operational conditions from previous works.

Building Material	**Bioreactor Type**	$k_L a$ [h^{-1}]	**Liquid volume [L]**	**Operational conditions**	**Reference**
Glass Stainless-steel	Stirred tank	7.92-316.44	0.6	100 to 500 RPM stirrer speed	(Özbek and Gayik, 2001)
		18-234	90	100 to 500 RPM stirrer speed and 0.5 to 2.0 vvm Q_g	(Li et al., 2018)
	Airlift	14-72	12	0.002 to 0.01 m/s U_{gr}	(Nikakhtari and Hill, 2005a, 2005b)
		10.8-54.0	1100	0.003 to 0.11 m/s U_{gr}	(Chisti and Jauregui-Haza, 2002)
Disposable plastic	Stirred tank	6.8-13	3	100 to 200 RPM stirrer speed and 0.05 to 0.1 vvm Q_g	(Kaiser et al., 2011)
		20-160	45	100 to 900 W/m^3 P/V and 0.0005 to 0.003 m/s U_g	(Dreher et al., 2013)
		9	1000	132 RPM stirrer speed and 0.015 vvm Q_g	(Löffelholz et al., 2014)
	Rocking	5-20	1	5°-10° rocking angle and 10-30 RPM rocking speed	(Ghasemi et al., 2019)
		10	20	15° rising angle and 0.12 vvm Q_g	(Terrier et al., 2007)
		50-300	12-120	15-35 RPM and 0.1 vvm Q_g (2D Cell-tainer® Bioreactor)	(Junne et al., 2013)
		10-71	2	10-40 RPM and 0.1 vvm Q_g	(Jones et al., 2017)
		1.62-142.52	3-10	10-40 RPM and 0.4 vvm Q_g	This work
	Orbital-shaken	2-70	5-15	65-120 RPM shaking speed and no active aeration	(Zhang et al., 2010)
		4-79	2.5-37.5	80-220 RPM shaking speed and 0.053 to 0.160 vvm Q_g	
		2-10	1000	40 RPM shaking speed and 0.025 vvm Q_g	(Zhang et al., 2010)

	Pneumatic (bubble column)	7-17	20	0.17 to 0.31 vvm Q_g	(Terrier et al., 2007)
	Pneumatic (air wheel)	20	10	0.05 to 0.50 vvm Q_g	(Kim et al., 2013)

A maximum achievable power input of 435 W/m^3 was reported by Löffelholz et al. (Löffelholz et al., 2014) using a stirred disposable bioreactor with a 2 L liquid volume, which was comparable in magnitude with the 3 L power input performance in this experiment. In addition, Kaiser et al. (Kaiser et al., 2017) reported a similar range of power inputs with various types of stirred disposable bioreactors, which were comparable to the power inputs achievable here with 3 L in the wave bioreactor. It was mentioned by Löffelholz et al. that a power input of 150 W/m^3 can be acceptable for mammalian cell culture in a stirred disposable bioreactor system, whereas in the wave bioreactor a much higher value was achievable. It is worth noting that previous works have confirmed that the wave bioreactor induces very low shear stresses in the liquid phase (Kalmbach et al., 2011; Marsh et al., 2017), and so such limitations on power input may not be relevant here. While a power input comparable to stirred tank and orbitally-shaken disposable bioreactors was observed in this study, the low shear stress in the liquid phase could be explained by the fact that the rocking motion moves the entire liquid volume and transports the mechanical power throughout the whole perimeter of the liquid body. In contrast, in a stirred tank system a high shear stress together with high mechanical power is introduced at the impeller tip and delivered into the liquid. Such differences in the power transfer mechanisms help to explain the unique high power input but low shear stress advantage in rocking bioreactors.

As shown in Figure 4-8, the power consumption of the wave bioreactor exhibited a periodic trend with maximum power consumption occurring at the turnaround of each rocking motion, and the minimum power was observed when the rocking platform returned to its horizontal position. This trend in the power consumption follows the previously reported oscillatory characteristics of liquid velocity for similar rocking disposable bioreactor systems (Kalmbach et al., 2011; Öncül et al., 2010; Zhan et al., 2019), some of which are also illustrated in Figure 4-8 for comparison.

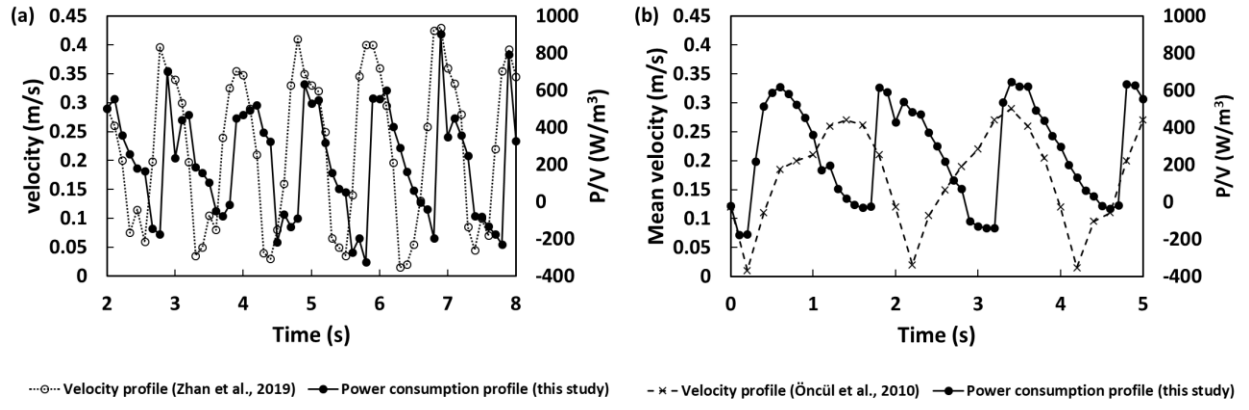

Figure 4-8 Comparison of the periodic trend of power consumption with previous works reporting velocity: (a) comparing with simulated velocity profile at centre position of the bag at 5 L liquid filling, 30 rpm and 7º rocking angle from Zhan et al. (Zhan et al., 2019), (b) comparing with simulated mean velocity along the center line of the 20 L bag with 7 L liquid filling, 15 rpm and 8º rocking angle from Öncül et al. (Öncül et al., 2010).

As shown in Figure 4-8 (a), the point velocity estimated by Zhan et al. (Zhan et al., 2019) using ANSYS CFD simulations at 30 rpm and 7º rocking angle for a 5 L liquid volume in a 10 L bag exhibited a similar oscillatory trend as the power input oscillation observed in this study with the same volumes (at 30 rpm and 8º rocking angle). The slight deviation in the phase of oscillation could be attributed to the slight difference in rocking angle. The power input trend at 20 rpm and 8º rocking angle with 6 L liquid in a 10 L bag from this study was compared with the previously reported mean center line velocity from Öncül et al. (Öncül et al., 2010) as shown in Figure 4-8 (b). Although the similar oscillatory trend was also verified in both works, the characteristics of the oscillation differed from each other significantly, which could possibly be ascribed to the differences in experimental conditions. In addition, a similar oscillatory trend was reported by Marsh et al (Marsh et al., 2017) as well in their fluid dynamic characterization of a 2 L bag at various rocking frequencies. This correlation between the variations in liquid velocity and power input reveals the direct impact of power input on liquid hydrodynamic characteristics in a wave bioreactor.

4.2.2 The influence of power input on volumetric mass transfer coefficient

Comparing all three types of power inputs (peak, average, and base), it is suggested that the net peak power input is more representative and important when characterizing the power input to the liquid for the following reasons. First, the net peak power input better reflected the impact of operating conditions (rocking frequency, rocking angle and, in some cases, liquid volume) while the trends of the net base and average power inputs tended to indicate less differences between the operating conditions. Secondly, net peak power input occurred when the rocking platform reversed direction back from the lowest point which is also at the highest tilting angle. It was also at this point in the rocking cycle where the entrainment of air by the wave occurred. According to our earlier work, most of the gas-liquid mass transfer is accomplished by such a breaking-wave air entrainment process compared to surface gas-liquid mass transfer alone (Bai et al., 2019). Since the net peak power input appears to be more closely aligned with wave-breaking it should be the better basis for correlating mass transfer performance.

By analogy with many previous studies on gas-liquid mass transfer in stirred-tank bioreactors, the dependence of $k_L a$ on power input was explored, with the results shown in Figure 4-9. The relationship between the volumetric mass transfer coefficient and the specific power input can be divided into two separate sections, based on the trend depicted in Figure 4-9 (a) and (b). It was noted that the $k_L a$ increased proportionally and without much variability as the power input increased up to approximately 400 W/m^3 for the 8^o rocking angle and 600 W/m^3 for the 12^o rocking angle. P/V at this lower range was observed to be relatively independent of the influence from the liquid and bag volumes. As the power input was further increased above each threshold of 400 W/m^3 and 600 W/m^3, respectively, the $k_L a$ increased more rapidly in a non-linear trend. However, this trend was observed to have more variability depending on the bag geometry for both rocking angles. For example, the same 30% liquid filling fraction would yield different relationships between $k_L a$ and power input for different bag sizes, while $k_L a$ for 6, 8 and 10 L in the same bag size would yield a similar relationship between the two variables.

For model analysis all the bag and liquid volumes were combined for the purpose of developing an approximate characterization. A power law model was tested against the experimental data to provide an empirical correlation between the $k_L a$ and peak P/V which showed an acceptable approximation with the 8^o rocking angle data as shown in Figure 4-9 (a) and good agreement with the 12^o rocking angle data as shown in Figure 4-9 (b).

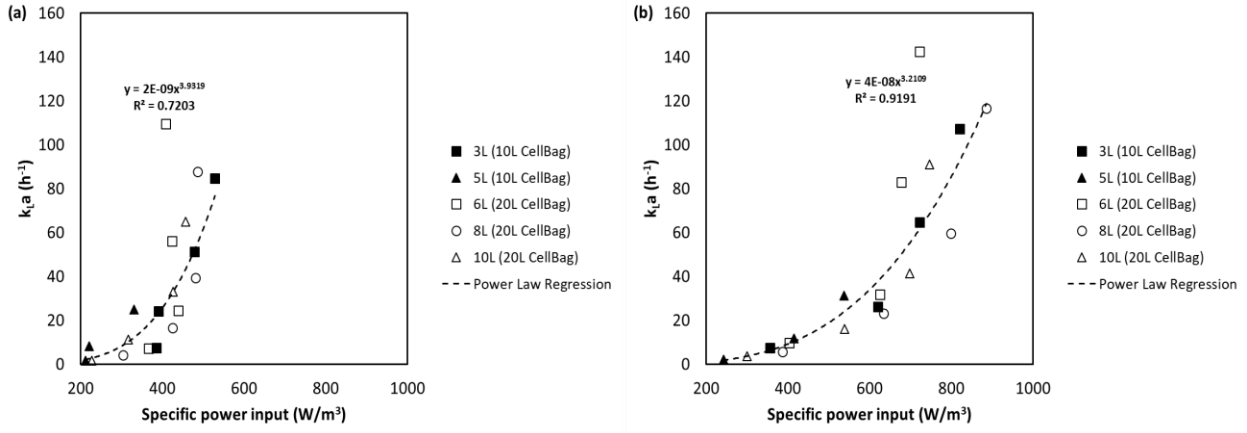

Figure 4-9 The dependence of volumetric mass transfer coefficient on specific power input with varied liquid volumes in two bag geometries at (a) 8º rocking angle and (b) 12º rocking angle. Power law regressions combine all volumes and bag geometries.

The relationship between $k_L a$ and P/V shown in Figure 4-9 (a) and (b) indicated that operating the wave bioreactor above 400 and 600 W/m^3 thresholds would be effective in rapidly improving the gas-liquid mass transfer capacity of the bioreactor. This power input level was achievable by increasing the rocking angle and frequency in combination. Increasing the rocking angle would be a much more feasible practice (within the mechanical limits of the device) as the higher rocking frequency would induce the 'out-of-phase' movement of the liquid, with a decreasing effectiveness for power delivery into the liquid as illustrated previously for net peak power in Figure 4-6.

Compared with the stirred tank disposable bioreactors data summarized in Table 4-4, the wave bioreactor was more proficient in gas-liquid mass transfer, probably by introducing more energy into the liquid as was indicated by a comparatively higher $k_L a$ and P/V simultaneously. For example, the maximum achievable P/V and $k_L a$ for the stirred tank disposable bioreactor reported by Kaiser et al. were 37.9 W/m^3 and 35.9 h^{-1}, respectively, at 1.5 L liquid volume with a tip speed of 0.8 m/s and an aeration rate of 0.25 vvm. In this work, the P/V could reach 800 W/m^3 and $k_L a$ could achieve 100 h^{-1} with a 3 L liquid volume. Compared with an orbitally shaken bioreactor at 10 L and 20 L bag volumes (Klöckner et al., 2013b), the $k_L a$ of the wave bioreactor was higher at a lower filling level of 30% (25% in the work of Klöckner et al.) and remained comparable as the filling level increased to 50%.

4.2.3 The influence of power input on mixing time

The degree of homogeneity in a bioreactor is important for ensuring optimal growth conditions throughout, and it is related to the mixing time that can be experimentally measured (Kawase and Moo-Young, 1989). The mixing times in stirred-tank bioreactors have often been correlated with rotational speed as part of the Reynolds number, which is a representation of the specific power input and fluid properties (Hadjiev et al., 2006). Therefore, a similar relationship was sought for the rocking bioreactor, with the results shown in Figure 4-10. The mixing time data revealed that as the specific power input decreased, a rapid increase in mixing time existed in the 200 to 400 W/m^3 range, which represented a much poorer mixing performance in the bioreactor. Although not as significant at lower liquid volumes of 3 and 5 L in a 10 L bioreactor, the mixing performance would deteriorate as the liquid volume increased in a larger bag volume. As illustrated in one study with color mixing characterization (Jones et al., 2017), a unique mixing mechanism in the wave bioreactor determines that mixing of the liquid in the horizontal direction was slower compared with its robust vertical mixing alongside the platform rocking at lower rocking intensity. As the bioreactor bag volume increased from 10 L to 20 L, the width of the bag was elongated (from 26.5 cm at 3 L liquid volume to 48.0 cm at 6 L liquid volume) while the length of the bag remained unchanged, and this impaired the mixing of the liquid in the horizontal direction. This could explain the poor mixing performance found at low power input conditions which corresponds to the low rocking frequency and smaller rocking angle.

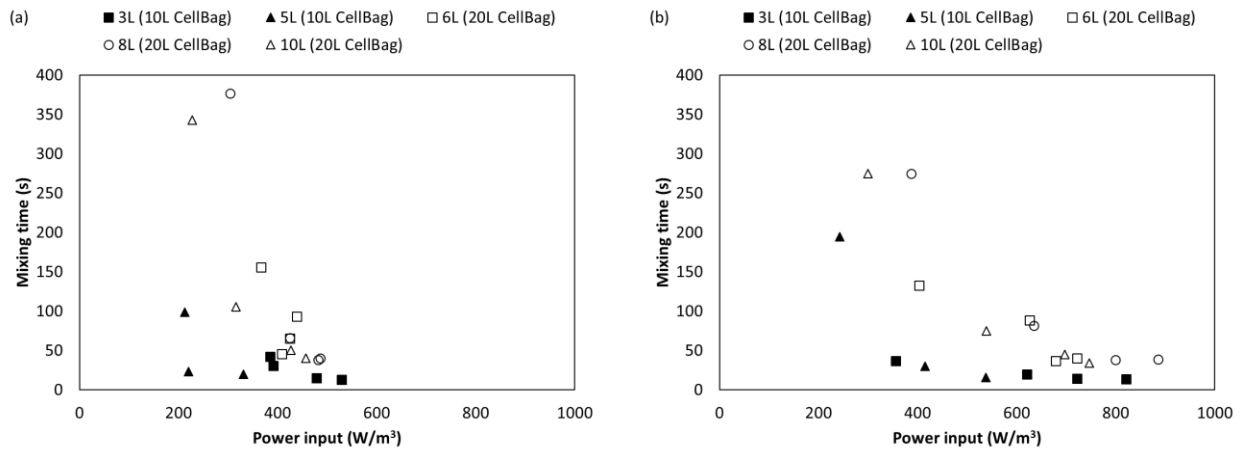

Figure 4-10 The correlation between mixing time and specific power input with various liquid volumes at (a) 8° rocking angle and (b) 12° rocking angles.

The correlation of mixing time and power input was found to be significantly dependent on rocking angles. Figure 4-10 (a) and (b) exhibited different patterns with respect to the dependence of mixing time on power input. A lower rocking angle was shown to be more effective in liquid mixing given the shorter mixing time achieved using a lower power input at an 8° rocking angle, compared with the 12° angle results. This phenomenon also draws attention to the possible conflict between gas-liquid mass transfer and liquid mixing capacity in the wave bioreactor. A possible explanation for such a contradiction was that the higher rocking angle could induce a subsequently higher velocity of the liquid approaching the edge of the bag. This facilitated the mixing along the bag width dimension but may have hampered the mixing along the perpendicular bag length dimension. This would result in less liquid movement in one direction which could potentially undermine the overall mixing time performance at lower rocking frequencies despite the increased rocking angle.

Despite the insufficient horizontal liquid movement and longer mixing time, a higher $k_L a$ requires the maximal conversion of mechanical energy into a vertical velocity of the liquid which then could be utilized as momentum for a more effective wave generation. Such wave generation has been shown to be more effective in improving the gas-liquid mass transfer capacity compared with the surface aeration mechanism. Such interactions among $k_L a$, t_m and P/V reveal the complexity of characterizing mass transfer and its dependence on P/V in a wave bioreactor, and sometimes a trade-off might be required at low rocking intensity conditions to balance the demand for both t_m

and $k_L a$. However, in most applications the oxygen transfer is a more potentially limiting factor than mixing time and such trade-offs may not be necessary in practice.

Phenolphthalein was used to visualize pH changes during the mixing experiments to identify trends or problems in mixing. Obvious and noticeable dead zones in mixing were only observed at the lowest rocking frequency of 10 rpm, which suggested that the mixing capacity of the rocking bioreactor at the 10 and 20 L scale was enough under most typical operating conditions. For bioprocesses running for many hours, the mixing times of approximately 50 s measured here are relatively short and should be suitable for most process control purposes.

4.3 Improvement of Mass Transfer Capacity through a Cross-over Baffle Design

4.3.1 The influence of diagonal cross-over baffle on the mixing performance in the rocking bioreactor

Figure 4-11 (a) - (f) illustrated the mixing performance using a phenolphthalein indicator at 10 rpm with 5 L liquid volume loaded in a 10 L bioreactor, as an example. The t_m in this case was 98.7 ± 5.8 s. It could be observed from Figure 4-11 (a) - (f) that the mixing in the liquid spread out in two directions simultaneously i.e. longitudinally along the length of the bag and horizontally along width of the bag. Since the longitudinal mixing was consistent with the rocking motion generated by the bioreactor, it was much more effective for the mixing in this direction while in contrast the mixing in the horizontal direction was less effective. The installation of the cross-over baffle aimed to divert part of the longitudinal momentum delivered from the rocking motor into the horizontal direction. This was expected to help distribute momentum required for mixing more evenly in the bioreactor.

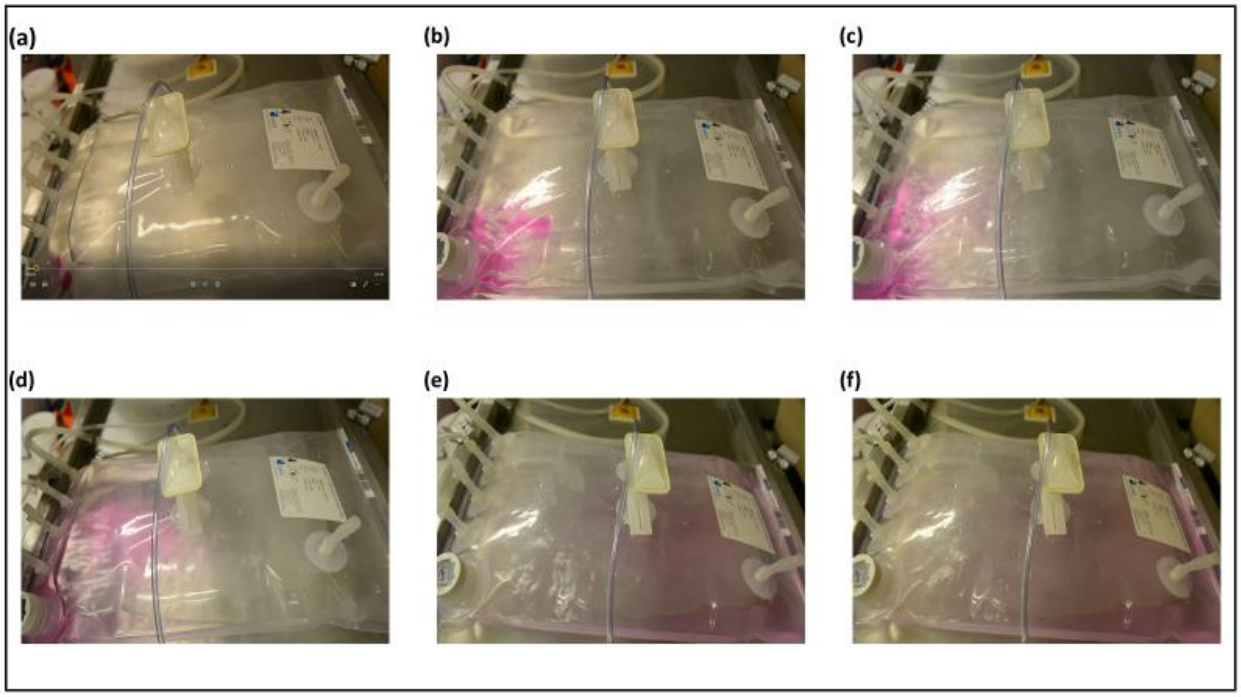

Figure 4-11 Phenolphthalein visualization of the mixing in a 10 L Cell Bag with a 5 L 0.05% wt phenolphthalein indicator solution at (a) 0 s injection (b) 10 s after injection (c) 20 s after injection (d) 40 s after injection (e) 60 s after injection and (f) 90 s after injection

Two main parameters representing the mass transfer capacity in the bioreactors, namely mixing time t_m and volumetric mass transfer coefficient $k_L a$, were examined in this study to determine if the external baffle installed on the rocking tray could significantly improve the mass transfer capacity of the bioreactor. Figure 4-12 (a) shows that first the t_m decreased rapidly as the rocking frequency increased starting from 10 rpm up to 40 rpm while the impact of rocking angle on the t_m varied depending on the rocking frequency. A higher rocking angle (12^o) was proven to generate better mixing performance represented by a lower t_m when the rocking frequency was at 10 rpm. As the rocking frequency rose above 20 rpm, the difference in mixing performance brought by rocking angle was negligible. Insufficient mixing was found to exist under 5 L, especially for rocking frequencies of 10 and 20 rpm, with t_m reaching over 100 s. In comparison, t_m under 3 L liquid volume was much lower across all rocking frequency conditions. The cross-over baffle was effective in improving the mixing performance of the bioreactor at both 3 and 5 L liquid volume as illustrated by Figure 4-12 (b), where t_m was maintained below 100 s even with

the lowest rocking frequency and rocking angle. Furthermore, the impact of the rocking angle was minimized for all rocking frequencies when the baffle was installed on the rocking platform.

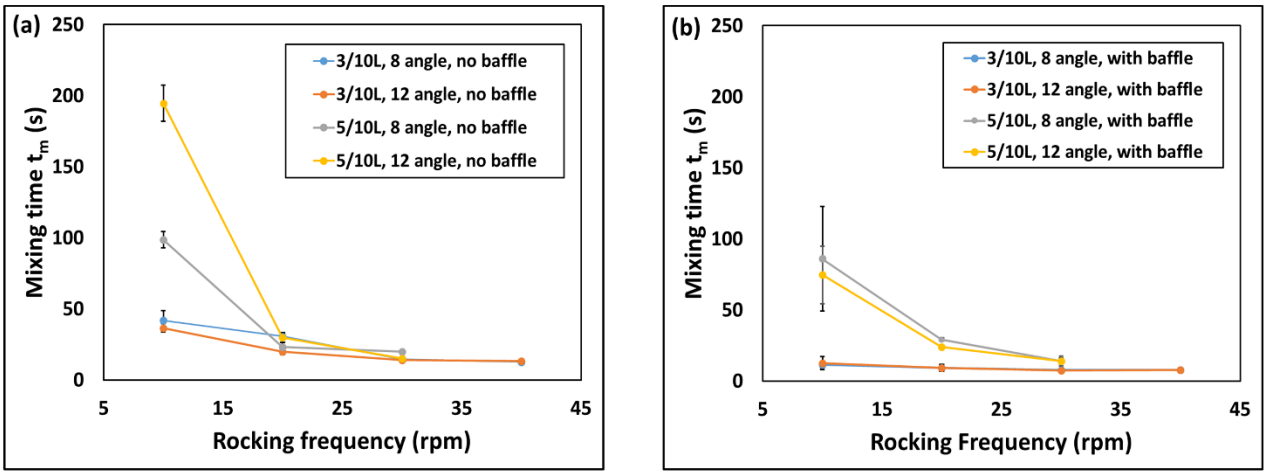

Figure 4-12 Mixing time (t_m) with 3 L and 5 L liquid volumes in the 10 L bag between 10 rpm and 40 rpm rocking frequency and two rocking angles. (a) mixing time in the control group without any baffle installed and (b) mixing time with the rod cross-over baffle installed on the rocking tray.

As the bioreactor was scaled up to the 20 L bag, effective mixing was harder to achieve as illustrated by Figure 4-13 (a). Comparing with Figure 4-12 (a) at 10 L bioreactor volume, doubling the bioreactor further increased the t_m especially at a low rocking frequency of 10 rpm. Mixing time (t_m) was elevated above 350 s for both 8 and 10 L liquid volume with an 8^o rocking angle. Increasing the rocking angle from 8^o to 12^o was not as effective in improving mixing capacity as it was in the 10 L bioreactor as the difference of t_m between 8^o and 12^o rocking angle was not very significant. Despite the rapid decreasing trend of t_m as the rocking frequency increased, t_m still ranged between 66 and 105.3 s at a 20 rpm rocking frequency for a liquid volume between 6 and 10 L.

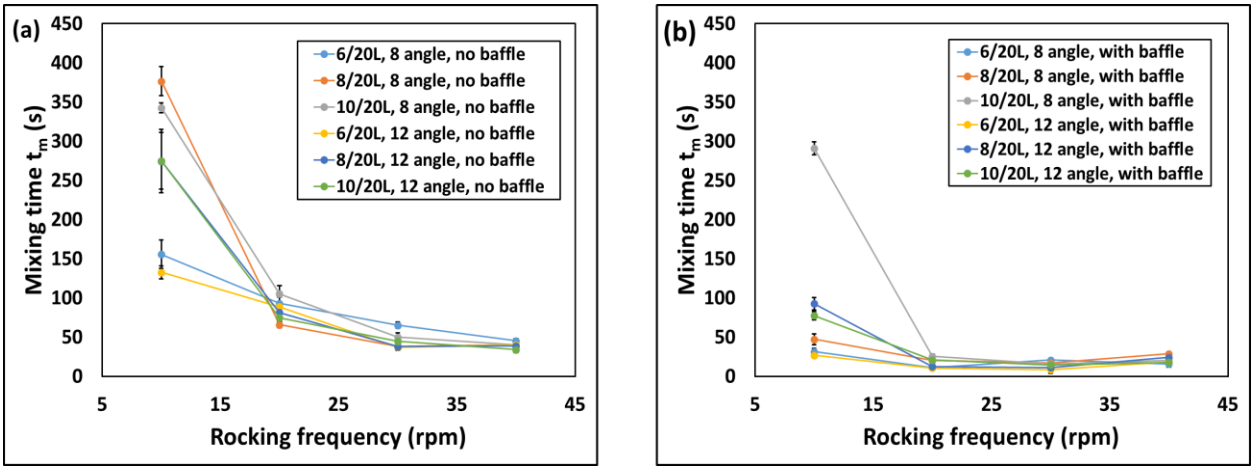

Figure 4-13 Mixing time (t_m) with 6, 8 and 10 L liquid volumes in the 20 L bag between 10 rpm and 40 rpm rocking frequency and two rocking angles (8° and 12° respectively). (a) mixing time in the control group without any baffle installed; (b) mixing time with a rod cross-over baffle installed on the rocking tray.

Installing the baffle in a 20 L scale bioreactor would significantly reduce the t_m as shown in Figure 4-13 (b), especially at the low 10 rpm rocking frequency. Except for the insufficient mixing still existing with 10 L liquid volume at a 8° rocking angle condition with t_m reaching 290.7 s, t_m under all other rocking conditions could drop below 100 s. With rocking angle set at 8°, the highest t_m at 20 rpm was 25.3 s with 10 L liquid volume and was further decreased to 17.3 s as the rocking frequency increased to 30 rpm. As the rocking angle was elevated to 12°, mixing performance could be further enhanced. The t_m at 10 rpm was decreased to 77.3 s compared to the 290.7 s t_m achieved at a 8° rocking angle. When the rocking frequency increased to 20 rpm, the highest t_m was 20.7 s with a 10 L liquid volume and this value was decreased to 14.7 s at 30 rpm.

Compared with the no baffle control group results, installing the baffle could reduce t_m under all rocking frequencies and angles. Such improvement however was more substantial at the low 10 rpm rocking frequency combined with a 12° rocking angle than the rest of rocking conditions. This was due to lower t_m achieved when rocking frequency was increased which left only narrow room for the baffle to cut the t_m a step further. Additionally, insufficient mixing mostly occurred under the 10 rpm rocking conditions which rendered the baffle much more effective in improving the mixing capacity of the bioreactor at this low rocking frequency. Further increasing the rocking

frequency up to 40 rpm was observed to provide rather limited improvement on mixing performance at both 8° and 12° rocking angles. The lowest t_m at 40 rpm was 16 s with 6 L liquid volume and 8° rocking angle while at 30 rpm, t_m could reach as low as 11.3 s. This indicated that excessive rocking frequency was not helpful in achieving better mixing performance and thus unnecessary for a baffle equipped bioreactor system.

Proposed explanations for such improvements from baffle installation on mixing capacity of the bioreactor looked into two perspectives. Firstly, as mentioned in the visualization of the mixing performance in the rocking bioreactor that the 1-dimensional rocking motion of the bioreactor generated much more momentum for liquid moving along the longitudinal direction than the horizontal direction and thus mainly facilitated the mixing along the rocking direction. However, the mixing in the horizontal direction would be undermined as the mixing indicator was seen trapped or moving slowly along the width of the bag as illustrated by Figure 4-9 (a) – (f). A baffle installed in between the rocking tray and bioreactor bag helped divert some of the liquid in a direction perpendicular to the 1-dimensional rocking motion. Secondly, small vortices were noticed right at the downstream edge of the baffle. Such vortex-intense region could create increasing eddy turbulence which was argued to be beneficial for the effective mixing in the vessel and thus could possibly contribute to the improved mixing capacity of the bioreactor.

4.3.2 The influence of diagonal cross-over baffle on the gas-liquid mass transfer performance in the rocking bioreactor

Contrary to an expected beneficial effect brought by a baffle on the mixing performance of the rocking bioreactor, the influence of the baffle on the gas-liquid mass transfer was more complex than initially imagined. As summarized in Figure 4-14, installing the baffle could increase $k_L a$ at 10 rpm most significantly. When the rocking frequency was increased to 20 rpm, the improvement of $k_L a$ from the baffle diminished and the difference between the control group and baffle group was negligible at this rocking frequency. As the rocking frequency further increased to 30 and 40 rpm, it was discovered that installing the baffle undermined the gas-liquid mass transfer capacity of the bioreactor.

At an 8° rocking angle, installing the baffle could improve the $k_L a$ from 7.35 ± 0.33 to 9.85 ± 0.93 with a 3 L liquid volume. With a 6 L liquid volume, $k_L a$ could improve from 7.18 ± 0.94 to 13.14 ± 0.35. At a 12° rocking angle, installing the baffle could increase the $k_L a$ from 7.33 ± 0.23 to 13.55 ± 0.63 with a 3 L liquid volume. With 6 L liquid volume, $k_L a$ could improve from 9.82 ± 0.43 to 15.81 ± 0.41. However the $k_L a$ with or without baffle at 5, 8 and 10 L volumes didn't show any distinguishable difference.

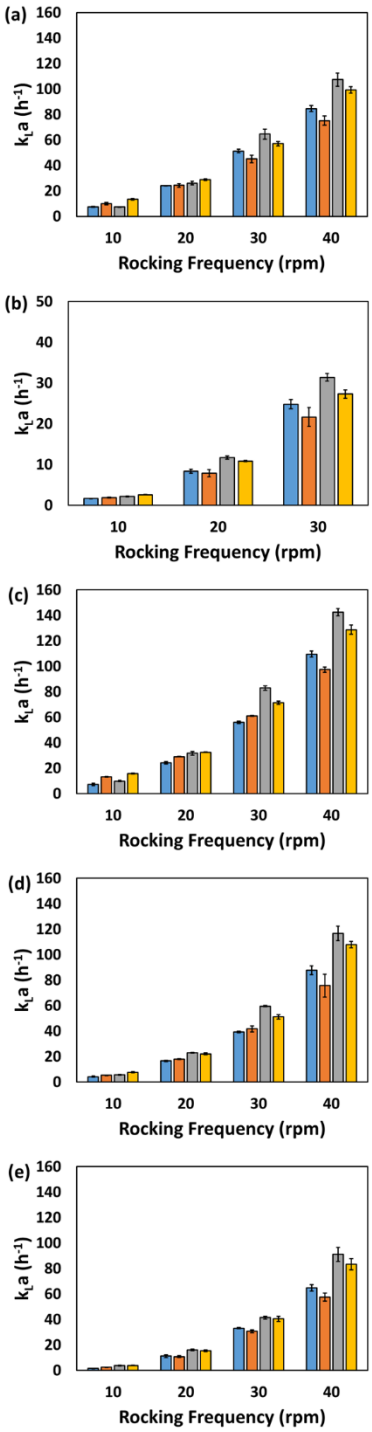

Figure 4-14 Impact of the baffle on k_La under varied conditions including control group without baffle with 8º rocking angle (blue column), baffle installed with 8º rocking angle (orange column), control group without baffle with 12º rocking angle (grey column) and

baffle installed with 12º rocking angle (yellow column) at (a) 3 L, (b) 5 L, (c) 6 L, (d) 8 L and (e) 10 L liquid volumes.

Possible explanations for such results stemmed from several aspects. As discussed in Section 4.1, when developing the mechanistic $k_L a$ model there were two distinctive gas-liquid mass transfer mechanisms occurring in the rocking bioreactor. When the rocking frequency was low, surface aeration played a more influential role in transporting oxygen from the gas phase into the liquid phase. Installing baffle was shown to create a vortex-intense region and such a region could possibly enhance the gas-liquid mass transfer (Kadic and Heindel, 2014). This could explain the improvement of $k_L a$ at the low 10 rpm conditions. As the rocking frequency increased to 30 or 40 rpm, the wave air entrainment mechanism started to become the dominant mass transfer mechanism and in such situations sufficient momentum along the rocking direction was needed in order to generate waves strong enough in height, width, and velocity to capture as much air as possible during the entrainment. The baffle in such scenarios would undermine the wave strength since it diverted a certain portion of the longitudinal momentum into the horizontal direction and by doing so the momentum delivered to the wave formation would subsequently be decreased. This could explain the reduced $k_L a$ observed when baffle was present at the 30 and 40 rpm operating conditions.

4.4 Improvement of Mass Transfer Capacity through a Porous Plastic Sparger

4.4.1 The improvement in $k_L a$ from sparger compared with surface aeration

Figure 4-15 shows the enhancement of the $k_L a$ for the bioreactor with the addition of a porous tube sparger. Current results indicated an effective improvement at low rocking frequency and later we could supplement more data on a different liquid volume and also try to dissect the $k_L a$ from surface and sparger distinctively to illustrate the effect of sparger.

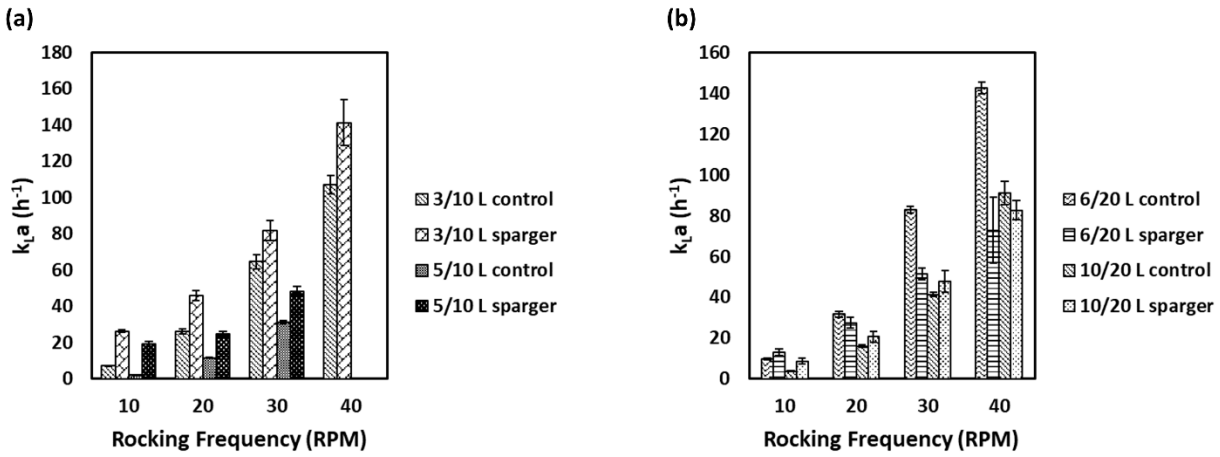

Figure 4-15 Comparison of $k_L a$ improvement between sparger equipped bioreactor (labelled as sparger) and original bioreactor (labelled as control) at two liquid volumes with (a) using a hydrophobic 5 cm long 5 µm sparger and (b) using a hydrophilic 5 cm long 5 µm sparger. 5 L at 40 rpm data was not measured due to flooding of filter during experiments.

It was illustrated in Figure 4-15 (a) that the $k_L a$ of the sparger-equipped bioreactor was increased for all rocking frequencies at both 3 and 5 L liquid volumes. While the $k_L a$ increase was nearly 3-fold for 3 L and 8-fold for 5 L at 10 rpm, such improvement was getting narrower as the rocking frequency increased starting from 10 rpm up to 40 rpm. This could be attributed to two possible reasons: 1) another form of mass transfer which was wave air entrainment gas-liquid oxygen mass transfer mechanism helped boost the $k_L a$ of the rocking bioreactor during high rocking frequency operations, especially at 30 and 40 rpm (Bai et al., 2019), 2) the strong wave motion generated at high rocking frequency might trap the bubbles generated from sparger and their distribution within

the liquid body. As illustrated in Figure 4-15 (b), in comparison with the hydrophobic sparger installed in the 10 L bag container, the hydrophilic sparger installed in 20 L bag container provided inconsistent improvement on $k_L a$. The hydrophilic sparger in the 20 L bag was observed to enhance the $k_L a$ at a 10 L liquid volume but was not effective for a 6 L liquid volume, especially when the rocking frequency reached 30 rpm and higher. However, it was shown by both figures that spargers installed in the bioreactor could improve the $k_L a$ despite their wettability at low rocking frequencies between 10 and 20 rpm, which is the commonly adopted rocking frequency range for mammalian cell growth applications. Such an improvement in $k_L a$ offers potential for debottlenecking the oxygen limitation encountered in high-density mammalian cell growth in a small-scale disposable bioreactor batch operation which was currently realized mostly through perfusion or fed-batch operations (Clincke et al., 2013a, 2013b).

Table 4-5 A cross-comparison of the $k_L a$ performance among varied types of bioreactors

Bioreactor type	Material	Mixing design	Liquid volume (L)	Agitation (RPM)	Sparging (vvm)	Max $k_L a$ achievable (h^{-1})	Reference
Stirred tank	Glass	N/A	0.6	500	0.3	316.4	(Özbek and Gayik, 2001)
	Plastic film	N/A	45	375	0.44	175	(Dreher et al., 2014b)
	Hard Plastic	N/A	1 - 2.5	200	0.25	39.5	(Kaiser et al., 2011)
Orbitally shaken	Glass	N/A	5	130	N/A	9	(Zhang et al., 2009)
	Hard plastic	N/A	0.6	220	N/A	40	(Monteil et al., 2013)
Rocking	Plastic film	1 Dimensional	10	30	0.1	4	(Singh, 1999)
		2 Dimensional	10	42	0.4	200	(Westbrook et al., 2014)
		Under-tow	20	N/A	0.125	12.9	(Terrier et al., 2007)
		1 Dimensional	10	40	0.4	82.58	This study
Pneumatic	Plastic film	Bubble column	20	N/A	0.49	16	(Terrier et al., 2007)
		Airlift	3	N/A	0.1	5.9	(Kwon et al., 2013)
	Hard plastic	Air wheel rotary	10	31	0.5	8.96	(Kim et al., 2013)

Due to variation on multiple operational parameters which could potentially impact the $k_L a$ and inconsistency of their characterization for different types of bioreactors. It is difficult to perform a consistent direct comparison among varied types of bioreactors. The data gathered in Table 4-5 aimed to provide an overview of the oxygen mass transfer capacity of varied bioreactors with similar range of working volumes first and if possible sharing similar agitation speeds and sparging flow rates. The stirred tank bioreactor was still the bioreactor capable of generating the highest $k_L a$ achievable among all types of bioreactors in comparison, however at the cost of potentially highest averaged shear stress brought by intensive agitation and bubble breaking. For growing mammalian cells, the stirred tank bioreactor has to reduce its agitation speed to between 100 to 200 rpm and rely on minimal submerged aeration which in most cases brings down its $k_L a$ below 200 h^{-1} which was still more than sufficient for mammalian cell culture growth. Except for the stirred tank, all other types of single-use bioreactor hold comparable and moderate $k_L a$ values which indicated a similar oxygenation capacity as shown by Table 4-5. With the sparger design installed, the modified rocking disposable bioreactor acquired a relatively higher $k_L a$ at the highest rocking frequency of 40 rpm. Such $k_L a$ performance was proven to be sufficient for CHO cells to grow up to 10^7 cells/mL (Jorjani and Ozturk, 1999; Ruffieux et al., 1998). When the rocking frequency was reduced to 30 rpm and 0.11 vvm, which was very close to the experimental conditions reported by Singh in his work, the $k_L a$ acquired in our study reached 31.35±1.33 h^{-1} which was still 10-fold higher than $k_L a$ originally reported (Singh, 1999). The highest $k_L a$ acquired from sparger equipped rocking bioreactor in this study could potentially support a robust growth of aerobic microbial cells up to medium scale (10 to 20 L) without a severe oxygen limitation observed by previous study (Glazyrina et al., 2010). However, the further scale-up for microbial cell growth purpose in the rocking bioreactor even with a sparger was still challenging as it was noticed that maintaining the same rocking frequency at a larger scale would be difficult to achieve, mainly due to the limited mechanical strength of the plastic film. This might require that either the sparger length is further elongated to generate more bubbles or to reduce the pore size of the spager which are common approaches adopted for bubble column or airlift bioreactor design. However, such modifications should be approached carefully because of additional shear stresses on cells from breaking bubbles as well as foaming issues induced by fine bubbles.

4.4.2 $k_L a$ dependence on flowrates under varied rocking frequency and liquid volume

Gas flowrate was determined to be a key parameter affecting the $k_L a$ of the bioreactor, especially under sparged conditions during the bioreactor operation. For the sparger-modified rocking disposable bioreactor, the impact of gas flowrate on the bioreactor $k_L a$ was examined as illustrated in Figure 4-16 in which the $k_L a$ values under various gas flowrates are summarized.

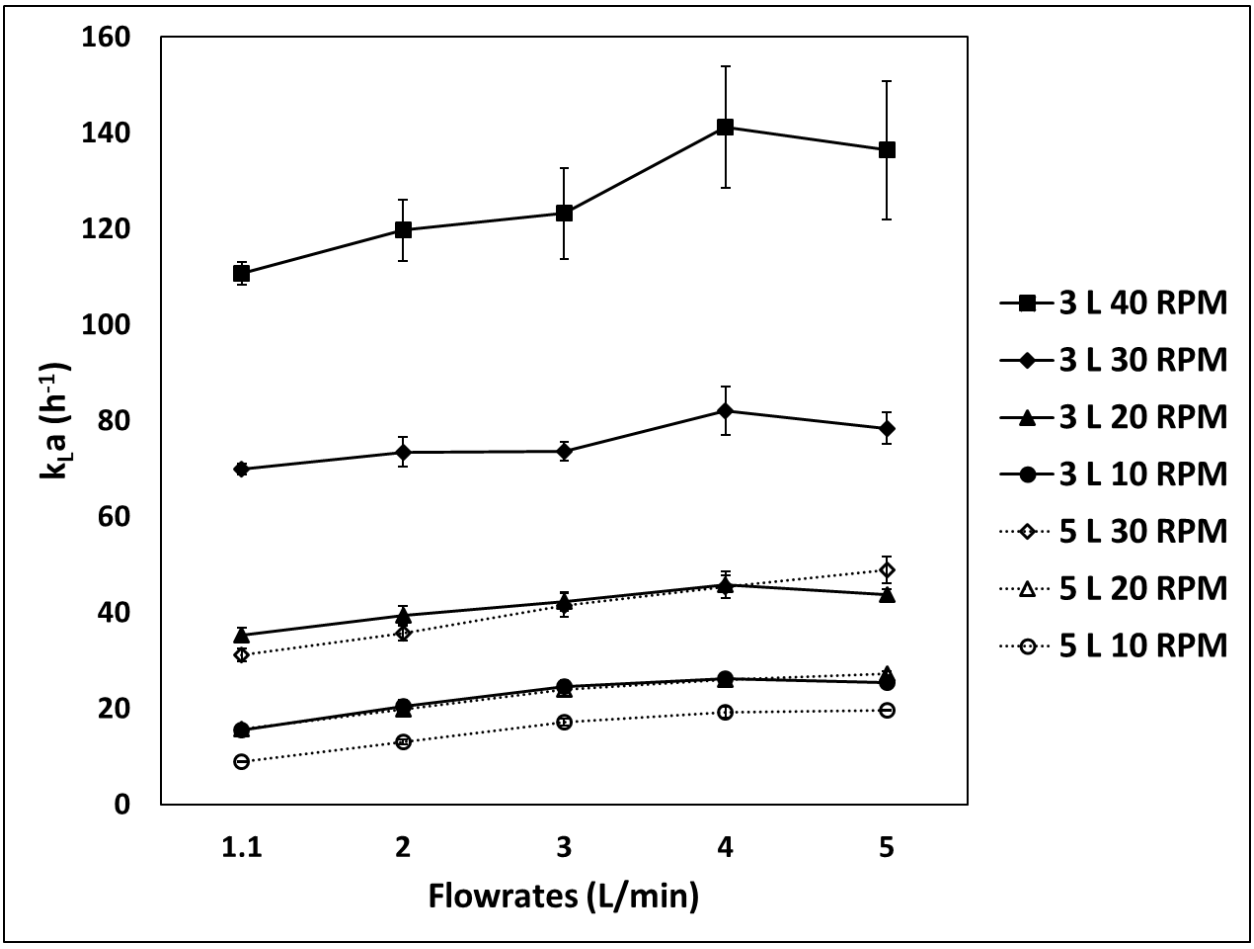

Figure 4-16 Impact of different air flowrates on gas-liquid mass transfer coefficients at 3 L liquid volume (solid filled data points) and 5 L liquid volume (empty filled data points) at 10 rpm (sphere), 20 rpm (triangle), 30rpm (diamond) and 40 rpm (square) respectively.

It was shown that for 3 L liquid volume, the $k_L a$ would improve with the increasing air flowrate up to 4 L/min and then slightly decreased at the highest 5 L/min air flowrate. A similar improvement was confirmed under the 5 L liquid volume condition with the only difference that $k_L a$ continued to improve to the highest capacity at highest 5 L/min air flowrate. As the sparging was enhanced, the bubbles distributed in the liquid would affect the wave formation within the liquid body. The higher flowrate would then create not only a larger amount of bubbles but also a higher momentum carried by bubbles into the liquid which could impose a negative effect on the wave formation. As the wave air entrainment would be the more efficient gas-liquid mass transfer mechanism at higher rocking frequencies, the disturbance of the bubbles induced from very high air flow rate would surpass the enhancement it generated through increase gas-liquid specific interfacial area a. At a 5 L liquid volume, the increased a would continuously improve the $k_L a$ up to the highest 5 L/min air flowrate while the negative effect had yet taken dominance at such level of flowrate. Such results indicated a superior scalability of the sparger for higher liquid volume in the same bag volume. The trend of $k_L a$ dependence on flowrates under 5 L with 20 rpm was shown close to the trend discovered under 3 L with 10 rpm and comparable similarity between 5 L with 30 rpm and 3 L with 20 rpm existed as well.

Traditionally when studying the dependence of $k_L a$ on gas flowrate in a stirred tank bioreactor, a semi-empirical power-law model has been applied which exhibited a good fit across various scales. In this study, as it was observed that sparger installed in the bioreactor could contribute to a significant amount of gas-liquid mass transfer capacity, it was reasonable to characterize the dependence of $k_L a$ on superficial gas velocity U_g in the similar manner applied previously for sparged stirred tank or pneumatic driven bioreactors. The first question to be answered was how the U_g was defined for a rocking bioreactor equipped with a porous air sparger. Previous studies characterized the U_g by dividing the total gas volume passing through the gas-liquid interface by the total area of a nominal gas-liquid interface which was connected to the geometrical diameter of the vessel. Such a definition was found to be problematic for application to a rocking bioreactor as the nominal gas-liquid interface area was constantly changing and difficult to be either estimated or measured. To resolve this challenge, an alternative definition of U_g was proposed based on the

division of total air volume passing through the sparger by the effective area A_e of the porous sparger surface which was defined by following equation (4.12):

$$A_e = A_{cylinder} \cdot \emptyset \tag{4.12}$$

The correlation between the ln($k_L a$) and ln(U_g) was plotted in Figure 4-17 to firstly verify the validity of our proposed definition of U_g and secondly to investigate the dependence of $k_L a$ on U_g in the sparger modified rocking bioreactor.

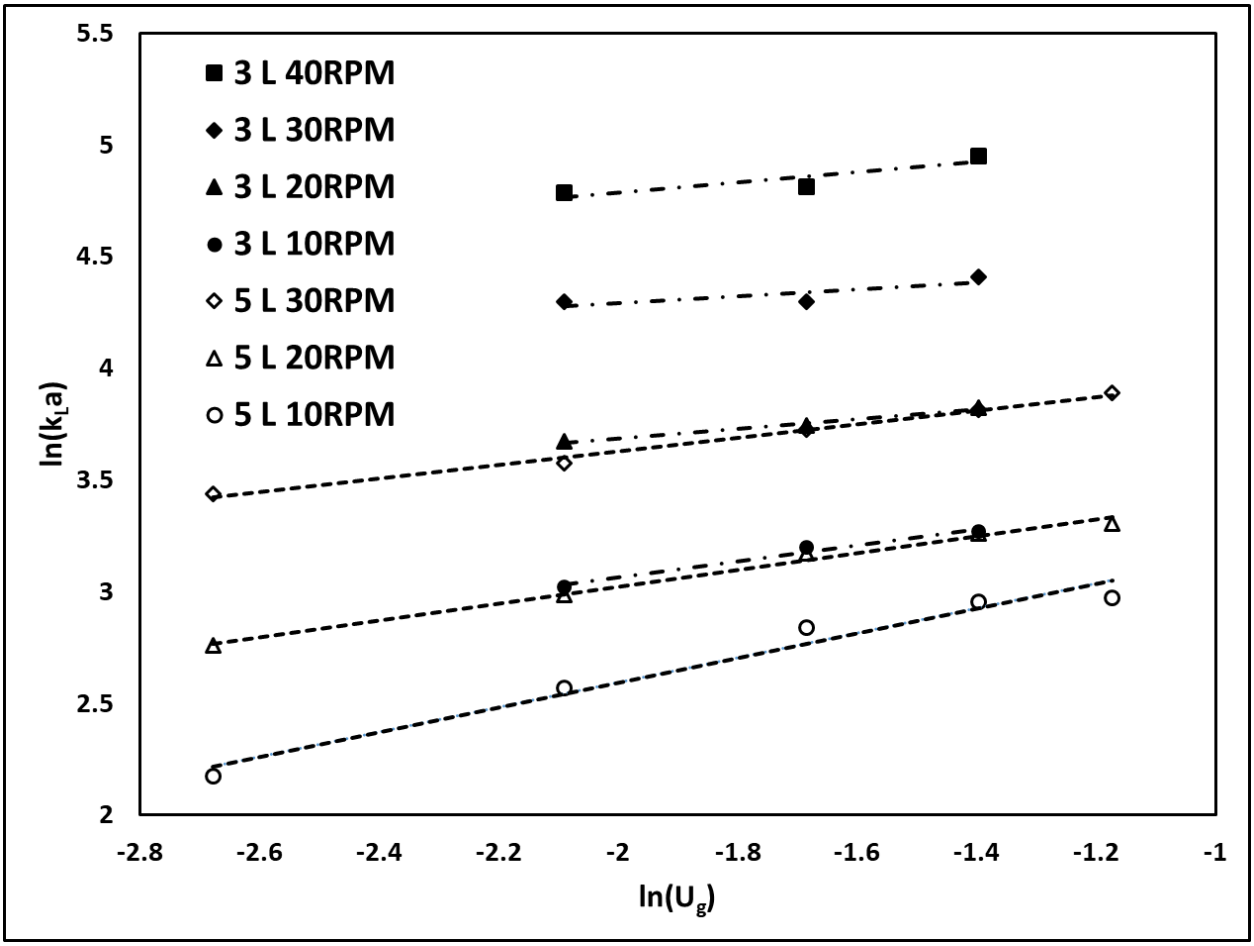

Figure 4-17 A linear regression established between ln($k_L a$) and ln(U_g) for 3 L (dash dot lines) and 5 L (square dot lines) at 10 rpm (sphere), 20 rpm (triangle), 30 rpm (diamond) and 40 rpm (filled square). 5 L at 40 rpm data was not measured due to flooding of filter during experiments.

It was shown in Figure 4-17 that the connection between ln($k_L a$) and ln(U_g) was well characterized by a linear regression model which indicated that the power-law model commonly applied for pneumatic or sparged stirred tank bioreactor might be as well applied for a rocking bioreactor equipped with a porous sparger as long as it contributed the majority of the gas-liquid mass transfer capacity for the bioreactor. Such a linear trend might also validate the proposed definition of superficial gas velocity for the rocking bioreactor with a sparger installed. It should be noticed that while the exponential factor of the power law model for 20 and 30 rpm at 5 L and 10 and 20 rpm at 3 L was uniform, the rest of operational conditions hold significant difference among each other. For 30 and 40 rpm at 3 L liquid volume, such inconsistency could be explained by the wave motion induced impact on the bubble formation on the sparger surface as well as its distribution in the liquid body. The deviation for 10 rpm at 3 L liquid volume might indicate that the power-law model application should take the role of surface aeration as well into consideration. Such influence was insignificant for stirred or airlifted vessel but played a relatively more influential role in the rocking bioreactor, especially when the liquid volume was low and surface area was at its maximum.

4.4.3 The influence of wettability on bubble formation, distribution and subsequently overall $k_L a$ of the bioreactor

An examination on the role of wettability affecting the $k_L a$ was performed based on several prior investigations reporting that bubble sizes in the liquid phase might be related to the wettability of the material surface (Kukizaki and Wada, 2008; Wesley et al., 2016). In this study, the role of wettability was investigated by using 2 spargers with the same geometrical dimensions but different wettability (either hydrophobic or hydrophilic).

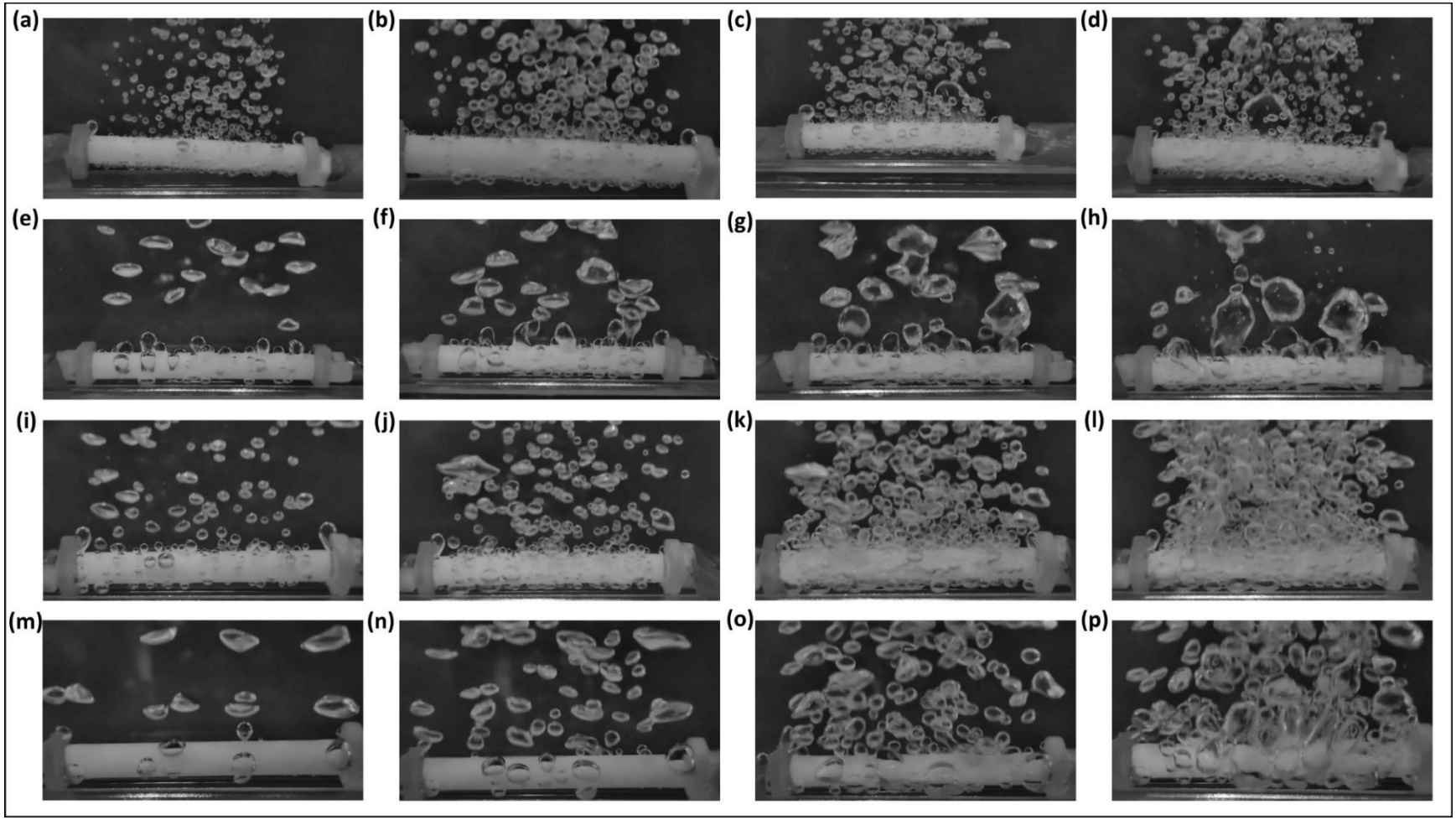

Figure 4-18 Formation of bubbles on a 5 cm long sparger surface and their distribution in the liquid phase under following conditions: (a)-(d) 5 µm hydrophilic sparger with 0.5, 1, 2 and 4 L/min air flow rates; (e)-(h) 5 µm hydrophobic sparger with 0.5, 1, 2 and 4 L/min air flow rates; (i)-(l) 10 µm hydrophobic sparger with 0.5,1,2 and 4 L/min air flow rates; (m)-(p) 50 µm hydrophobic sparger with 0.5, 1, 2 and 4 L/min air flow rates.

Figure 4-18 illustrates in detail the bubble morphology observed on both hydrophobic and hydrophilic sparger surfaces under various flowrates and sparger pore sizes. By comparing Figure 4-18 (e) - (h) with Figure 4-18 (a) - (d), it is seen that despite having the same pore geometry (5 μm d_p), the bubbles formed on the hydrophobic surface tended to coalesce more rapidly on the sparger surface before being released from pores into the aqueous phase. In contrast, bubbles formed on the hydrophilic surface were less likely to coalesce on the surface but were released with a smaller bubble size. Since the initial bubble sizes released from the sparger surfaces were different, their rates of coalescence and break-up in the liquid phase were different as well (Prince and Blanch, 1990). The difference in sparger surface wettability could affect the shape of the bubbles as reflected in Figure 4-18 (a) - (h) which shared the same nominal pore diameter but different wettability. The circularity (defined as $\frac{4\pi A_s}{p^2}$) of the bubbles released from the hydrophilic sparger was distributed densely within 0.85 – 1 while the bubbles from hydrophobic sparger with the same pore size was seen to distribute mostly around 0.75 (data shown in the Appendix). The mean Sauter diameters were 0.61 mm for the 5 μm hydrophilic sparger and 1.04 mm for 10 μm hydrophobic sparger while for 5 μm and 50 μm hydrophobic spargers these values were relatively higher at 1.54 mm and 1.96 mm respectively. Additionally, it was observed that bubbles were attached to the hydrophilic sparger surface for a longer time compared to those formed on the hydrophobic surface before they were released into the liquid. This was probably attributed to the balance of buoyancy against material surface wettability effect and surface tension of the liquid in combination. Such an observation was consistent to previously reported studies on the bubble formation related to wettability of the orifice surface (Lin et al., 1994).

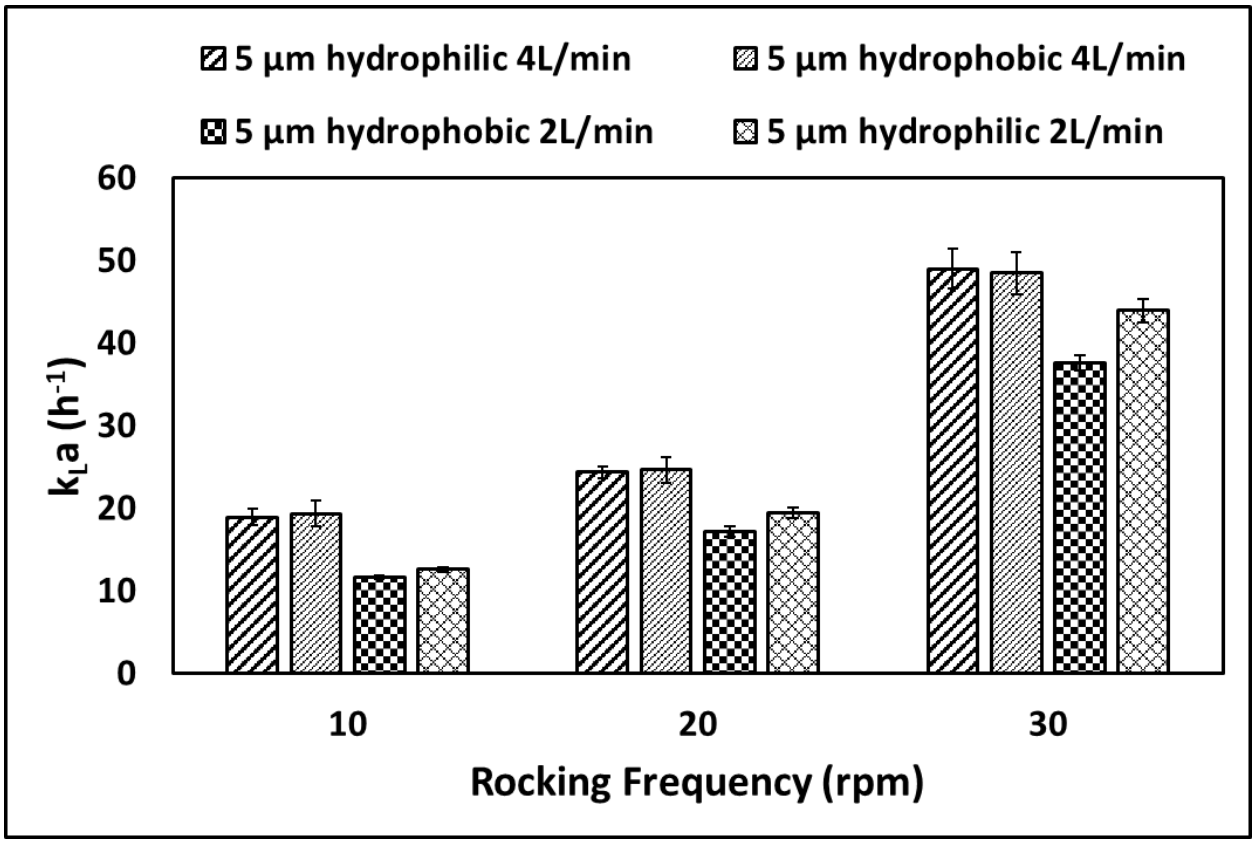

Figure 4-19 k_La of the bioreactor at two different air flowrates with either hydrophobic or hydrophilic sparger installed.

When examining material effects on the macroscopic performance of k_La, it was discovered that the influence of the wettability of the sparger surface would be neutralized by the flow rate as it increased. As shown in Figure 4-19, the k_La value was seen to be affected slightly by the sparger wettability at an air flow rate of 2 L/min. When the air flow rate was increased to 4 L/min, despite the difference in sparger surface wettability, the k_La of the bioreactor no longer exhibited a significant difference. Comparing Figure 4-18 (c) and (d) with Figure 4-18 (g) and (h), despite the distinctive differences in bubble shape and density, the k_La did not show a significant difference.

Meanwhile, the $k_L a$ of various sparger pore sizes illustrated a clear difference between 10 µm and 50 µm spargers but a negligible difference between 5 µm and 10 µm spargers. Both observations indicated that the bubble attachment characteristics, instead of the bubbles' shape, might be the influential factor that directly contributed to the difference in $k_L a$ performance of the sparger. It was noted that previous studies focused on a flow rate ranging from 2.5 to 55 mL/min of a single hole flow rate which corresponds to 0.21 m/s to 4.67 m/s superficial air velocity venting from a single 250 µm diameter pore. In this study, such values fell between 0.07 and 0.25 m/s, based on the characterization of the pore area ratio using X-ray CT scanning and image processing methods.

Chapter 5 Conclusions and Recommendations

5.1 Conclusions

This thesis studied the gas-liquid mass transfer conditions in a rocking disposable bioreactor, revealing important process engineering effects (not previously evaluated comprehensively) in the connection between key mass transfer parameters and the operational parameters of the bioreactor. Conclusions drawn from this study are categorized into four main perspectives related to four major sections in the Results and Discussion chapter.

1. The model developed in Chapter 4.1 accounts for the separate contributions of oxygen gas–liquid mass transfer induced by not only surface aeration but also air entrainment by breaking waves during the back and forth rocking action. The model uses a combination of surface aeration and wave-breaking air entrainment mechanisms adapted from established ocean wave mechanics literature. This way of characterizing the gas–liquid mass transfer in the wave bioreactor is necessary for a comprehensive understanding and prediction of mass transfer in the bioreactor. The $k_L a$ calculated from derived semi-empirical correlations in this mechanistic model was shown to reasonably match the experimentally measured $k_L a$, but under less turbulent conditions (Reynolds number < 15,000) the $k_L a$ was substantially underestimated for some operating conditions. Such deviations require investigation of the flow patterns in more detail, although they appear to be primarily at very low $k_L a$ values which are of less practical importance. It was confirmed from this model that wave-breaking air entrainment and surface aeration each play different roles at various rocking conditions. Surface aeration was shown to account for the majority of gas–liquid mass transfer capacity at lower rocking frequencies and angles, while the air entrainment replaces surface aeration as the dominant contributor to gas-liquid mass transfer capacity as the rocking frequency and angle are increased. A sensitivity test of the model showed that the wave slope and wave phase speed are the two most critical variables affecting the

entrainment of air by the breaking wave. On the basis of the test results, as the wave slope and wave phase speed exceed certain threshold values, the $k_L a$ value increases rapidly which renders theprecise determination of such thresholds important to accurately characterize the gas-liquid mass transfer induced by breaking waves in these bioreactors. By borrowing knowledge from ocean wave mechanism studies, an enhanced understanding of gas-liquid mass transfer mechanism in the rocking disposable bioreactor is formed and this may be applicable and useful for the scale-up and optimization of this disposable bioprocess.

2. The results from Chapter 4.2 indicate that a simple electrical method based on current monitoring at a constant voltage would be a reliable method for measurement of the rocking disposable bioreactor power input. The results were comparable in overall trend of average power inputs to previously reported work using either a CFD technique or a calorimetry method. Additionally, itis suggested that peak power input, is more suitable for characterizing the power input in this type of bioreactor. The peak power input exhibited an oscillatory behavior corresponding to the rocking motion, and the gas-liquid mass transfer was closely correlated with the peak power input. In general, gas-liquid mass transfer was observed to increase and mixing time to decrease with increased power input, as achieved through a combination of increased rocking angle and frequency. Moreover, the trend in the increase of $k_L a$ with specific power input could be approximated empirically by a power-law model. Mixing time was observed to rapidly decrease and stabilized at values generally less than 50 s at the 20 L bag scale once power input reached a level of approximately 400 W/m^3 or higher for an 8^o rocking angle. However, larger rocking angles may increase the mixing time at the same power input through mechanisms that need further examination. These observations are consistent with consideration of the prevailing fluid mechanics conditions.

3. The results from Chapter 4.3 revealed that installing a diagonal cross-over baffle in between the rocking tray and the bioreactor bag could reduce the mixing time (t_m) of the bioreactor. Such a reduction was more significant as the liquid volume increased, or as the rocking frequency decreased. Hence the baffle proved to be most effective at 10 to 20 rpm with liquid volume of 5 and 10 L respectively. This reduction in t_m could be attributed to the diversion of liquid flow from a 1-D direction in alignment with the rocking motion to a more 2-D directions. On the other hand, installing the baffle resulted in a decrease in the $k_L a$, especially as the rocking frequency increased and liquid volume decreased. This is because air entrainment by wave plays a more influential role in mass transfer when the rocking frequency is higher, or the liquid volume is lower. The presence of the baffle diverted part of momentum away from the rocking direction. Although this helps reduce t_m by creating a 2-D mixing pattern, this diverted momentum results in a decreased fluid velocity reaching the edge of bag which undermines the strength of the wave. The dampened strength of the wave reduces air entrainment and leads to a relatively lower $k_L a$ compared with control groups without baffles.

4. Based on the results from Chapter 4.4, it was demonstrated that installing a porous tube sparger in a disposable rocking bioreactor holds the potential for improving the oxygen gas-liquid mass transfer performance of the bioreactor, especially when the rocking intensity (rocking frequency and angle combined) of the bioreactor was mild. The highest achievable $k_L a$ in this work showed comparable or superior performance compared with other major types of bioreactor design, except for sparged stirred tank bioreactor system. The $k_L a$ of the modified bioreactor system exhibited a strong dependence on the gas flow conditions as well as the nominal pore size of the porous

sparger. However, wettability of the porous sparger surface was shown to only slightly affect the sparger performance at low gas flow. As the superficial gas velocity further increased, the difference brought by surface wettability was shown to be negligible.

5.2 Recommendations

Based on the progress and conclusions achieved in this study, the following aspects are recommended for future studies:

1. A further experimental validation of the established $k_L a$ model on a larger scale of rocking disposable bioreactor would help improve the robustness and applicability of the model. The data acquired from a larger-scale bioreactor study could also help validate the power input measurement method and examine the impact of power input on mass transfer capacity of the bioreactor.

2. Animal cells such as CHO or Sf-9 cells could be tested for their growth in the modified rocking disposable bioreactor with both sparger and baffle installed. This could further reveal the leverage between the potential damage induced from bubbles generation on animal cells and the benefits brought by improved t_m and $k_L a$ for cell growth and viable cell density. The presence of a live cell system could reveal the impact of dynamic oxygen consumption on the oxygen transfer capacity of the rocking bioreactor. This could also offer insight on the impact of the suspension fluid properties, such as the effect of lower surface tension due to proteinaceous materials, on t_m and $k_L a$ in a realistic scenario. Other medium components such as salts may affect bubble coalescence, and these effects could be studied as more realistic fermentation media

3. Potential improvements on the sparger design such as pore diameter, pore structure and sparger geometry are worth investigating as adjusting these parameters could potentially generate bubbles with finer diameters as well as more even bubble size distribution and thus further enhance the performance of the sparger such as increasing t_m and $k_L a$ as well as minimizing the extra shear stress brought by bubbling into the media.

4. A modified rocking disposable bioreactor could be combined with other process techniques such as microcarrier or perfusion cultivations. Microcarriers could support the growth of adherent cells or cells susceptible to shear stress in the rocking bioreactor and a perfusion process could enhance the cell density and productivity in a single batch. The improved mass transfer capacity achieved in this study could possibly further boost the performance of the bioreactor when coupled with these process intensification techniques.

Bibliography

Altaras, G.M., Eklund, C., Ranucci, C., Maheshwari, G., 2007. Quantitation of interaction of lipids with polymer surfaces in cell culture. Biotechnol. Bioeng. 96, 999–1007. https://doi.org/10.1002/bit.21171

Amer, M., Feng, Y., Ramsey, J.D., 2019. Using CFD simulations and statistical analysis to correlate oxygen mass transfer coefficient to both geometrical parameters and operating conditions in a stirred-tank bioreactor. Biotechnol. Prog. 35, 1–14. https://doi.org/10.1002/btpr.2785

Ansoni, J.L., Seleghim, P., 2016. Optimal industrial reactor design: Development of a multiobjective optimization method based on a posteriori performance parameters calculated from CFD flow solutions. Adv. Eng. Softw. 91, 23–35. https://doi.org/10.1016/j.advengsoft.2015.08.008

Arnold, L., Lee, K., Rucker-Pezzini, J., Lee, J.H., 2019. Implementation of Fully Integrated Continuous Antibody Processing: Effects on Productivity and COGm. Biotechnol. J. 14, 1–10. https://doi.org/10.1002/biot.201800061

Ascanio, G., Castro, B., Galindo, E., 2004. Measurement of power consumption in stirred vessels-a review. Chem. Eng. Res. Des. 82, 1282–1290. https://doi.org/10.1205/cerd.82.9.1282.44164

Bai, Y., Moo-Young, M., Anderson, W.A., 2019. A mechanistic model for gas–liquid mass transfer prediction in a rocking disposable bioreactor. Biotechnol. Bioeng. 116, 1986–1998. https://doi.org/10.1002/bit.27000

Bajgain, P., Mucharla, R., Wilson, J., Welch, D., Anurathapan, U., Liang, B., Lu, X., Ripple, K., Centanni, J.M., Hall, C., Hsu, D., Couture, L.A., Gupta, S., Gee, A.P., Heslop, H.E., Leen, A.M., Rooney, C.M., Vera, J.F., 2014. Optimizing the production of suspension cells using the G-Rex M series. Mol. Ther. - Methods Clin. Dev. 1, 14015.

https://doi.org/10.1038/mtm.2014.15

Bandyopadhyay, B., Humphrey, A.E., Taguchi, H., 1967. Dynamic measurement of the volumetric oxygen transfer coefficient in fermentation systems. Biotechnol. Bioeng. 9, 533–544. https://doi.org/10.1002/bit.260090408

Blenkinsopp, C.E., Chaplin, J.R., 2007. Void fraction measurements in breaking waves. Proc. R. Soc. A Math. Phys. Eng. Sci. 463, 3151–3170. https://doi.org/10.1098/rspa.2007.1901

Büchs, J., Lotter, S., Milbradt, C., 2001. Out-of-phase operating conditions, a hitherto unknown phenomenon in shaking bioreactors. Biochem. Eng. J. 7, 135–141. https://doi.org/10.1016/S1369-703X(00)00113-3

Bunnak, P., Allmendinger, R., Ramasamy, S. V., Lettieri, P., Titchener-Hooker, N.J., 2016. Life-cycle and cost of goods assessment of fed-batch and perfusion-based manufacturing processes for mAbs. Biotechnol. Prog. 32, 1324–1335. https://doi.org/10.1002/btpr.2323

Cataldo, A.L., Burgstaller, D., Hribar, G., Jungbauer, A., Satzer, P., 2020. Economics and ecology: Modelling of continuous primary recovery and capture scenarios for recombinant antibody production. J. Biotechnol. 308, 87–95. https://doi.org/10.1016/j.jbiotec.2019.12.001

Chisti, Y., Jauregui-Haza, U.J., 2002. Oxygen transfer and mixing in mechanically agitated airlift bioreactors, Biochemical Engineering Journal.

Cirés, S., Alvarez-Roa, C., Heimann, K., 2015. First use of the WAVE^{TM} disposable rocking bioreactor for enhanced bioproduct synthesis by N2-fixing cyanobacteria. Biotechnol. Bioeng. 112, 621–626. https://doi.org/10.1002/bit.25455

Clincke, M.-F.F., Mölleryd, C., Samani, P.K., Lindskog, E., Fäldt, E., Walsh, K., Chotteau, V., 2013a. Very high density of Chinese hamster ovary cells in perfusion by alternating

tangential flow or tangential flow filtration in WAVE bioreactor™-part II: Applications for antibody production and cryopreservation. Biotechnol. Prog. 29, 768–777. https://doi.org/10.1002/btpr.1703

Clincke, M.-F.F., Mölleryd, C., Zhang, Y., Lindskog, E., Walsh, K., Chotteau, V., 2013b. Very high density of CHO cells in perfusion by ATF or TFF in WAVE bioreactor™: Part I: Effect of the cell density on the process. Biotechnol. Prog. 29, 754–767. https://doi.org/10.1002/btpr.1704

Coronel, J., Behrendt, I., Bürgin, T., Anderlei, T., Sandig, V., Reichl, U., Genzel, Y., 2019. Influenza A virus production in a single-use orbital shaken bioreactor with ATF or TFF perfusion systems. Vaccine 37, 7011–7018. https://doi.org/10.1016/j.vaccine.2019.06.005

Danckwerts, P. V., 1951. Significance of Liquid-Film Coefficients in Gas Absorption. Ind. Eng. Chem. 43, 1460–1467. https://doi.org/10.1021/ie50498a055

de Sá da Silva, J., Mizukami, A., Gonzalez Gil, L. V., Valeria de Campos, J., B.G. Assis, O., Tadeu Covas, D., Swiech, K., Torres Suazo, C.A., 2019. Improving wave-induced motion bioreactor performance for human mesenchymal stromal cell expansion. Process Biochem. 84, 143–152. https://doi.org/10.1016/j.procbio.2019.06.004

de Sousa Pinto, D., Bandeiras, C., de Almeida Fuzeta, M., Rodrigues, C.A.V., Jung, S., Hashimura, Y., Tseng, R.J., Milligan, W., Lee, B., Ferreira, F.C., Lobato da Silva, C., Cabral, J.M.S., 2019. Scalable Manufacturing of Human Mesenchymal Stromal Cells in the Vertical-Wheel Bioreactor System: An Experimental and Economic Approach. Biotechnol. J. 14, 1–9. https://doi.org/10.1002/biot.201800716

Decarli, M.C., dos Santos, D.P., Astray, R.M., Ventini-Monteiro, D.C., Jorge, S.A.C., Correia, D.M., de Sá da Silva, J., Rocca, M.P., Langoni, H., Menozzi, B.D., Pereira, C.A., Suazo, C.A.T., 2018. DROSOPHILA S2 cell culture in a WAVE Bioreactor:

potential for scaling up the production of the recombinant rabies virus glycoprotein. Appl. Microbiol. Biotechnol. 102, 4773–4783. https://doi.org/10.1007/s00253-018-8962-0

Deike, L., Melville, W.K., Popinet, S., 2016. Air entrainment and bubble statistics in breaking waves. J. Fluid Mech. 801, 91–129. https://doi.org/10.1017/jfm.2016.372

Delafosse, A., Calvo, S., Collignon, M.-L., Toye, D., 2018. Comparison of hydrodynamics in standard stainless steel and single-use bioreactors by means of an Euler-Lagrange approach. Chem. Eng. Sci. 188, 52–64. https://doi.org/10.1016/J.CES.2018.01.034

Ding, W., 2013. Determination of Extractables and Leachables from Single-Use Systems. Chemie Ing. Tech. 85, 186–196. https://doi.org/10.1002/cite.201200113

Dorival-García, Noemí, Bones, J., 2017. Evaluation of solvent systems for optimized extractables studies of single use bioprocessing solutions. J. Chromatogr. A 1513, 69–77. https://doi.org/10.1016/j.chroma.2017.06.066

Dorival-García, N., Bones, J., 2017. Monitoring leachables from single-use bioreactor bags for mammalian cell culture by dispersive liquid-liquid microextraction followed by ultra high performance liquid chromatography quadrupole time of flight mass spectrometry. J. Chromatogr. A 1512, 51–60. https://doi.org/10.1016/J.CHROMA.2017.06.077

Dorival-García, N., Carillo, S., Ta, C., Roberts, D., Comstock, K., Lofthouse, S., Ciceri, E., D'Silva, K., Kierans, G., Kaisermayer, C., Lindeberg, A., Bones, J., 2018. Large-Scale Assessment of Extractables and Leachables in Single-Use Bags for Biomanufacturing. Anal. Chem. 90, 9006–9015. https://doi.org/10.1021/acs.analchem.8b01208

Dreher, T., Dreher, T., Husemann, U., Zahnow, C., Wilde, D. De, Adams, T., Greller, G., de Wilde, D., Adams, T., Greller, G., 2013. High Cell Density Escherichia coli Cultivation in Different Single-Use Bioreactor Systems. Chemie Ing. Tech. 85, 162–171. https://doi.org/10.1002/cite.201200122

Dreher, T., Husemann, U., Adams, T., de Wilde, D., Greller, G., 2014a. Design space definition for a stirred single-use bioreactor family from 50 to 2000 L scale. Eng. Life Sci. 14, 304–310. https://doi.org/10.1002/elsc.201300067

Dreher, T., Walcarius, B., Husemann, U., Klingenberg, F., Zahnow, C., Adams, T., de Wilde, D., Casteels, P., Greller, G., 2014b. Microbial High Cell Density Fermentations in a Stirred Single-Use Bioreactor, in: Eibl, D., Eibl, R. (Eds.), Disposable Bioreactors II. Springer Berlin Heidelberg, Berlin, Heidelberg, pp. 127–147. https://doi.org/10.1007/10_2013_189

Ducci, A., Weheliye, W.H., 2014. Orbitally shaken bioreactors-viscosity effects on flow characteristics. AIChE J. 60, 3951–3968. https://doi.org/10.1002/aic.14608

Duncan, J.H., 1981. An Experimental Investigation of Breaking Waves Produced by a Towed Hydrofoil. Proc. R. Soc. Lond. A. Math. Phys. Sci. https://doi.org/10.2307/2397189

Eibl, R., Eibl, D., 2008. Design And Use Of The Wave Bioreactor For Plant Cell Culture, in: Plan Tissue Culture Engineering. Springer Netherlands, Dordrecht, pp. 203–227. https://doi.org/10.1007/978-1-4020-3694-1_12

Eibl, R., Kaiser, S., Lombriser, R., Eibl, D., 2010a. Disposable bioreactors: The current state-of-the-art and recommended applications in biotechnology. Appl. Microbiol. Biotechnol. 86, 41–49. https://doi.org/10.1007/s00253-009-2422-9

Eibl, R., Werner, S., Eibl, D., 2010b. Bag bioreactor based on wave-induced motion: Characteristics and applications. Adv. Biochem. Eng. Biotechnol. 115, 55–87. https://doi.org/10.1007/10_2008_15

Emmerling, V. V., Pegel, A., Milian, E.G., Venereo-Sanchez, A., Kunz, M., Wegele, J., Kamen, A.A., Kochanek, S., Hoerer, M., 2016. Rational plasmid design and bioprocess optimization to enhance recombinant adeno-associated virus (AAV) productivity in

mammalian cells. Biotechnol. J. 11, 290–297. https://doi.org/10.1002/biot.201500176

Farid, S.S., Washbrook, J., Titchener-Hooker, N.J., 2008. Combining Multiple Quantitative and Qualitative Goals When Assessing Biomanufacturing Strategies under Uncertainty. Biotechnol. Prog. 21, 1183–1191. https://doi.org/10.1021/bp050070f

Farid, S.S., Washbrook, J., Titchener-Hooker, N.J., 2005. Decision-support tool for assessing biomanufacturing strategies under uncertainty: Stainless steel versus disposable equipment for clinical trial material preparation. Biotechnol. Prog. 21, 486–497. https://doi.org/10.1021/bp049692b

Fortescue, G.E., Pearson, J.R.A., 1967. On gas absorption into a turbulent liquid. Chem. Eng. Sci. 22, 1163–1176. https://doi.org/10.1016/0009-2509(67)80183-0

Gagliardi, C., Khalil, M., Foster, A.E., 2019. Streamlined production of genetically modified T cells with activation, transduction and expansion in closed-system G-Rex bioreactors. Cytotherapy 21, 1246–1257. https://doi.org/10.1016/j.jcyt.2019.10.006

Garcia-Ochoa, F., Gomez, E., 2009. Bioreactor scale-up and oxygen transfer rate in microbial processes: An overview. Biotechnol. Adv. 27, 153–176. https://doi.org/10.1016/J.BIOTECHADV.2008.10.006

Garcia-Ochoa, F., Gomez, E., Santos, V.E., Merchuk, J.C., 2010. Oxygen uptake rate in microbial processes: An overview. Biochem. Eng. J. 49, 289–307. https://doi.org/10.1016/j.bej.2010.01.011

George, M., Farooq, M., Dang, T., Cortes, B., Liu, J., Maranga, L., 2010. Production of cell culture (MDCK) derived Live Attenuated Influenza Vaccine (LAIV) in a fully disposable platform process. Biotechnol. Bioeng. 106, 906–917. https://doi.org/10.1002/bit.22753

Ghasemi, A., Bozorg, A., Rahmati, F., Mirhassani, R., Hosseininasab, S., 2019. Comprehensive study on Wave bioreactor system to scale up the cultivation of and

recombinant protein expression in baculovirus-infected insect cells. Biochem. Eng. J. 143, 121–130. https://doi.org/10.1016/J.BEJ.2018.12.011

Glazyrina, J., Materne, E.M., Dreher, T., Storm, D., Junne, S., Adams, T., Greller, G., Neubauer, P., 2010. High cell density cultivation and recombinant protein production with Escherichia coli in a rocking-motion-type bioreactor. Microb. Cell Fact. 9, 42. https://doi.org/10.1186/1475-2859-9-42

Gottschalk, U., Brorson, K., Shukla, A.A., 2012. The need for innovation in biomanufacturing. Nat. Biotechnol. 30, 489–492. https://doi.org/10.1038/nbt.2263

Grein, T.A., Leber, J., Blumenstock, M., Petry, F., Weidner, T., Salzig, D., Czermak, P., 2016. Multiphase mixing characteristics in a microcarrier-based stirred tank bioreactor suitable for human mesenchymal stem cell expansion. Process Biochem. 51, 1109–1119. https://doi.org/10.1016/j.procbio.2016.05.010

Hadjiev, D., Sabiri, N.E., Zanati, A., 2006. Mixing time in bioreactors under aerated conditions. Biochem. Eng. J. 27, 323–330. https://doi.org/10.1016/J.BEJ.2005.08.009

Hammond, M., Marghitoiu, L., Lee, H., Perez, L., Rogers, G., Nashed-Samuel, Y., Nunn, H., Kline, S., 2014. A cytotoxic leachable compound from single-use bioprocess equipment that causes poor cell growth performance. Biotechnol. Prog. 30, 332–337. https://doi.org/10.1002/btpr.1869

Hammond, M., Nunn, H., Rogers, G., Lee, H., Marghitoiu, A.-L., Perez, L., Nashed-Samuel, Y., Anderson, C., Vandiver, M., Kline, S., 2013. Identification of a Leachable Compound Detrimental to Cell Growth in Single-Use Bioprocess Containers. PDA J. Pharm. Sci. Technol. 67, 123–134. https://doi.org/10.5731/pdajpst.2013.00905

Hanley, P.J., Mei, Z., Durett, A.G., da Graca Cabreira-Harrison, M., Klis, M., Li, W., Zhao, Y., Yang, B., Parsha, K., Mir, O., Vahidy, F., Bloom, D., Rice, R.B., Hematti, P., Savitz, S.I., Gee, A.P., 2014. Efficient manufacturing of therapeutic mesenchymal

stromal cells with the use of the Quantum Cell Expansion System. Cytotherapy 16, 1048–1058. https://doi.org/10.1016/j.jcyt.2014.01.417

Heshusius, S., Heideveld, E., Burger, P., Thiel-Valkhof, M., Sellink, E., Varga, E., Ovchynnikova, E., Visser, A., Martens, J.H.A., von Lindern, M., van den Akker, E., 2019. Large-scale in vitro production of red blood cells from human peripheral blood mononuclear cells. Blood Adv. 3, 3337–3350. https://doi.org/10.1182/bloodadvances.2019000689

Higbie, R., 1935. The rate of absorption of a pure gas into still liquid during short periods of exposure. Inst. Chem. Eng. 35, 36–60. https://doi.org/10.1017/CBO9780511805134.010

Hillig, F., Annemüller, S., Chmielewska, M., Pilarek, M., Junne, S., Neubauer, P., 2013. Bioprocess development in single-use systems for heterotrophic marine microalgae. Chemie-Ingenieur-Technik 85, 153–161. https://doi.org/10.1002/cite.201200143

Ikonomou, L., Schneider, Y.J., Agathos, S.N., 2003. Insect cell culture for industrial production of recombinant proteins. Appl. Microbiol. Biotechnol. 62, 1–20. https://doi.org/10.1007/s00253-003-1223-9

Imseng, N., Steiger, N., Frasson, D., Sievers, M., Tappe, A., Greller, G., Eibl, D., Eibl, R., 2014. Single-use wave-mixed versus stirred bioreactors for insect-cell / BEVS-based protein expression at benchtop scale. Eng. Life Sci. 14, 264–271. https://doi.org/10.1002/elsc.201300131

Ishii-Watabe, A., Hirose, A., Katori, N., Hashii, N., Arai, S., Awatsu, H., Eiza, A., Hara, Y., Hattori, H., Inoue, T., Isono, T., Iwakura, M., Kajihara, D., Kasahara, N., Matsuda, H., Murakami, S., Nakagawa, T., Okumura, T., Omasa, T., Takuma, S., Terashima, I., Tsukahara, M., Tsutsui, M., Yano, T., Kawasaki, N., 2015. Approaches to Quality Risk Management When Using Single-Use Systems in the Manufacture of Biologics. AAPS PharmSciTech 16, 993–1001. https://doi.org/10.1208/s12249-015-0368-z

Janakiraman, V., Kwiatkowski, C., Kshirsagar, R., Ryll, T., Huang, Y.M., 2015. Application of high-throughput mini-bioreactor system for systematic scale-down modeling, process characterization, and control strategy development. Biotechnol. Prog. 31, 1623–1632. https://doi.org/10.1002/btpr.2162

Jenke, D.R., Zietlow, D., Garber, M.J., Sadain, S., Reiber, D., Terbush, W., 2007. Accumulation of organic compounds leached from plastic materials used in biopharmaceutical process containers. PDA J. Pharm. Sci. Technol. 61, 286–302.

Jenkins, M.J., Farid, S.S., 2018. Cost-effective bioprocess design for the manufacture of allogeneic CAR-T cell therapies using a decisional tool with multi-attribute decision-making analysis. Biochem. Eng. J. 137, 192–204. https://doi.org/10.1016/j.bej.2018.05.014

Jones, S.M.J., Louw, T.M., Harrison, S.T.L., 2017. Energy consumption due to mixing and mass transfer in a wave photobioreactor. Algal Res. 24, 317–324. https://doi.org/10.1016/J.ALGAL.2017.03.001

Jorjani, P., Ozturk, S.S., 1999. Effects of cell density and temperature on oxygen consumption rate for different mammalian cell lines. Biotechnol. Bioeng. 64, 349–356. https://doi.org/10.1002/(SICI)1097-0290(19990805)64:3<349::AID-BIT11>3.0.CO;2-V

Junne, S., Solymosi, T., Oosterhuis, N., Neubauer, P., 2013. Cultivation of cells and microorganisms in wave-mixed disposable bag bioreactors at different scales. Chemie-Ingenieur-Technik 85, 57–66. https://doi.org/10.1002/cite.201200149

Kadarusman, J., Bhatia, R., McLaughlin, J., Lin, W.R., 2005. Growing Cholesterol-Dependent NS0 Myeloma Cell Line in the Wave Bioreactor System: Overcoming Cholesterol-Polymer Interaction by Using Pretreated Polymer or Inert Fluorinated Ethylene Propylene. Biotechnol. Prog. 21, 1341–1346. https://doi.org/10.1021/BP050091+

Kadic, E., Heindel, T.J., 2014. An Introduction to Bioreactor Hydrodynamics and Gas-Liquid Mass Transfer, An Introduction to Bioreactor Hydrodynamics and Gas-Liquid Mass Transfer. https://doi.org/10.1002/9781118869703

Kaiser, S.C., Eibl, R., Eibl, D., 2011. Engineering characteristics of a single-use stirred bioreactor at bench-scale: The Mobius CellReady 3L bioreactor as a case study. Eng. Life Sci. 11, 359–368. https://doi.org/10.1002/elsc.201000171

Kaiser, S.C., Werner, S., Jossen, V., Kraume, M., Eibl, D., 2017. Development of a method for reliable power input measurements in conventional and single-use stirred bioreactors at laboratory scale. Eng. Life Sci. 17, 500–511. https://doi.org/10.1002/elsc.201600096

Kalmbach, A., Genzel, Y., Reichl, U., Bordás, R., Öncül, A.A., Thévenin, D., Genzel, Y., Reichl, U., 2011. Experimental Characterization of Flow Conditions in 2- and 20-L Bioreactors with Wave-Induced Motion. Biotechnol. Prog. 27, 402–409. https://doi.org/10.1002/btpr.516

Kawase, Y., Moo-Young, M., 1989. Mixing time in bioreactors. J. Chem. Technol. Biotechnol. 44, 63–75. https://doi.org/10.1002/jctb.280440107

Kelley, B., 2009. Industrialization of mAb production technology: The bioprocessing industry at a crossroads. MAbs 1, 443–452. https://doi.org/10.4161/mabs.1.5.9448

Kelly, P.S., Dorival-García, N., Paré, S., Carillo, S., Ta, C., Alarcon Miguez, A., Coleman, O., Harper, E., Shannon, M., Henry, M., Connolly, L., Clynes, M., Meleady, P., Bones, J., Barron, N., 2019. Improvements in single-use bioreactor film material composition leads to robust and reliable Chinese hamster ovary cell performance. Biotechnol. Prog. 35. https://doi.org/10.1002/btpr.2824

Kelly, W., Veigne, S., Li, X., Subramanian, S.S., Huang, Z., Schaefer, E., 2018. Optimizing performance of semi-continuous cell culture in an ambr15^{TM} microbioreactor using dynamic flux balance modeling. Biotechnol. Prog. 34, 420–431.

https://doi.org/10.1002/btpr.2585

Kim, J.C., Seong, J.H., Lee, B., Hashimura, Y., Groux, D., Oh, D.J., 2013. Evaluation of a novel pneumatic bioreactor system for culture of recombinant Chinese hamster ovary cells. Biotechnol. Bioprocess Eng. 18, 801–807. https://doi.org/10.1007/s12257-012-0558-4

Klöckner, W., Diederichs, S., Büchs, J., 2013a. Orbitally Shaken Single-Use Bioreactors, in: Advances in Biochemical Engineering/Biotechnology. pp. 45–60. https://doi.org/10.1007/10_2013_188

Klöckner, W., Gacem, R., Anderlei, T., Raven, N., Schillberg, S., Lattermann, C., Büchs, J., 2013b. Correlation between mass transfer coefficient kLa and relevant operating parameters in cylindrical disposable shaken bioreactors on a bench-to-pilot scale. J. Biol. Eng. 7, 1–14. https://doi.org/10.1186/1754-1611-7-28

Klöckner, W., Tissot, S., Wurm, F., Büchs, J., 2012. Power input correlation to characterize the hydrodynamics of cylindrical orbitally shaken bioreactors. Biochem. Eng. J. 65, 63–69. https://doi.org/10.1016/j.bej.2012.04.007

Kreye, S., Stahn, R., Nawrath, K., Goralczyk, V., Zoro, B., Goletz, S., 2019. A novel scale-down mimic of perfusion cell culture using sedimentation in an automated microbioreactor (SAM). Biotechnol. Prog. 35, 1–11. https://doi.org/10.1002/btpr.2832

Kropp, C., Kempf, H., Halloin, C., Robles-Diaz, D., Franke, A., Scheper, T., Kinast, K., Knorpp, T., Joos, T.O., Haverich, A., Martin, U., Zweigerdt, R., Olmer, R., 2016. Impact of Feeding Strategies on the Scalable Expansion of Human Pluripotent Stem Cells in Single-Use Stirred Tank Bioreactors. Stem Cells Transl. Med. 5, 1289–1301. https://doi.org/10.5966/sctm.2015-0253

Kuiper, M., Spencer, C., Fäldt, E., Vuillemez, A., Holmes, W., Samuelsson, T., Gruber, D., Castan, A., 2019. Repurposing fed-batch media and feeds for highly productive CHO

perfusion processes. Biotechnol. Prog. 35. https://doi.org/10.1002/btpr.2821

Kukizaki, M., Wada, T., 2008. Effect of the membrane wettability on the size and size distribution of microbubbles formed from Shirasu-porous-glass (SPG) membranes. Colloids Surfaces A Physicochem. Eng. Asp. https://doi.org/10.1016/j.colsurfa.2007.10.005

Kurt, T., Marbà-Ardébol, A.-M., Turan, Z., Neubauer, P., Junne, S., Meyer, V., 2018. Rocking Aspergillus: morphology-controlled cultivation of Aspergillus niger in a wave-mixed bioreactor for the production of secondary metabolites. Microb. Cell Fact. 17, 128. https://doi.org/10.1186/s12934-018-0975-y

Kwon, J., Yang, Y., Cheon, S., Nam, H., Jin, G., Kim, D., 2013. Bioreactor engineering using disposable technology for enhanced production of hCTLA4Ig in transgenic rice cell cultures. Biotechnol. Bioeng. 110, 2412–2424. https://doi.org/10.1002/bit.24916

Lamarre, E., Melville, W.K., 1991. Air entrainment and dissipation in breaking waves. Nature 351, 469–472. https://doi.org/10.1038/351469a0

Lambrechts, T., Papantoniou, I., Viazzi, S., Bovy, T., Schrooten, J., Luyten, F.P., Aerts, J.M., 2016. Evaluation of a monitored multiplate bioreactor for large-scale expansion of human periosteum derived stem cells for bone tissue engineering applications. Biochem. Eng. J. 108, 58–68. https://doi.org/10.1016/j.bej.2015.07.015

Lamont, J.C., Scott, D.S., 1970. An eddy cell model of mass transfer into the surface of a turbulent liquid. AIChE J. 16, 513–519. https://doi.org/10.1002/aic.690160403

Lang, H.J., 1947. Cost relationships in preliminary cost estimation. Chem. Eng 54, 27.

Langer, E.S., Rader, R.A., 2014. Single-use technologies in biopharmaceutical manufacturing: A 10-year review of trends and the future. Eng. Life Sci. 14, 238–243. https://doi.org/10.1002/elsc.201300090

Larena, A., Pinto, G., 1991. Analysis of the relationship between surface roughness and

reflectometrical measurement of polyethylene films. Mater. Lett. 11, 309–311. https://doi.org/10.1016/0167-577X(91)90209-O

Lawson, T., Kehoe, D.E., Schnitzler, A.C., Rapiejko, P.J., Der, K.A., Philbrick, K., Punreddy, S., Rigby, S., Smith, R., Feng, Q., Murrell, J.R., Rook, M.S., 2017. Process development for expansion of human mesenchymal stromal cells in a 50 L single-use stirred tank bioreactor. Biochem. Eng. J. 120, 49–62. https://doi.org/10.1016/J.BEJ.2016.11.020

Lee, B., Fang, D., Croughan, M., Carrondo, M., Paik, S.-H., 2011. Characterization of novel pneumatic mixing for single-use bioreactor application. BMC Proc. 5, O12. https://doi.org/10.1186/1753-6561-5-S8-O12

Lehmann, N., Dittler, I., Lämsä, M., Ritala, A., Rischer, H., Eibl, D., Oksman-Caldentey, K.-M., Eibl, R., 2014. Disposable Bioreactors for Cultivation of Plant Cell Cultures, in: Production of Biomass and Bioactive Compounds Using Bioreactor Technology. Springer Netherlands, Dordrecht, pp. 17–46. https://doi.org/10.1007/978-94-017-9223-3_2

Leinonen, H.M., Lipponen, E.M., Valkama, A.J., Hynynen, H., Oruetxebarria, I., Turkki, V., Olsson, V., Kurkipuro, J., Samaranayake, H., Määttä, A.M., Parker, N.R., Ylä-Herttuala, S., Lesch, H.P., 2019. Preclinical Proof-of-Concept, Analytical Development, and Commercial Scale Production of Lentiviral Vector in Adherent Cells. Mol. Ther. - Methods Clin. Dev. 15, 63–71. https://doi.org/10.1016/j.omtm.2019.08.006

Li, F., Shen, A., Amanullah, A., 2013. Cell Culture Processes in Monoclonal Antibody Production, in: Pharmaceutical Sciences Encyclopedia. John Wiley & Sons, Inc., Hoboken, NJ, USA, pp. 1–38. https://doi.org/10.1002/9780470571224.pse506

Li, G., Li, H., Wei, G., He, X., Xu, S., Chen, K., Ouyang, P., Ji, X., 2018. Hydrodynamics, mass transfer and cell growth characteristics in a novel microbubble stirred bioreactor

employing sintered porous metal plate impeller as gas sparger. Chem. Eng. Sci. 192, 665–677. https://doi.org/10.1016/j.ces.2018.08.025

Lin, J.N., Banerji, S.K., Yasuda, H., 1994. Role of Interfacial Tension in the Formation and the Detachment of Air Bubbles. 1. A Single Hole on a Horizontal Plane Immersed in Water. Langmuir 10, 936–942. https://doi.org/10.1021/la00015a054

Liu, C.M., Hong, L.N., 2001. Development of a shaking bioreactor system for animal cell cultures. Biochem. Eng. J. 7, 121–125. https://doi.org/10.1016/S1369-703X(00)00111-X

Löffelholz, C., Kaiser, S.C., Kraume, M., Eibl, R., Eibl, D., 2014. Dynamic Single-Use Bioreactors Used in Modern Liter- and m3- Scale Biotechnological Processes: Engineering Characteristics and Scaling Up, in: Eibl, D., Eibl, R. (Eds.), Disposable Bioreactors II. Springer Berlin Heidelberg, Berlin, Heidelberg, pp. 1–44. https://doi.org/10.1007/10_2013_187

Lopes, A.G., 2015. Single-use in the biopharmaceutical industry: A review of current technology impact, challenges and limitations. Food Bioprod. Process. 93, 98–114. https://doi.org/10.1016/j.fbp.2013.12.002

Lu, J. Te, Chung, Y.C., Chan, Z.R., Hu, Y.C., 2005. A novel oscillating bioreactor BelloCell: Implications for insect cell culture and recombinant protein production. Biotechnol. Lett. 27, 1059–1065. https://doi.org/10.1007/s10529-005-8450-3

Maier, U., Büchs, J., 2001. Characterisation of the gas-liquid mass transfer in shaking bioreactors, Biochemical Engineering Journal.

Maltby, R., Tian, S., Chew, Y.M.J., 2018. Computational studies of a novel magnetically driven single-use-technology bioreactor: A comparison of mass transfer models. Chem. Eng. Sci. 187, 157–173. https://doi.org/10.1016/J.CES.2018.05.006

Marghitoiu, L., Liu, J., Lee, H., Perez, L., Fujimori, K., Ronk, M., Hammond, M.R., Nunn,

H., Lower, A., Rogers, G., Nashed-Samuel, Y., 2015. Extractables Analysis of Single-Use Flexible Plastic Biocontainers. PDA J. Pharm. Sci. Technol. 69, 49–58. https://doi.org/10.5731/pdajpst.2015.01001

Marsh, D.T.J., Lye, G.J., Micheletti, M., Odeleye, A.O.O., Ducci, A., Osborne, M.D., Lilly, E., 2017. Fluid dynamic characterization of a laboratory scale rocked bag bioreactor. AIChE J. 63, 4177–4187. https://doi.org/10.1002/aic.15734

McCready, M.J., Vassiliadou, E., Hanratty, T.J., 1986. Computer simulation of turbulent mass transfer at a mobile interface. AIChE J. 32, 1108–1115. https://doi.org/10.1002/aic.690320707

McKenzie, E.A., Abbott, W.M., 2018. Expression of recombinant proteins in insect and mammalian cells. Methods 147, 40–49. https://doi.org/10.1016/j.ymeth.2018.05.013

Mennan, C., Garcia, J., Roberts, S., Hulme, C., Wright, K., 2019. A comprehensive characterisation of large-scale expanded human bone marrow and umbilical cord mesenchymal stem cells. Stem Cell Res. Ther. 10, 99. https://doi.org/10.1186/s13287-019-1202-4

Mikola, M., Seto, J., Amanullah, A., 2007. Evaluation of a novel Wave Bioreactor® cellbag for aerobic yeast cultivation. Bioprocess Biosyst. Eng. 30, 231–241. https://doi.org/10.1007/s00449-007-0119-y

Minow, B., Seidemann, J., Tschoepe, S., Gloeckner, A., Neubauer, P., 2014a. Harmonization and characterization of different single-use bioreactors adopting a new sparger design 272–282. https://doi.org/10.1002/elsc.201300130

Minow, B., Tschoepe, S., Regner, A., Populin, M., Reiser, S., Noack, C., Neubauer, P., 2014b. Biological performance of two different 1000 L single-use bioreactors applying a simple transfer approach. Eng. Life Sci. 14, 283–291. https://doi.org/10.1002/elsc.201300147

Monteil, D.T., Shen, X., Tontodonati, G., Baldi, L., Hacker, D.L., Wurm, F.M., 2016. Disposable orbitally shaken TubeSpin bioreactor 600 for Sf9 cell cultivation in suspension. Anal. Biochem. 505, 26–28. https://doi.org/10.1016/j.ab.2016.04.009

Monteil, D.T., Tontodonati, G., Ghimire, S., Baldi, L., Hacker, D.L., Bürki, C.A., Wurm, F.M., 2013. Disposable 600-mL orbitally shaken bioreactor for mammalian cell cultivation in suspension. Biochem. Eng. J. 76, 6–12. https://doi.org/10.1016/j.bej.2013.04.008

Moog, D.B., Jirka, G.H., 1999. Air-Water Gas Transfer in Uniform Channel Flow. J. Hydraul. Eng. 125, 3–10. https://doi.org/10.1061/(ASCE)0733-9429(1999)125:1(3)

Müller, M., Husemann, U., Greller, G., Meusel, W., Kraume, M., 2018. Heat transfer characteristics of a stirred single-use bioreactor. Biochem. Eng. J. 140, 168–177. https://doi.org/10.1016/J.BEJ.2018.09.022

Müller, M., Meusel, W., Husemann, U., Greller, G., Kraume, M., 2017. Measurement of heat transfer coefficients in stirred single-use bioreactors by the decay of hydrogen peroxide. Eng. Life Sci. 17, 1234–1243. https://doi.org/10.1002/elsc.201700099

Nakagawa, H., Nezu, I., Ueda, H., 1975. Turbulence of Open Channel Flow over Smooth and Rough Beds. Proc. Japan Soc. Civ. Eng. 1975, 155–168. https://doi.org/10.2208/jscej1969.1975.241_155

Nankervis, B., Jones, M., Vang, B., Brent Rice, R., Coeshott, C., Beltzer, J., 2018. Optimizing T Cell Expansion in a Hollow-Fiber Bioreactor. Curr. Stem Cell Reports 4, 46–51. https://doi.org/10.1007/s40778-018-0116-x

Nezu, I., Rodi, W., 1986. Open-channel Flow Measurements with a Laser Doppler Anemometer. J. Hydraul. Eng. 112, 335–355. https://doi.org/10.1061/(ASCE)0733-9429(1986)112:5(335)

Nikakhtari, H., Hill, G.A., 2005a. Enhanced Oxygen Mass Transfer in an External Loop

Airlift Bioreactor Using a Packed Bed. Ind. Eng. Chem. Res. 44, 1067–1072. https://doi.org/10.1021/ie0494925

Nikakhtari, H., Hill, G.A., 2005b. Hydrodynamic and oxygen mass transfer in an external loop airlift bioreactor with a packed bed. Biochem. Eng. J. 27, 138–145. https://doi.org/10.1016/j.bej.2005.08.014

Nogueira, D.E.S., Rodrigues, C.A.V., Carvalho, M.S., Miranda, C.C., Hashimura, Y., Jung, S., Lee, B., Cabral, J.M.S., 2019. Strategies for the expansion of human induced pluripotent stem cells as aggregates in single-use Vertical-Wheel^{TM} bioreactors. J. Biol. Eng. 13, 1–14. https://doi.org/10.1186/s13036-019-0204-1

Novais, J.L., Titchener-Hooker, N.J., Hoare, M., 2001. Economic comparison between conventional and disposables-based technology for the production of biopharmaceuticals. Biotechnol. Bioeng. 75, 143–153. https://doi.org/10.1002/bit.1182

Odeleye, A.O.O., Marsh, D.T.J., Osborne, M.D., Lye, G.J., Micheletti, M., 2014. On the fluid dynamics of a laboratory scale single-use stirred bioreactor. Chem. Eng. Sci. 111, 299–312. https://doi.org/10.1016/j.ces.2014.02.032

Öncül, A.A., Kalmbach, A., Genzel, Y., Reichl, U., Thévenin, D., 2010. Characterization of flow conditions in 2 L and 20 L wave bioreactors® using computational fluid dynamics. Biotechnol. Prog. 26, 101–110. https://doi.org/10.1002/btpr.312

Özbek, B., Gayik, S., 2001. The studies on the oxygen mass transfer coefficient in a bioreactor. Process Biochem. 36, 729–741. https://doi.org/10.1016/S0032-9592(00)00272-7

Palomares, L.A., Ramírez, O.T., 1996. The effect of dissolved oxygen tension and the utility of oxygen uptake rate in insect cell culture. Cytotechnology 22, 225–237. https://doi.org/10.1007/BF00353943

Pereira Chilima, T.D., Moncaubeig, F., Farid, S.S., 2018. Impact of allogeneic stem cell

manufacturing decisions on cost of goods, process robustness and reimbursement. Biochem. Eng. J. 137, 132–151. https://doi.org/10.1016/j.bej.2018.04.017

Peters, M.S., Timmerhaus, K.D., 1991. Plant design and economics for chemical engineers, 4th ed. McGraw-Hill, New York, NY.

Petrides, D., Harrison, R.G., Todd, P.W., Rudge, S.R., Petrides, D.P., 2015. Bioprocess Design and Economics Bioseparations Science and Engineering. Oxford University Press.

Phillips, O.M., 1985. Spectral and statistical properties of the equilibrium range in wind-generated gravity waves. J. Fluid Mech. 156, 505. https://doi.org/10.1017/S0022112085002221

Pietrzykowski, M., Flanagan, W., Pizzi, V., Brown, A., Sinclair, A., Monge, M., 2013. An environmental life cycle assessment comparison of single-use and conventional process technology for the production of monoclonal antibodies. J. Clean. Prod. 41, 150–162. https://doi.org/10.1016/j.jclepro.2012.09.048

Pilarek, M., Sobieszuk, P., Wierzchowski, K., Dąbkowska, K., 2018. Impact of operating parameters on values of a volumetric mass transfer coefficient in a single-use bioreactor with wave-induced agitation. Chem. Eng. Res. Des. 136, 1–10. https://doi.org/10.1016/J.CHERD.2018.04.012

Powers, A.D., Piras, B.A., Clark, R.K., Lockey, T.D., Meagher, M.M., 2016. Development and Optimization of AAV hFIX Particles by Transient Transfection in an iCELLis ® Fixed-Bed Bioreactor. Hum. Gene Ther. Methods 27, 112–121. https://doi.org/10.1089/hgtb.2016.021

Prince, M.J., Blanch, H.W., 1990. Bubble coalescence and break-up in air-sparged bubble columns. AIChE J. 36, 1485–1499. https://doi.org/10.1002/aic.690361004

Rahimi, M.J., Sitaraman, H., Humbird, D., Stickel, J.J., 2018. Computational fluid dynamics

study of full-scale aerobic bioreactors: Evaluation of gas–liquid mass transfer, oxygen uptake, and dynamic oxygen distribution. Chem. Eng. Res. Des. 139, 283–295. https://doi.org/10.1016/j.cherd.2018.08.033

Ramasamy, S.V., Titchener-Hooker, N.J., Lettieri, P., 2015. Life cycle assessment as a tool to support decision making in the biopharmaceutical industry: Considerations and challenges. Food Bioprod. Process. 94, 297–305. https://doi.org/10.1016/j.fbp.2014.03.009

Rao, G., Moreira, A., Brorson, K., 2009. Disposable bioprocessing: The future has arrived. Biotechnol. Bioeng. 102, 348–356. https://doi.org/10.1002/bit.22192

Raven, N., Rasche, S., Kuehn, C., Anderlei, T., Klöckner, W., Schuster, F., Henquet, M., Bosch, D., Büchs, J., Fischer, R., Schillberg, S., 2015. Scaled-up manufacturing of recombinant antibodies produced by plant cells in a 200-L orbitally-shaken disposable bioreactor. Biotechnol. Bioeng. 112, 308–321. https://doi.org/10.1002/bit.25352

Rodrigues, C.A., Silva, T.P., Nogueira, D.E., Fernandes, T.G., Hashimura, Y., Wesselschmidt, R., Diogo, M.M., Lee, B., Cabral, J.M., 2018. Scalable culture of human induced pluripotent cells on microcarriers under xeno-free conditions using single-use vertical-wheel^{TM} bioreactors. J. Chem. Technol. Biotechnol. 93, 3597–3606. https://doi.org/10.1002/jctb.5738

Rodrigues, M.E., Costa, A.R., Henriques, M., Azeredo, J., Oliveira, R., 2012. Wave characterization for mammalian cell culture: Residence time distribution. N. Biotechnol. 29, 402–408. https://doi.org/10.1016/j.nbt.2011.10.006

Romero, L., Melville, W.K., Kleiss, J.M., 2012. Spectral Energy Dissipation due to Surface Wave Breaking. J. Phys. Oceanogr. 42, 1421–1444. https://doi.org/10.1175/JPO-D-11-072.1

Ruffieux, P.A., Von Stockar, U., Marison, I.W., 1998. Measurement of volumetric (OUR)

and determination of specific (qO2) oxygen uptake rates in animal cell cultures. J. Biotechnol. 63, 85–95. https://doi.org/10.1016/S0168-1656(98)00046-7

Schirmaier, C., Jossen, V., Kaiser, S.C., Jüngerkes, F., Brill, S., Safavi-Nab, A., Siehoff, A., van den Bos, C., Eibl, D., Eibl, R., 2014. Scale-up of adipose tissue-derived mesenchymal stem cell production in stirred single-use bioreactors under low-serum conditions. Eng. Life Sci. 14, 292–303. https://doi.org/10.1002/elsc.201300134

Schlaeppi, J.M., Henke, M., Mahnke, M., Hartmann, S., Schmitz, R., Pouliquen, Y., Kerins, B., Weber, E., Kolbinger, F., Kocher, H.P., 2006. A semi-automated large-scale process for the production of recombinant tagged proteins in the Baculovirus expression system. Protein Expr. Purif. 50, 185–195. https://doi.org/10.1016/j.pep.2006.06.021

Shirahata, H., Hirao, M., Sugiyama, H., 2017. Decision-Support Method for the Choice Between Single-Use and Multi-Use Technologies in Sterile Drug Product Manufacturing. J. Pharm. Innov. 12, 1–13. https://doi.org/10.1007/s12247-016-9264-7

Shukla, A.A., Gottschalk, U., 2013. Single-use disposable technologies for biopharmaceutical manufacturing. Trends Biotechnol. 31, 147–154. https://doi.org/10.1016/J.TIBTECH.2012.10.004

Singh, V., 1999. Disposable bioreactor for cell culture using wave-induced agitation. Cytotechnology 30, 149–158. https://doi.org/10.1023/A:1008025016272

Sousa, M.F.Q., Silva, M.M., Giroux, D., Hashimura, Y., Wesselschmidt, R., Lee, B., Roldão, A., Carrondo, M.J.T., Alves, P.M., Serra, M., 2015. Production of oncolytic adenovirus and human mesenchymal stem cells in a single-use, Vertical-Wheel bioreactor system: Impact of bioreactor design on performance of microcarrier-based cell culture processes. Biotechnol. Prog. 31, 1600–1612. https://doi.org/10.1002/btpr.2158

Stettler, M., Zhang, X., Hacker, D.L., De Jesus, M., Wurm, F.M., 2007. Novel orbital shake bioreactors for transient production of CHO derived IgGs. Biotechnol. Prog. 23, 1340–

1346. https://doi.org/10.1021/bp070219i

Sun, B., Zhao, D., Zhang, X., Gu, T., Yu, X., Sun, S., Zhao, X., Wei, L., Liu, D., Yan, H., Meng, X., Kong, W., Xu, F., Yang, P., Jiang, C., 2016. Development a scalable production process for truncated human papillomavirus type-6 L1 protein using WAVE Bioreactor and hollow fiber membrane. Appl. Microbiol. Biotechnol. 100, 1231–1240. https://doi.org/10.1007/s00253-015-6974-6

Terrier, B., Courtois, D., Hénault, N., Cuvier, A., Bastin, M., Aknin, A., Dubreuil, J., Pétiard, V., 2007. Two new disposable bioreactors for plant cell culture: The wave and undertow bioreactor and the slug bubble bioreactor. Biotechnol. Bioeng. 96, 914–923. https://doi.org/10.1002/bit.21187

Timmins, N.E., Athanasas, S., Günther, M., Buntine, P., Nielsen, L.K., 2011. Ultra-High-Yield Manufacture of Red Blood Cells from Hematopoietic Stem Cells. Tissue Eng. Part C Methods 17, 1131–1137. https://doi.org/10.1089/ten.tec.2011.0207

Timmins, N.E., Kiel, M., Günther, M., Heazlewood, C., Doran, M.R., Brooke, G., Atkinson, K., 2012. Closed system isolation and scalable expansion of human placental mesenchymal stem cells. Biotechnol. Bioeng. 109, 1817–1826. https://doi.org/10.1002/bit.24425

Tribe, L.A., Briens, C.L., Margaritis, A., 1995. Determination of the volumetric mass transfer coefficient (kLa) using the dynamic “gas out–gas in” method: Analysis of errors caused by dissolved oxygen probes, Biotechnology and Bioengineering. Wiley Subscription Services, Inc., A Wiley Company. https://doi.org/10.1002/bit.260460412

Tsai, A.C., Liu, Y., Yuan, X., Chella, R., Ma, T., 2017. Aggregation kinetics of human mesenchymal stem cells under wave motion. Biotechnol. J. 12, 1–13. https://doi.org/10.1002/biot.201600448

Turney, D.E., Banerjee, S., 2013. Air–water gas transfer and near-surface motions. J. Fluid

Mech. 733, 588–624. https://doi.org/10.1017/jfm.2013.435

Uslu, U., Erdmann, M., Wiesinger, M., Schuler, G., Schuler-Thurner, B., 2019. Automated Good Manufacturing Practice–compliant generation of human monocyte-derived dendritic cells from a complete apheresis product using a hollow-fiber bioreactor system overcomes a major hurdle in the manufacture of dendritic cells for cancer vaccine. Cytotherapy 21, 1166–1178. https://doi.org/10.1016/j.jcyt.2019.09.001

Valkama, A.J., Leinonen, H.M., Lipponen, E.M., Turkki, V., Malinen, J., Heikura, T., Ylä-Herttuala, S., Lesch, H.P., 2018. Optimization of lentiviral vector production for scale-up in fixed-bed bioreactor. Gene Ther. 25, 39–46. https://doi.org/10.1038/gt.2017.91

Ventini-Monteiro, D., Dubois, S., Astray, R.M., Castillo, J., Pereira, C.A., 2015. Insect cell entrapment, growth and recovering using a single-use fixed-bed bioreactor. Scaling up and recombinant protein production. J. Biotechnol. 216, 110–115. https://doi.org/10.1016/j.jbiotec.2015.10.013

Vermasvuori, R., Hurme, M., 2011. Economic comparison of diagnostic antibody production in perfusion stirred tank and in hollow fiber bioreactor processes. Biotechnol. Prog. 27, 1588–1598. https://doi.org/10.1002/btpr.676

Wang, L., Hu, H., Yang, J., Wang, F., Kaisermayer, C., Zhou, P., 2012. High Yield of Human Monoclonal Antibody Produced by Stably Transfected Drosophila Schneider 2 Cells in Perfusion Culture Using Wave Bioreactor. Mol. Biotechnol. 52, 170–179. https://doi.org/10.1007/s12033-011-9484-5

Wang, L., Ridgway, D., Gu, T., Moo-Young, M., 2003. Effects of process parameters on heterologous protein production in Aspergilus niger fermentation. J. Chem. Technol. Biotechnol. 78, 1259–1266. https://doi.org/10.1002/jctb.898

Weber, W., Weber, E., Geisse, S., Memmert, K., 2002. Optimisation of protein expression and establishment of the Wave Bioreactor for Baculovirus/insect cell culture.

Cytotechnology 38, 77–85. https://doi.org/10.1023/A:1021102015070

Weheliye, W., Yianneskis, M., Ducci, A., 2013. On the fluid dynamics of shaken bioreactors- flow characterization and transition. AIChE J. 59, 334–344. https://doi.org/10.1002/aic.13943

Werner, S., Olownia, J., Egger, D., Eibl, D., 2013. An Approach for Scale-Up of Geometrically Dissimilar Orbitally Shaken Single-Use Bioreactors. Chemie Ing. Tech. 85, 118–126. https://doi.org/10.1002/cite.201200153

Wesley, D.J., Smith, R.M., Zimmerman, W.B., Howse, J.R., 2016. Influence of Surface Wettability on Microbubble Formation. https://doi.org/10.1021/acs.langmuir.5b03743

Westbrook, A., Scharer, J., Moo-Young, M., Oosterhuis, N., Perry Chou, C., 2014. Application of a two-dimensional disposable rocking bioreactor to bacterial cultivation for recombinant protein production. Biochem. Eng. J. 88, 154–161. https://doi.org/10.1016/j.bej.2014.04.011

Whitman, W.G., 1923. The Two-Film Theory of Gas Absorption. Chem. Metall. Eng. 29, 148.

Wurm, F.M., 2004. Production of recombinant protein therapeutics in cultivated mammalian cells. Nat. Biotechnol. 22, 1393–1398. https://doi.org/10.1038/nbt1026

Xenopoulos, A., 2015. A new, integrated, continuous purification process template for monoclonal antibodies: Process modeling and cost of goods studies. J. Biotechnol. 213, 42–53. https://doi.org/10.1016/j.jbiotec.2015.04.020

Xu, P., Clark, C., Ryder, T., Sparks, C., Zhou, J., Wang, M., Russell, R., Scott, C., 2017. Characterization of TAP Ambr 250 disposable bioreactors, as a reliable scale-down model for biologics process development. Biotechnol. Prog. 33, 478–489. https://doi.org/10.1002/btpr.2417

Xu, S., Hoshan, L., Jiang, R., Gupta, B., Brodean, E., O'Neill, K., Seamans, T.C., Bowers, J.,

Chen, H., 2017. A practical approach in bioreactor scale-up and process transfer using a combination of constant P/V and vvm as the criterion. Biotechnol. Prog. 33, 1146–1159. https://doi.org/10.1002/btpr.2489

Yang, J., Guertin, P., Jia, G., Lv, Z., Yang, H., Ju, D., 2019. Large-scale microcarrier culture of HEK293T cells and Vero cells in single-use bioreactors. AMB Express 9. https://doi.org/10.1186/s13568-019-0794-5

Zhan, C., Hagrot, E., Brandt, L., Chotteau, V., 2019. Study of hydrodynamics in Wave Bioreactors by Computational Fluid Dynamics reveals a resonance phenomenon. Chem. Eng. Sci. 193, 53–65. https://doi.org/10.1016/J.CES.2018.08.017

Zhang, X., Bürki, C.A., Stettler, M., De Sanctis, D., Perrone, M., Discacciati, M., Parolini, N., DeJesus, M., Hacker, D.L., Quarteroni, A., Wurm, F.M., 2009. Efficient oxygen transfer by surface aeration in shaken cylindrical containers for mammalian cell cultivation at volumetric scales up to 1000 L. Biochem. Eng. J. 45, 41–47. https://doi.org/10.1016/j.bej.2009.02.003

Zhang, X., Stettler, M., de Sanctis, D., Perrone, M., Parolini, N., Discacciati, M., de Jesus, M., Hacker, D., Quarteroni, A., Wurm, F., 2010. Use of orbital shaken disposable bioreactors for mammalian cell cultures from the milliliter-scale to the 1,000-liter scale. Adv. Biochem. Eng. Biotechnol. 115, 33–53. https://doi.org/10.1007/10_2008_18

Zhu, L., Han, W., Song, B., Wang, Z., 2018a. Characterizing the fluid dynamics in the flow fields of cylindrical orbitally shaken bioreactors with different geometry sizes. Eng. Life Sci. 18, 570–578. https://doi.org/10.1002/elsc.201700170

Zhu, L., Monteil, D.T., Wang, Y., Song, B., Hacker, D.L., Wurm, M.J., Li, X., Wang, Z., Wurm, F.M., 2018b. Fluid dynamics of flow fields in a disposable 600-mL orbitally shaken bioreactor. Biochem. Eng. J. 129, 84–95. https://doi.org/10.1016/J.BEJ.2017.10.019

Appendix A

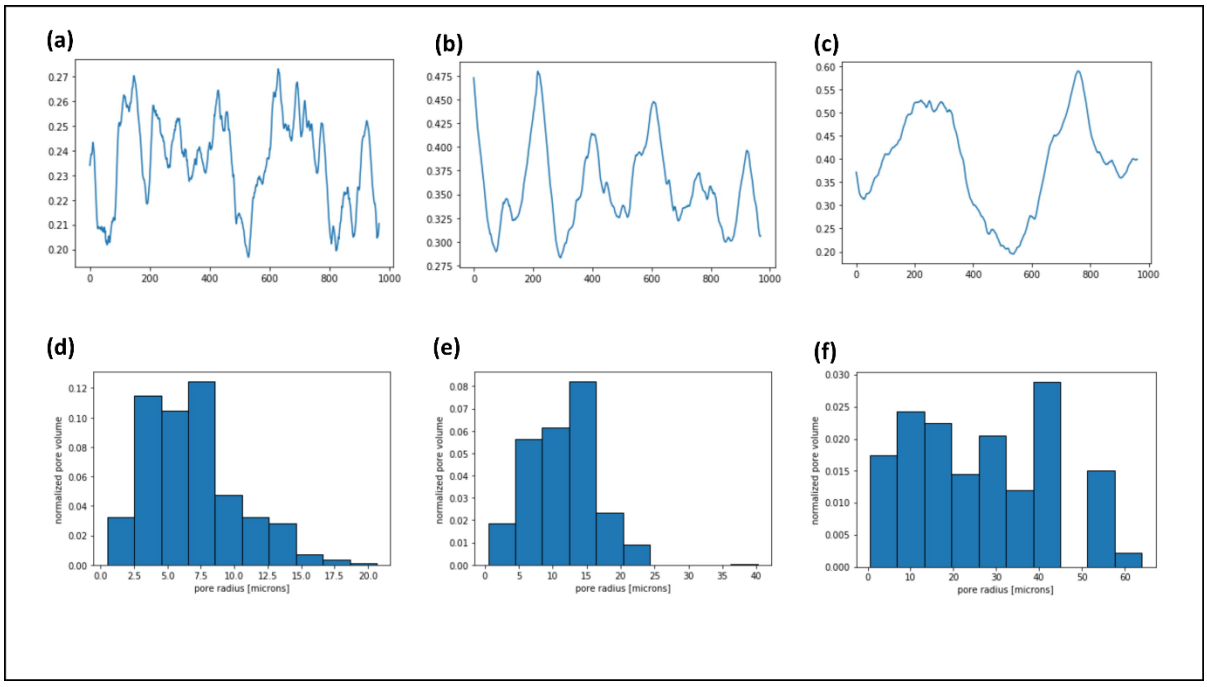

Figure A-1 Illustration of the area fraction distribution and pore size distribution of three spargers used in this study with 5, 10 and 50 µm nominal porosity.

Summary of original $k_L a$ data acquired from control group (original bag design) and baffle installed group.

No Baffle (Control)
Baffle
Sparger

kLa measurements

3L DI water, 8 angle, 10 L bag	repeat 1	repeat 2	repeat 3	Average	Std
10 rpm	7.46	6.98	7.61	7.35	0.32909
20 rpm	24.29	24.01	24.07	24.12333	0.147422
30 rpm	52.33	51.87	49.72	51.30667	1.39321
40 rpm	86.75	82.08	84.96	84.59667	2.356106

5L DI water, 8 angle, 10 L bag	repeat 1	repeat 2	repeat 3	Average	Std
10 rpm	1.67	1.67	1.6	1.646667	0.040415
20 rpm	8.09	8	8.88	8.323333	0.484183
30 rpm	24.28	24.05	26.09	24.80667	1.117333
40 rpm	N/A	N/A	N/A	N/A	N/A

6L DI water, 8 angle, 20 L bag	repeat 1	repeat 2	repeat 3	Average	Std
10 rpm	6.59	6.67	8.27	7.176667	0.947699
20 rpm	24.35	23.28	25.29	24.30667	1.0057
30 rpm	57.19	55.33	55.65	56.05667	0.994451
40 rpm	111.23	106.8	110.61	109.5467	2.398798

3L DI water, 12 angle, 10 L bag	repeat 1	repeat 2	repeat 3	Average	Std
10 rpm	7.54	7.08	7.38	7.333333	0.233524
20 rpm	27.67	24.81	25.82	26.1	1.450414
30 rpm	69.17	62.88	61.68	64.57667	4.022938
40 rpm	103.18	112.97	105.76	107.3033	5.074193

5L DI water, 12 angle, 10 L bag	repeat 1	repeat 2	repeat 3	Average	Std
10 rpm	2.11	2.24	2.29	2.213333	0.092916
20 rpm	11.24	11.97	11.82	11.67667	0.38553
30 rpm	30.41	32.29	31.43	31.37667	0.941134
40 rpm	N/A	N/A	N/A	N/A	N/A

6L DI water, 12 angle, 20 L bag	repeat 1	repeat 2	repeat 3	Average	Std
10 rpm	9.54	10.32	9.61	9.823333	0.431548
20 rpm	30.13	32.96	31.95	31.68	1.43419
30 rpm	81.03	84.07	83.75	82.95	1.670449
40 rpm	144.65	139.3	143.62	142.5233	2.838597

3L DI water, 8 angle, 10 L bag	repeat 1	repeat 2	repeat 3	Average	Std
10 rpm	9.49	9.15	10.91	9.85	0.933595
20 rpm	23.85	23.35	26.01	24.40333	1.413695
30 rpm	44.54	42.51	48.39	45.14667	2.986576
40 rpm	74.88	71.66	79	75.18	3.679185

5L DI water, 8 angle, 10 L bag	repeat 1	repeat 2	repeat 3	Average	Std
10 rpm	1.97	1.94	1.72	1.876667	0.136504
20 rpm	8.83	7.02	7.76	7.87	0.91
30 rpm	23.95	19.32	21.68	21.65	2.315146
40 rpm	N/A	N/A	N/A	N/A	N/A

6L DI water, 8 angle, 20 L bag	repeat 1	repeat 2	repeat 3	Average	Std
10 rpm	13.38	13.31	12.73	13.14	0.356791
20 rpm	29.03	29.14	29.08	29.08333	0.055076
30 rpm	61.33	60.99	60.85	61.05667	0.246847
40 rpm	95.85	96.5	99.84	97.39667	2.140802

3L DI water, 12 angle, 10 L bag	repeat 1	repeat 2	repeat 3	Average	Std
10 rpm	13.85	12.82	13.99	13.55333	0.638931
20 rpm	28.78	28.3	29.56	28.88	0.635925
30 rpm	57.93	55.1	58.22	57.08333	1.723727
40 rpm	98.6	97.12	102.04	99.25333	2.524229

5L DI water, 12 angle, 10 L bag	repeat 1	repeat 2	repeat 3	Average	Std
10 rpm	2.62	2.53	2.56	2.57	0.045826
20 rpm	11	10.8	10.73	10.84333	0.140119
30 rpm	28.41	27.17	26.27	27.28333	1.074492
40 rpm	N/A	N/A	N/A	N/A	N/A

6L DI water, 12 angle, 20 L bag	repeat 1	repeat 2	repeat 3	Average	Std
10 rpm	16.21	15.83	15.38	15.80667	0.415492
20 rpm	32.41	32.68	32.4	32.49667	0.15885
30 rpm	72.71	71.13	70.41	71.41667	1.176492
40 rpm	132.58	128.07	125.42	128.69	3.620041

Summary of original $k_L a$ data acquired from control group (original bag design) and baffle installed group (cont'd).

No Baffle (Control)												
Baffle												
Sparger												
8L DI water, 8 angle, 20 L bag	repeat 1	repeat 2	repeat 3	Average	Std		10L DI water, 8 angle, 20 L bag	repeat 1	repeat 2	repeat 3	Average	Std
10 rpm	4.59	4.23	3.74	4.186667	0.426654		10 rpm	1.52	1.65	1.7	1.623333	0.092916
20 rpm	17.21	16.38	16.25	16.61333	0.520801		20 rpm	10.1	11.94	11.71	11.25	1.002547
30 rpm	39.9	39.33	38.8	39.34333	0.550121		30 rpm	33.52	33.26	32.56	33.11333	0.496521
40 rpm	84.66	91.36	87.37	87.79667	3.370317		40 rpm	62.17	65.58	66.93	64.89333	2.453168
8L DI water, 12 angle, 20 L bag	repeat 1	repeat 2	repeat 3	Average	Std		10L DI water, 12 angle, 20 L bag	repeat 1	repeat 2	repeat 3	Average	Std
10 rpm	5.38	5.83	5.72	5.643333	0.234592		10 rpm	3.48	3.97	3.82	3.756667	0.251064
20 rpm	22.89	23.37	22.87	23.04333	0.283078		20 rpm	15.4	16.57	16.1	16.02333	0.588756
30 rpm	59.8	58.98	59.77	59.51667	0.465009		30 rpm	40.29	42.53	41.53	41.45	1.122141
40 rpm	110.11	119.18	120.7	116.6633	5.726014		40 rpm	84.71	93.65	94.88	91.08	5.550757
8L DI water, 8 angle, 20 L bag	repeat 1	repeat 2	repeat 3	Average	Std		10L DI water, 8 angle, 20 L bag	repeat 1	repeat 2	repeat 3	Average	Std
10 rpm	5.25	5.41	5.15	5.27	0.131149		10 rpm	2.51	2.46	2.57	2.513333	0.055076
20 rpm	18.07	17.67	18.2	17.98	0.276225		20 rpm	10.11	10.82	11.59	10.84	0.740203
30 rpm	39.49	41.54	44.26	41.76333	2.39283		30 rpm	29.75	30.61	32.02	30.79333	1.146051
40 rpm	67.29	74.6	85.12	75.67	8.96303		40 rpm	57.21	60.8	54.56	57.52333	3.131778
8L DI water, 12 angle, 20 L bag	repeat 1	repeat 2	repeat 3	Average	Std		10L DI water, 12 angle, 20 L bag	repeat 1	repeat 2	repeat 3	Average	Std
10 rpm	7.57	8.12	7.18	7.623333	0.472264		10 rpm	3.7	4.07	4.1	3.956667	0.222785
20 rpm	21.75	23.09	21.53	22.12333	0.844354		20 rpm	14.8	16.01	15.58	15.46333	0.613379
30 rpm	50.06	53.11	50.47	51.21333	1.655305		30 rpm	38.59	42.75	40.16	40.5	2.100738
40 rpm	108.29	110.08	105.32	107.8967	2.404253		40 rpm	79.4	88.02	82.64	83.35333	4.354048

Summary of original t_m data acquired from control group and baffle installed group.

No Baffle (Control)																		
Baffle																		
Mixing time measurements																		
3L DI water, 8 angle, 10 L bag	repeat 1	repeat 2	repeat 3	Average	Std		5L DI water, 8 angle, 10 L bag	repeat 1	repeat 2	repeat 3	Average	Std		6L DI water, 8 angle, 10 L bag	repeat 1	repeat 2	repeat 3	Average	Std
10 rpm	46	46	34	42	6.928203		10 rpm	102	102	92	98.66667	5.773503		10 rpm	170	162	135	155.6667	18.33939
20 rpm	28	32	32	30.66667	2.309401		20 rpm	26	24	20	23.33333	3.05505		20 rpm	95	100	84	93	8.185353
30 rpm	16	14	14	14.66667	1.154701		30 rpm	20	20	20	20	0		30 rpm	62	64	70	65.33333	4.163332
40 rpm	12	12	14	12.66667	1.154701		40 rpm	N/A	N/A	N/A	N/A	N/A		40 rpm	42	46	48	45.33333	3.05505
3L DI water, 12 angle, 10 L bag	repeat 1	repeat 2	repeat 3	Average	Std		5L DI water, 12 angle, 10 L bag	repeat 1	repeat 2	repeat 3	Average	Std		6L DI water, 12 angle, 10 L bag	repeat 1	repeat 2	repeat 3	Average	Std
10 rpm	34	36	40	36.66667	3.05505		10 rpm	180	202	202	194.6667	12.70171		10 rpm	126	130	142	132.6667	8.326664
20 rpm	22	18	20	20	2		20 rpm	26	32	32	30	3.464102		20 rpm	87	89	90	88.66667	1.527525
30 rpm	14	14	14	14	0		30 rpm	14	16	16	15.33333	1.154701		30 rpm	35	36	40	37	2.645751
40 rpm	12	14	14	13.33333	1.154701		40 rpm	N/A	N/A	N/A	N/A	N/A		40 rpm	38	40	42	40	2
3L DI water, 8 angle, 10 L bag	repeat 1	repeat 2	repeat 3	Average	Std	lnx	5L DI water, 8 angle, 10 L bag	repeat 1	repeat 2	repeat 3	Average	Std		6L DI water, 8 angle, 10 L bag	repeat 1	repeat 2	repeat 3	Average	Std
10 rpm	10	14	10	11.33333	2.309401	2.302585	10 rpm	60	70	128	86	36.71512		10 rpm	30	28	36	31.33333	4.163332
20 rpm	8	12	8	9.333333	2.309401	2.995732	20 rpm	30	28	30	29.33333	1.154701		20 rpm	10	10	14	11.33333	2.309401
30 rpm	8	8	8	8	0	3.401197	30 rpm	14	16	12	14	2		30 rpm	22	20	20	20.66667	1.154701
40 rpm	8	8	8	8	0	3.688879	40 rpm	N/A	N/A	N/A	N/A	N/A		40 rpm	12	16	20	16	4
3L DI water, 12 angle, 10 L bag	repeat 1	repeat 2	repeat 3	Average	Std		5L DI water, 12 angle, 10 L bag	repeat 1	repeat 2	repeat 3	Average	Std		6L DI water, 12 angle, 10 L bag	repeat 1	repeat 2	repeat 3	Average	Std
10 rpm	18	10	10	12.66667	4.618802		10 rpm	62	64	98	74.66667	20.23199		10 rpm	28	26	26	26.66667	1.154701
20 rpm	12	8	8	9.333333	2.309401		20 rpm	24	24	24	24	0		20 rpm	10	8	14	10.66667	3.05505
30 rpm	8	6	8	7.333333	1.154701		30 rpm	10	16	16	14	3.464102		30 rpm	6	6	14	8.666667	4.618802
40 rpm	8	8	8	8	0		40 rpm	N/A	N/A	N/A	N/A	N/A		40 rpm	18	18	20	18.66667	1.154701

Summary of original t_m data acquired from control group and baffle installed group (cont'd).

No Baffle (Control)												
Baffle												
8L DI water, 8 angle, 10 L bag	repeat 1	repeat 2	repeat 3	Average	Std		10L DI water, 8 angle, 10 L bag	repeat 1	repeat 2	repeat 3	Average	Std
10 rpm	398	368	364	376.6667	18.58315		10 rpm	344	348	336	342.6667	6.110101
20 rpm	66	70	62	66	4		20 rpm	108	114	94	105.3333	10.2632
30 rpm	42	40	32	38	5.291503		30 rpm	44	52	54	50	5.291503
40 rpm	38	38	44	40	3.464102		40 rpm	40	44	36	40	4
8L DI water, 12 angle, 10 L bag	repeat 1	repeat 2	repeat 3	Average	Std		10L DI water, 12 angle, 10 L bag	repeat 1	repeat 2	repeat 3	Average	Std
10 rpm	318	238	268	274.6667	40.41452		10 rpm	243	268	314	275	36.01389
20 rpm	86	74	84	81.33333	6.429101		20 rpm	80	70	74	74.66667	5.033223
30 rpm	34	40	40	38	3.464102		30 rpm	38	50	46	44.66667	6.110101
40 rpm	38	40	38	38.66667	1.154701		40 rpm	38	34	30	34	4
8L DI water, 8 angle, 10 L bag	repeat 1	repeat 2	repeat 3	Average	Std		10L DI water, 8 angle, 10 L bag	repeat 1	repeat 2	repeat 3	Average	Std
10 rpm	54	40	48	47.33333	7.023769		10 rpm	288	300	284	290.6667	8.326664
20 rpm	18	20	22	20	2		20 rpm	26	28	22	25.33333	3.05505
30 rpm	16	16	20	17.33333	2.309401		30 rpm	14	18	16	16	2
40 rpm	28	30	28	28.66667	1.154701		40 rpm	20	20	20	20	0
8L DI water, 12 angle, 10 L bag	repeat 1	repeat 2	repeat 3	Average	Std		10L DI water, 12 angle, 10 L bag	repeat 1	repeat 2	repeat 3	Average	Std
10 rpm	88	88	102	92.66667	8.082904		10 rpm	78	82	72	77.33333	5.033223
20 rpm	14	12	12	12.66667	1.154701		20 rpm	22	20	20	20.66667	1.154701
30 rpm	12	10	12	11.33333	1.154701		30 rpm	14	14	16	14.66667	1.154701
40 rpm	24	22	26	24	2		40 rpm	16	20	18	18	2

Summary of original $k_L a$ data acquired from sparger group

Short Sparger (5cm)								
	2019-05-06	2019-05-07						
5micron, hydrophobic	2019-06-05	2019-06-10	2019-05-13	2019-04-17	2019-04-17	2019-04-18		
3L DI water, 12 angle, 10 L bag 4L/min	repeat 4	repeat 5	repeat 6	repeat 1	repeat 2	repeat 3	Average	Std
10 rpm	27.12	25.06	26.16	26.52	26.39	26.36	26.2683333	0.67582296
20 rpm	43.44	43.00	43.65	49.25	47.83	47.69	45.81	2.74324625
30 rpm	78.48	76.97	76.45	89.05	81.97	88.07	81.8316667	5.56546644
40 rpm	148.86	126.55	N/A	148.18	N/A	N/A	141.196667	12.6889414
5 micron, hydrophobic	2019-08-20	2019-08-20	2019-08-20	2019-08-20	2019-10-07	2019-10-07		
5L DI water, 12 angle, 10 L bag 4L/min	repeat 1	repeat 2	repeat 3	repeat 4	repeat 5	repeat 6	Average	Std
10 rpm	20.68	18.01	17.32	18.63	20.24	21.14	19.3366667	1.56198165
20 rpm	24.70	23.3	23.01	23.85	25.71	27.07	24.6066667	1.55713412
30 rpm	50.76	49.33	46.32	44.61	48.78	50.94	48.4566667	2.5180045
40 rpm	N/A	N/A	N/A	N/A	N/A	N/A	#DIV/0!	#DIV/0!
10 micron, hydrophobic	2019-05-28	2019-05-28	2019-05-29	2019-05-29	2019-08-21	2019-08-21		
5L DI water, 12 angle, 10 L bag 4L/min	repeat 1	repeat 2	repeat 3	repeat 4	repeat 5	repeat 6	Average	Std
10 rpm	20.69	19.18	18.79	17.94	14.93	15.48	17.835	2.23016367
20 rpm	27.13	25.64	26.47	24.77	21.30	21.21	24.42	2.57666451
30 rpm	46.14	44.19	48.12	42.67	44.29	44.96	45.0616667	1.87626668
40 rpm	N/A	N/A	N/A	N/A	N/A	N/A	#DIV/0!	#DIV/0!
50 micron, hydrophobic	2019-08-22	2019-08-22	2019-08-23	2019-08-24	2019-09-10	2019-09-10		
5L DI water, 12 angle, 10 L bag 4L/min	repeat 1	repeat 2	repeat 3	repeat 4	repeat 5	repeat 6	Average	Std
10 rpm	10.28	10.56	11.72	11.8	13.84	14.21	12.0683333	1.6365869
20 rpm	15.27	16.11	16.74	17.38	20.02	20.05	17.595	2.01473323
30 rpm	35.80	37.03	38.12	39.41	41.51	42.57	39.0733333	2.61059891
40 rpm	N/A	N/A	N/A	N/A	N/A	N/A	#DIV/0!	#DIV/0!
5 micron, hydrophilic	2019-09-17	2019-09-16	2019-09-16	2019-09-17	2019-09-17	2019-09-17		
5L DI water, 12 angle, 10 L bag 4L/min	repeat 1	repeat 2	repeat 3	repeat 4	repeat 5	repeat 6	Average	Std
10 rpm	18.04	20	20.24	18.52	18.51	18.12	18.905	0.96435989
20 rpm	23.88	24.71	25.57	24.12	24.12	23.54	24.3233333	0.72062935
30 rpm	48.34	49.91	51.65	45.63	51.22	47.18	48.9883333	2.36148611
40 rpm	N/A	N/A	N/A	N/A	N/A	N/A	#DIV/0!	#DIV/0!
5 micron, hydrophilic	2019-11-24	2019-11-25	2019-11-25	2019-11-26	2019-11-26	2019-11-28		
6L DI water, 12 angle, 20 L bag 4L/min	repeat 1	repeat 2	repeat 3	repeat 4	repeat 5	repeat 6	Average	Std
10 rpm	10.37	12.24	12.59	13.83	13.97	15.5	13.0833333	1.76072334
20 rpm	22.96	26.33	26.96	28.22	30.29	29.72	27.4133333	2.66300332
30 rpm	48.75	51.27	51	48.79	54.65	55.5	51.66	2.86280981
40 rpm	63.2	61.1	61.18	103.13	75.13	73.72	72.91	16.0635363
	2019-11-25							
5 micron, hydrophilic	2019-11-26	2019-11-25	2019-11-26	2019-11-26	2019-11-28	2019-11-28		
10L DI water, 12 angle, 20 L bag 4L/min	repeat 1	repeat 2	repeat 3	repeat 4	repeat 5	repeat 6	Average	Std
10 rpm	7.65	6.33	9.67	9.43	9.81	9.55	8.74	1.42395225
20 rpm	17.00	17.71	22.04	21.91	22.77	23.12	20.7583333	2.68367969
30 rpm	40.29	42.63	48.41	50.02	54.24	51.67	47.8766667	5.38228081
40 rpm	82.84	74.54	84.08	80.8	88.71	84.48	82.575	4.71835459

5micron, hydrophobic	2019-06-04	2019-06-04	2019-06-11	2019-06-11		
5L DI water, 12 angle, 10 L bag same Ug	repeat 1	repeat 2	repeat 3	repeat 4	Average	Std
10 rpm	8.85	8.9	8.75	8.69	8.7975	0.095
20 rpm	15.55	15.56	16.05	15.94	15.775	0.258005
30 rpm	31.9	29.15	31.67	31.82	31.135	1.326763
40 rpm	N/A	N/A	N/A	N/A	N/A	N/A
5micron, hydrophobic	2019-05-30	2019-05-30	2019-06-04	2019-06-04		
5L DI water, 12 angle, 10 L bag 2L/min	repeat 1	repeat 2	repeat 3	repeat 4	Average	Std
10 rpm	13.44	13.57	12.81	12.38	13.05	0.556477
20 rpm	19.97	21.05	19.2	18.82	19.76	0.984107
30 rpm	37.06	37.17	34.52	34.15	35.725	1.612751
40 rpm	N/A	N/A	N/A	N/A	N/A	N/A
5micron, hydrophobic	2019-05-28	2019-05-28	2019-05-29	2019-05-29		
5L DI water, 12 angle, 10 L bag 3L/min	repeat 1	repeat 2	repeat 3	repeat 4	Average	Std
10 rpm	16.59	16.57	18.25	17.14	17.1375	0.78729
20 rpm	23.47	22.36	25.68	23.73	23.81	1.38099
30 rpm	39.57	39.69	44.79	41.81	41.465	2.443788
40 rpm	N/A	N/A	N/A	N/A	N/A	N/A
5micron, hydrophobic	2019-05-28	2019-05-28	2019-05-29	2019-05-29		
5L DI water, 12 angle, 10 L bag 4L/min	repeat 1	repeat 2	repeat 3	repeat4	Average	Std
10 rpm	20.69	19.18	18.79	17.94	19.15	1.149812
20 rpm	27.13	25.64	26.47	24.77	26.0025	1.023112
30 rpm	46.14	44.19	48.12	42.67	45.28	2.366812
40 rpm	N/A	N/A	N/A	N/A	N/A	N/A
5micron, hydrophobic	2019-06-03	2019-06-03	2019-06-11	2019-06-11		
5L DI water, 12 angle, 10 L bag 5L/min	repeat 1	repeat 2	repeat 3	repeat4	Average	Std
10 rpm	19.46	19.42	19.6	19.75	19.5575	0.14975
20 rpm	27.59	26.89	27.08	27.56	27.28	0.349571
30 rpm	51.79	45.44	50.28	47.99	48.875	2.772105
40 rpm	N/A	N/A	N/A	N/A	N/A	N/A